Abstract

The Qumushan (QMS) syn-collisional granodiorite, which is located in the eastern section of the North Qilian Orogen at the northern margin of the Greater Tibetan Plateau, has typical adakitic characteristics and also contains abundant mafic magmatic enclaves (MMEs). This recognition offers an unprecedented insight into the petrogenesis of both the adakitic host granodiorite and the enclosed MMEs. The MMEs and their host granodiorites share many characteristics in common, including identical crystallization age (~430 Ma), same mineralogy, similar mineral chemistry and whole-rock isotopic compositions, indicating their genetic link. The MMEs are most consistent with being of cumulate origin formed at earlier stages of the same magmatic system that produced the QMS adakitic granodiorite. Subsequent replenishment of adakitic magmas could have disturbed the cumulate piles as "MMEs" dispersed in the adakitic granodiorite host during emplacement. The geochemical data and petrogenetic modeling of trace elements suggest that the QMS adakitic host granodiorite is most consistent with fractional crystallization dominated by the mineral assemblage of the MMEs. The parental magma for the QMS granodiorite is best explained as resulting from partial melting of the ocean crust together with recycled terrigenous sediments during continental collision, which may have also experienced interaction with mantle peridotite during ascent.

Highlights:

1. The QMS adakitic granodiorites and their MMEs formed at ~430 Ma.

2. The MMEs are cumulate rocks formed at earlier stages of the same magmatic systems.

3. The QMS adakitic granodiorites resulted from fractional crystallization dominated by mineral assemblages represented by the MMEs.

4. The parental magma for the QMS granodiorite is best explained as resulting from partial melting of the ocean crust together with recycled terrigenous sediments during continental collision, which may have also experienced interaction with mantle peridotite during ascent.

Syn-collisional adakitic granodiorites formed by fractional crystallization: insights from their enclosed mafic magmatic enclaves (MMEs) in the Qumushan pluton, North Qilian Orogen at the northern margin of the Tibetan Plateau

Shuo Chen [a,b*], Yaoling Niu [a, c*], Jiyong Li [a,b], Wenli Sun [a], Yu Zhang [d], Yan Hu[a,b], Fengli Shao [a,b]

[a] Institute of Oceanology, Chinese Academy of Sciences, Qingdao 266071, China.

[b] University of Chinese Academy of Sciences, Beijing 100049, China

[c] Department of Earth Sciences, Durham University, Durham DH1 3LE, UK

[d] School of Earth Sciences, Lanzhou University, Lanzhou 730000, China

***Corresponding authors:**

Mr. Shuo Chen (chenshuo528@foxmail.com)

Professor Yaoling Niu (yaoling.niu@foxmail.com)

Abstract

The Qumushan (QMS) syn-collisional granodiorite, which is located in the eastern section of the North Qilian Orogen at the northern margin of the Greater Tibetan Plateau, has typical adakitic characteristics and also contains abundant mafic magmatic enclaves (MMEs). This recognition offers an unprecedented insight into the petrogenesis of both the adakitic host granodiorite and the enclosed MMEs. The MMEs and their host granodiorites share many characteristics in common, including identical crystallization age (~430 Ma), same mineralogy, similar mineral chemistry and whole-rock isotopic compositions, indicating their genetic link. The MMEs are most consistent with being of cumulate origin formed at earlier stages of the same magmatic system that produced the QMS adakitic granodiorite. Subsequent replenishment of adakitic magmas could have disturbed the cumulate piles as "MMEs" dispersed in the adakitic granodiorite host during emplacement. The geochemical data and petrogenetic modeling of trace elements suggest that the QMS adakitic host granodiorite is most consistent with fractional crystallization dominated by the mineral assemblage of the MMEs. The parental magma for the QMS granodiorite is best explained as resulting from partial melting of the ocean crust together with recycled terrigenous sediments during continental collision, which may have also experienced interaction with mantle peridotite during ascent.

Keywords: Adakitic rocks; Mafic magmatic enclaves; Cumulate; Syn-collisional granodiorite; North Qilian Orogen

1. **Introduction**

"Adakite" was introduced by Defant and Drummond (1990) after the name of Adak Island in the Aleutian arc. It refers to a group of intermediate-felsic igneous rocks observed in modern oceanic and continental arcs genetically associated with seafloor subduction. They are characterized by high Sr, light rare earth elements (REEs), Sr/Y (>40) and La/Yb (>20), low Y and heavy REEs, and lack of obvious Eu anomalies. It was initially considered that adakites were derived by partial melting of young (≤ 25Myrs) and warm subducting/subducted ocean crust in subduction zones (Defant and Drummond, 1990). The origin of adakite has since been one of the most popular subjects of research in igneous petrology due to its use for tectonic finger-printing (see Castillo, 2006, 2012), yet recent studies have shown that adakite or rocks with adakitic compositions can be produced in various ways and in different settings (Castillo et al., 1999; Xu et al., 2002; Chung et al., 2003, 2005; Wang et al., 2005, 2007; Macpherson et al., 2006; RodrIguez et al., 2007; Streck et al., 2007; He et al., 2013; Chen et al., 2013a; Song et al., 2014a). Because adakite is defined on the basis of certain trace element characteristics as detailed above, geochemistry in combination with experimental geochemistry has been widely used to discuss the petrogenesis of adakites and adakitic rocks (e.g., Defant and Drummond, 1990; Sen and Dunn, 1994; Castillo et al., 1999; Xu et al., 2002; Wang et al., 2005; Xiong et al., 2005; Castillo, 2006, 2012). However, a petrological approach is essential for petrological problems and is expected to offer insights into the petrogenesis of adakites and adakitic rocks. Indeed, mafic magmatic enclaves (MMEs) hosted in adakitic rocks have been recently recognized, and the processes of the MME formation may offer a fresh perspective on the petrogenesis of the adakitic host (e.g., RodrIguez et al., 2007; Chen et al., 2013b).

In this paper, we report our petrological, mineralogical and geochemical analyses and

63 trace-element modeling on an MME-bearing adakitic pluton well exposed in the eastern section of the
64 North Qilian orogenic belt (NQOB) (Fig. 1a). This pluton was previously studied using the "standard"
65 geochemical method with the MMEs being overlooked (e.g., Wang et al., 2006a; Tseng et al., 2009; Yu
66 et al., 2015). Here we present a simple but effective model of fractional crystallization to successfully
67 address both the origin of MMEs and their host adakitic granodiorite.

68 **2. Geological setting**

69 The NW-SE-trending NQOB is located between the Alashan Block to the northeast and the Qilian
70 Block to the southwest, and is offset to the northwest by the Altyn-Tagh Fault (Fig.1a). It is made up of
71 Early Paleozoic subduction-zone complexes including ophiolitic melanges, blueschists and eclogites,
72 Silurian flysch formations, Devonian molasse, and Carboniferous to Triassic sedimentary cover
73 sequences (Fig. 1a) (Song et al., 2007, 2013; Zhang et al., 2007). It is composed of three subunits, i.e.,
74 (1) the southern ophiolite belt, (2) the middle arc magmatic belt and (3) the northern back-arc basin
75 ophiolite-volcanic belt (Fig. 1a) (Song et al., 2007, 2013; Zhang et al., 2007; Chen et al., 2014). It is
76 generally accepted that the NQOB is an Early Paleozoic suture zone, which records a long tectonic
77 history from seafloor spreading/subduction to the ultimate continental collision and mountain-building
78 (see Song et al., 2013). The Qumushan (QMS) pluton we studied is about 60km^2 in outcrop located in
79 the eastern section of the NQOB. It lies approximately 10 km southeast of the Baojishan (BJS) pluton
80 (Fig.1b). The QMS pluton intruded the Ordovician sedimentary and metamorphic rocks of Yingou
81 group (Fig.1b). MMEs are widespread in the host granodiorite (Fig. 2a).

3. Analytical methods

3.1. Zircon U–Pb ages

Zircons were separated by using combined methods of heavy liquid and magnetic techniques before hand-picking under a binocular microscope. The selected zircons were set in an epoxy mount that was polished to expose zircon interiors. Cathodoluminescence (CL) images were taken at China University of Geosciences in Wuhan (CUGW) to examine the internal structure of individual zircon grains. The zircon U-Pb dating was done using LA-ICP-MS at China University of Geosciences in Beijing (CUGB). The instrument consists of an Agilent 7500a quadrupole inductively coupled plasma mass spectrometry (ICP-MS) coupled with a UP-193 Solid-State laser (193 nm, New Wave Research Inc.). Laser spot size was set to be ~30μm. Zircon 91500 (Wiedenbeck et al., 1995) and a secondary standard zircon TEMORA (417 Ma) (Black et al., 2003) was used as an external standard. The analytical procedure is given in Song et al. (2010a). Isotopic ratios and element concentrations of zircons were calculated using GLITTER (ver. 4.4, Macquarie University). Common Pb correction was applied using the method of Andersen (2002). Results are given in Appendix 1.

3.2. Mineral compositions

Mineral chemistry was determined using a JXA-8100 microprobe at Chang'an University, China. The operating conditions were a 15 kV accelerating potential with a probe current of 10 nA and the electron beam diameter of 1μm. Results are given in Appendix 2 and Appendix 3.

3.3. Major and trace elements

The bulk-rock major and trace elements were analyzed using Leeman Prodigy inductively coupled

plasma-optical emission spectroscopy (ICP-OES) and Agilent-7500a inductively coupled plasma mass spectrometry (ICP-MS) at CUGB, respectively. The analytical uncertainties are generally less than 1% for most major elements with the exception of TiO_2 (~1.5%) and P_2O_5 (~2.0%). The loss on ignition was measured by placing 1 g of sample powder in the furnace at 1000°C for several hours before cooling in a desiccator and reweighting. The analytical details are given in Song et al. (2010b). The data are presented in Appendix 4.

3.4. Whole-rock Sr-Nd-Hf isotopes

Whole-rock Sr-Nd-Hf isotopic analyses were done in Guangzhou Institute of Geochemistry, Chinese Academy of Sciences (GIG-CAS). The rock powders were digested and dissolved in HF-HNO_3 acid mixtures and dried on a hot-plate. Sr-Nd-Hf fractions were separated using small Sr Spec resin columns to obtain Sr and Nd-Hf bearing fractions. Sr isotopic compositions were determined using a Neptune Plus multi-collector ICP-MS (MC-ICP-MS) following Ma et al. (2013a). Nd fractions were then separated by passing through cation columns followed by HDEHP columns. Separation of Hf from the matrix and rare earth elements was carried out using a combined method of Eichrom RE and HDEHP columns. Nd and Hf isotopic compositions were determined using a Micromass Isoprobe MC-ICP-MS following Li et al. (2009) and Ma et al. (2013b). Repeated analysis of NBS-987 run during the same period of sample analysis gave $^{87}Sr/^{86}Sr$=0.710283±27 (2σ, n=13). Repeated analysis of BHVO-2 and JB-3 during the same period of sample analysis yielded $^{143}Nd/^{144}Nd$ 0.512977±14 (2σ, n=8) and 0.513053±18 (2σ, n=13), respectively. During the course of this study, the mean $^{176}Hf/^{177}Hf$ ratios for BHVO-2 and JB-3 are respectively 0.283099±15 (2σ, n = 13) and 0.283216 ± 15 (2σ, n=6). All measured $^{87}Sr/^{86}Sr$, $^{143}Nd/^{144}Nd$ and $^{176}Hf/^{177}Hf$ ratios were normalized to $^{86}Sr/^{88}Sr$

= 0.1194, $^{146}Nd/^{144}Nd$ =0.7219 and $^{179}Hf/^{177}Hf$ = 0.7325, respectively. The USGS rock standards JB-3 and BHVO-2 run with our samples give values consistent with the reported reference values (GeoREM, http://georem.mpch-mainz.gwdg.de/). Results are given in Appendix 5.

4. Petrography and mineral chemistry

4.1. Granodiorite

The QMS pluton is of granodioritic composition with a mineral assemblage of plagioclase (45 vol. %–50 vol. %), quartz (35 vol. %-42 vol. %), amphibole (3 vol. %-10 vol. %), biotite (2 vol. %-10 vol. %), minor K-feldspar, and accessory minerals such as apatite, sphene, zircon and Fe-Ti oxides (Fig. 2d). Plagioclase crystals are euhedral to subhedral, and are of oligoclase composition with An_{12-24} (Fig. 3a). Zoned-plagioclase crystals display normal zoning with more anorthitic cores rimmed by less calcic compositions (Fig. 3a). Amphibole is always present as euhedral to subhedral crystals despite the variably small abundances (Fig. 2d). Amphibole grains are usually homogeneous and rarely display disequilibrium textures. Amphiboles from the host granodiorite can be classified as edenite (Appendix 3, Fig. 4) following Leake et al. (1997). They have medium SiO_2, and low TiO_2 (0.37-1.24 wt. %), Na_2O (0.87-1.48 wt. %) and K_2O (0.29-1.69 wt. %).

4.2. Mafic magmatic enclave

MMEs are abundant in the QMS pluton (Fig. 2a), showing varying shape and size from centimeters to tens of centimeters in diameter (Fig. 2a). They differ from the host by having finer grain-size (Figs. 2a-c), but have the same mineralogy albeit with greater mafic modes (e.g., 35-50 vol.% amphibole, 5-15 vol.% biotite, 40-50 vol.% plagioclase, minor quartz, K-feldspar, along with accessory

minerals such as apatite, sphene, zircon and Fe-Ti oxides), thus giving a dioritic bulk composition. Plagioclase mostly occurs as subhedral grains with compositions similar to those in the host granodiorite. Zoned-plagioclase in the MMEs shows a compositional continuum with cores slightly more anorthitic than the rims (Fig. 3b). Amphibole in the MMEs is compositionally identical to that in the host granodiorite (Fig. 4). Biotite is yellow brown with subhedral to euhedral forms. The MMEs show no chilled margins nor textures of crystal resorption or reactive overgrowth. These rocks mainly exhibit porphyritic-like textures.

5. Results

5.1. Zircon U–Pb ages

Four samples (2 host-MME pairs) were chosen for dating. In CL images (Figs. 5a, c), zircons from the host granodiorites (QMS12-04host and QMS12-10host) are transparent, colorless, and mostly euhedral columnar crystals of varying size (~150-300μm long with length/width ratio of 1:1-3:1) with well-developed oscillatory zoning. The zircons have varying U (~ 28-386 ppm) and Th (~ 69-423 ppm) with Th/U ratio of 0.3-1.4. All these characteristics are consistent with the zircons being of magmatic origin (Hoskin and Schaltegger, 2003). After excluding discordant ages, zircons from the two host granodiorite samples yielded weighted mean $^{206}Pb/^{238}U$ ages of 429.7 ±2.5 Ma (1σ, MSWD=0.15, n=23) and 431.5 ±2.6 Ma (1σ, MSWD=0.19, n=20), respectively (Figs. 5a, c), representing the crystallization age (~430 Ma) of the host granodiorite. These age data are in agreement with those in the literature (Tseng et al., 2009; Yu et al., 2015).

Zircons from the MMEs (QMS12-04MME and QMS12-10MME) show similar optical properties to those in the host with oscillatory zoning (Figs. 5b, d) and varying size (~150-200μm in length

length/width ratio of ~ 1:1-2:1). They have varying Th (27-548 ppm), U (50-541 ppm), and Th/U (0.1-2.4). They are also of magmatic origin. Zircons in the 2 MMEs yielded the same weighted mean ages as zircons in the host within error, i.e. 429.6 ±2.8 Ma (1σ, MSWD=0.48, n=18) and 431.2 ±2.8 Ma (1σ, MSWD=0.2, n=19), respectively (Figs. 5b, d).

5.2. Major and trace elements

Eleven representative QMS granodiorite samples and their hosted MMEs (including 5 host-MME pairs) were analyzed for whole-rock major and trace element compositions (Appendix 4). The granodiorite samples have high SiO_2 (64.37-65.49 wt.%), Al_2O_3 (16.09-17.61 wt.%), Na_2O (4.86-5.12 wt.%) and Na_2O/K_2O (2.11-3.82) with medium total alkalis (Na_2O+K_2O = 6.46-7.25 wt.%), and plot in the granodiorite field (Fig. 6a). They have low $Fe_2O_3^T$ (2.86-3.43 wt.%), MgO (2.14-2.60 wt.%) and CaO (3.60-4.10 wt.%). They are calc-alkaline (Fig. 6b) and metaluminous to weakly peraluminous (A/CNK= 0.93 to 1.03) (Fig. 6c), which is typical for I-type granitoids (Chappell and White, 1992). In contrast, the MMEs plot in the fields of diorite, monzodiorite and monzonite (Fig. 6a). They are compositionally high-K calc-alkaline to calc-alkaline (Fig. 6b), and metaluminous with A/CNK ranging from 0.74 to 0.84 (Fig. 6c). They have lower SiO_2 (52.06-58.59 wt.%), higher $Fe_2O_3^T$ (6.12-8.50 wt.%), MgO (5.09-7.22 wt.%), CaO (4.99-6.57 wt.%), P_2O_5 (0.49-1.01 wt.%), and slightly higher $Mg^{\#}$ (0.63-0.68; $Mg^{\#}=Mg/[Mg+Fe^{2+}]$) than the host granodiorites.

In the chondrite-normalized REE diagram, the QMS granodiorite samples are characterized by a relatively flat heavy REE (HREE) pattern ($[Dy/Yb]_N$ = 1.32-1.54), slightly negative to positive Eu anomalies (Eu/Eu*=0.88-1.13), and lower total REE contents (ΣREE=76-134 ppm) than the hosted MMEs. The REE patterns of the QMS granodiorites are similar to the field defined by the BJS

granodiorites (cf. Chen et al., 2015) (Fig. 7), but display greater light REE (LREE) enrichment ($[La/Sm]_N$ = 4.77-5.36). The MMEs show similar REE patterns, but have significantly higher HREEs (Fig. 7a, b), which is consistent with greater modes of REE-enriched minerals (e.g., amphibole, apatite and zircon). They have negative Eu anomalies (Eu/Eu*=0.6-0.8).

In the multi-element spider diagram (Fig. 8), the host granodiorite and MMEs both show enrichment of large ion lithophile elements (LILE, e.g., P, K, Pb) and depletion in high field strength elements (HFSE, e.g., Nb, Ta and Ti). Sr appears to have a positive anomaly in the host (Sr/Sr*=1.66-2.96), but varying anomalies for the MMEs (Sr/Sr*=0.5-1.19). In particular, compared to the BJS granodiorites (Chen et al., 2015), the QMS granodiorite samples have adakitic signatures with high Sr/Y and La/Yb ratios, and lower Y and Yb abundances, thus plotting in the adakite fields in the discrimination diagrams (Figs. 9a-b), while most MMEs plot in the normal arc rock field.

5.3. Sr-Nd-Hf isotopic geochemistry

Whole-rock Sr-Nd-Hf isotopic compositions for the MMEs and their host granodiorite are given in Appendix 5. The initial $^{87}Sr/^{86}Sr_{(t)}$, $\varepsilon_{Nd}(t)$ and $\varepsilon_{Hf}(t)$ values are calculated at 430 Ma using the zircon age data (see Fig. 5 above). On the plots of $^{87}Sr/^{86}Sr_{(t)}$, $\varepsilon_{Nd}(t)$ and $\varepsilon_{Hf}(t)$ against SiO_2 (Figs. 10j-l), both host granodiorite and MME samples are indistinguishable and overlapping within a narrow range (also see Appendix 5).

On SiO_2-variation diagrams (Fig. 10), the MMEs and their host granodiorite define linear trends for most elements (e.g., TiO_2, $Fe_2O_3^T$, MnO, MgO, CaO, P_2O_5, Eu and Hf abundances) and trace element ratio (e.g., Hf/Sm) (Figs. 10a-i), but show no correlations of initial Sr, Nd, and Hf isotopic compositions with SiO_2 (Figs. 10j-l).

6. Discussion

6.1. Petrogenesis of the mafic magmatic enclaves

Several models have been proposed for the origin of MMEs in the literature, including foreign xenoliths (usually country rocks; e.g., Vernon, 1983; Xu et al., 2006), refractory and residual phase assemblages derived from granitoid sources (e.g., the restite model; Chappell et al., 1987; Chappell and White, 1991), chilled material or cumulate of early-formed co-genetic crystals (e.g., Dodge and Kistler, 1990; Dahlquist, 2002; Donaire et al., 2005; RodrIguez et al., 2007; Niu et al., 2013; Huang et al., 2014; Chen et al., 2015), and basaltic melt material incompletely digested and homogenized during a magma mixing process (e.g., Vernon, 1983; Didier, 1987; Castro et al., 1990; Dorais et al., 1990; Barbarin and Didier, 1991; Chappell and White, 1991; Barbarin, 2005; Chen et al., 2009a, 2013b; Wang et al., 2013). We critically evaluate these interpretations below.

6.1.1. Textural and chemical relationships of the MMEs and their hosts

The textural and chemical relationships of the QMS MMEs and their host granodiorite concur with the findings for the BJS pluton (Chen et al., 2015), and are summarized as follows: (1) the MMEs in the QMS granodiorites are ellipsoidal, or elongate, show no chilled margins，no textures of crystal resorption nor reactive overgrowth, but exhibit typical magmatic texture (Figs. 2a-f); (2) they have a mineral assemblage identical to, and more mafic phases than, their host granodiorite (Figs. 2c-f); (3) they have mineral compositions (e.g., amphibole and plagioclase) identical to those of their host (Fig. 3-4); (4) they have the same age (~430 Ma) as their host (Fig. 5); (5) their different major and trace element abundances from their hosts are controlled largely by mineral modal proportions, i.e., MMEs

have greater modes of REE-enriched minerals (amphibole, apatite and zircon) and thus have higher MgO, Fe_2O_3, CaO and trace elements easily incorporated into these phases (e.g., TiO_2, P_2O_5, Hf and HREEs) (Figs. 10a-i); and (6) more importantly, they have overlapping and indistinguishable Sr-Nd-Hf isotopes with their host granodiorite (Figs. 10j-l).

Any successful models for the origin of MMEs must be consistent with these observations. Models for MMEs as foreign xenoliths from country rocks (e.g., Xu et al., 2006) can be readily rejected, as there is no evidence of reaction textures for the MMEs. Likewise, the identical age (~430 Ma) of the MMEs and their host as well as the magmatic textures, constitute a strong argument against the restite origin (e.g., Chappell et al., 1987). In addition, the MMEs do not contain peraluminous minerals and their metaluminous composition (Fig. 6c) also excludes their derivation by melting of peraluminous restites (Barbarin, 2005). Therefore, the most straightforward interpretation is that the MMEs and their hosts formed as different products of a common magmatic system.

6.1.2. Assessing the origin of magma mixing

Similar observations mentioned above between the MMEs and their host granitoids have been identified first by Pabst (1928) and by many others since then. The MMEs were thus described as "autoliths", referring to "cogenetic" or part of the same system. Despite the "autoliths" nature of the MMEs with the host, this interpretation has been questioned: (1) Why are isotopic values of some MMEs intermediate between those of crustal and mantle materials (e.g., DePaolo, 1981; Barbarin, 2005)? (2) Why are the MMEs fine-grained (e.g., Barbarin and Didier, 1991)? Because of these questions, a model of magma mixing between mantle-derived mafic magma and crust-derived felsic magma was proposed to address the above issues: (1) the intermediate isotopic values of the MMEs

247 were commonly interpreted as the result of magma mixing between a mantle-derived mafic magma and
248 a crust-derived felsic magma, because a mafic magma derived from upper mantle provides not only
249 material but also the heat necessary for melting and subsequently mixing with the crustal rocks (e.g.,
250 Barbarin, 2005); (2) the fine-grained MMEs were interpreted as due to quenching against host felsic
251 magmas (e.g., Vernon, 1984; Furman and Spera, 1985; Barbarin, 2005), owing to their higher liquidus
252 and solidus temperatures compared to felsic magmas. As a result, the magma mixing model has been
253 the most popular interpretation for the petrogenesis of the MMEs (see critical review by Niu et al.,
254 2013).

255 Actually, there are many compelling lines of evidence for magma mixing in many granitoids,
256 especially (1) where a clear isotopic contrast exists between the MMEs and the hosts (e.g., Holden et
257 al., 1987; Chen et al., 2009b; Liu et al., 2013); and (or) (2) where disequilibrium features occur in the
258 MMEs, e.g., complex zoning of clinopyroxene crystals that have distinctly low-MgO cores surrounded
259 by high-MgO rims (e.g., Chen et al., 2013a; Wang et al., 2013), or resorption textures or reversed
260 zoning of plagioclase (Pietranik et al., 2006; Chen et al., 2009a, 2009b). In the case of our study,
261 however, none of the above has been observed. Instead, many lines of evidence argue against the
262 magma mixing origin.

263 First, the MMEs and their host granodiorites in the QMS pluton have overlapping and
264 indistinguishable Sr-Nd-Hf isotopes (vs. isotopic contrast in magma mixing model). In spite of this,
265 some authors would still argue that the isotopic and mineral compositional similarity between the
266 enclaves and the host could result from chemical and isotopic equilibration during magma mixing, (e.g.,
267 Dorais et al., 1990; Barbarin, 2005; Chen et al., 2009b; Zhang et al., 2010) using some experimental
268 interpretations that isotopic equilibration is generally more easily achieved than chemical equilibration

(Lesher, 1990). However, we emphasize that it is physically unlikely that isotopes become homogenized whereas major and trace elements are not (Niu et al., 2013), because isotopes are "carried" by the relevant chemical elements and isotopic diffusion cannot take place without the diffusion of the "carrying" elements (Chen et al., 2015). In fact, there are two forceful arguments against thermal and chemical equilibration: (1) the MMEs exhibit no textures of crystal resorption or reactive overgrowth (Figs. 2b-c), and (2) plagioclase in the MMEs and their host granodiorite shows no compositional or textural disequilibrium (Fig. 3). In addition, although the fine-grained texture of the MMEs could be interpreted as resulting from quenching in the magma mixing model, quenching of the mafic magma would lead to a significantly high viscosity contrast between the solidified enclaves and the felsic host magma, thereby inhibiting deformation, mechanical mixing (Caricchi et al., 2012; Farner et al., 2014) and isotope homogenization between the MMEs and the host.

Second, strongly correlated variations between major and trace elements (Figs. 10a-i) are consistent with modal mineralogy control, as the result of magma evolution (i.e., the MMEs are cumulate and the host represents residual melt) rather than mixing of two magmas with entirely different origins because magma mixing is a complex, multi-stage process in which linear trends can be disturbed (e.g., Clemens, 1989; Donaire et al., 2005; Chen et al., 2015). Moreover, the distinctive high abundances of some elements in the MMEs, such as Zr and P (Fig. 11), cannot be explained by magma mixing because these elements are controlled by the presence of accessory phases, such as zircon and apatite. As shown in Fig. 11, mantle derived basaltic magmas would have much lower Zr and P_2O_5 than in the QMS MMEs. For example, quantitative calculations by Lee and Bachmann (2014) suggested that 10-20% melting of an upper mantle with 5 ppm Zr and 0.019 wt.% P_2O_5 (equivalent to that estimated for depleted mid-ocean ridge basalt mantle), would yield primary liquids with 25-50 ppm Zr and

0.1-0.2 wt.% P_2O_5. These concentrations are much lower than in the QMS MMEs. Additionally, boninites are thought to result from partial melting of highly depleted harzburgitic mantle peridotites induced by subduction-zone slab dehydration (Niu, 2005), but they also have lower Zr and P_2O_5 contents (Fig. 11). More importantly, magma mixing between a basalt with any silicic end-member (e.g., rhyolite) would generate a mixing array (Figs. 11a-b, the dash lines) totally different from the linear trend (Figs. 11a-b, the solid lines) defined by the QMS granodiorite and their MMEs. In contrast, all of these observations are consistent with the interpretation that the MMEs represent earlier cumulate with greater amounts of zircon and apatite than their hosts (e.g., Donaire et al., 2005).

6.1.3. Formation of the mafic magmatic enclaves

The foregoing observations, illustrations and discussion leave us with the best interpretation that the MMEs represent the earlier crystallized cumulate that were later disturbed by subsequent melt replenishment and induced magma convection in the magma chamber. As illustrated in Fig. 12, when a primitive magma body is emplaced into a cold environment (e.g., developing a magma chamber) with the wall-rock having temperatures below the liquidus of the magma, magma quench and rapid crystallization are inevitable because of the thermal contrast. For an andesitic primitive magma parental to the syn-collisional granitoids (Niu et al., 2013), the first major liquidus phases would be amphibole, biotite, plagioclase and accessory minerals such as zircon and apatite, and rapid quench will facilitate abundant nucleation without between-nuclei space for rapid growth, thus resulting in the formation of fine-grained cumulate (Chen et al., 2015). This is a fundamentally important petrologic concept with which any interpretation must comply. This early formed fine-grained mafic cumulate piles (largely plastic before complete solidification) can be readily disturbed by subsequent magma replenishment

and induced convection, resulting in the dispersion of the MMEs in the host granodiorite.

6.2 Petrogenesis of QMS adakitic granodiorite

6.2.1 Implication from the MMEs

Recently, mixing of basaltic and felsic magmas was proposed for the genesis of some high-Mg and low SiO_2 adakitic rocks from Mount Shasta and the North China Craton using the presence of ubiquitous MMEs as evidence (Chen et al., 2013b) and also based on the disequilibrium petrographic characteristics in high-Mg andesites (Streck et al., 2007; Chen et al., 2013a). This interpretation could be reasonable, but it is not the case here because there is no petrographic and compositional evidence for magma mixing as elaborated above. That is, the MMEs in the QMS adakitic granodiorite are not evidence for magma mixing, but rather they are of cumulate origin without direct asthenospheric mantle participation (e.g., Dahlquist, 2002). More importantly, the MMEs comprise dominantly amphibole and plagioclase, which are common cumulate minerals of andesitic melts. If the parental melts were basaltic, the typical cumulate from such evolved basaltic melt would be gabbro dominated by clinopyroxene and plagioclase (Chen et al., 2015). It can be inferred from this important petrological concept that the parental magmas of the MMEs and their host granodiorite was mafic andesitic (Niu et al., 2013; Chen et al., 2015).

6.2.2 Assessing the model of melting of mafic lower continental crust

To date, some intra-continental high-MgO or -$Mg^{\#}$ (also high Cr and Ni contents) adakitic rocks have been considered to originate from melting of delaminated lower crust (e.g., Xu et al., 2002; Gao et al., 2004; Wang et al., 2006b). By accepting and applying this model, it has been previously interpreted

that the QMS adakitic rocks were derived from delaminated lower crust, and they subsequently interacted with mantle peridotite during ascent (Tseng et al., 2009; Yu et al., 2015). Although this model seems plausible and applicable to the QMS adakitic rocks, it has more difficulties than certainties. First, the QMS adakitic granodiorites have lower $(Dy/Yb)_N$, $(La/Yb)_N$, and distinctive low K_2O/Na_2O ratios (Fig. 13b), which are significantly different from the composition of adakitic rocks inferred to be derived from partial melting of the thickened or delaminated lower continental crust. Second, the Nd and Hf isotopic data of the QMS adakitic granodiorite indicate a significant mantle input, which is also inconsistent with those of lower continental crust origin (Fig. 14a). Finally, the existence of the Paleo-Qilian ocean is manifested by the ophiolites and eclogites in the North Qilian orogenic belt; the ocean basin started its subduction at ~520 Ma, and was eventually closed at the end of the Ordovician (~445 Ma) followed by continental collision (see Song et al., 2013). Accordingly, the coeval (~430 Ma) MMEs and their adakitic host granodiorite of the QMS pluton are best interpreted as a magmatic response to the collision between the Qilian-Qaidam block and Alashan block, thereby being contrary to the environment of crustal extension required by a delaminated lower crustal origin. In fact, continuous lithosphere extension and delamination in the NQOB occurred at <400 Ma, which resulted in strong magmatic activity and formed a number of diorite-granodiorite-granite plutons with ages of ~400–360 Ma (Song et al., 2013, 2014b).

6.2.3 A fractional crystallization model for the petrogenesis of the QMS adakitic granodiorites

An origin of adakitic rocks by fractional crystallization has been proposed in the literature. However, it should be noted that all these crystallization models require basaltic parental magmas derived from the metasomatized mantle wedge in arc settings, such as in the complex Philippine arc

353 (Castillo et al., 1999; Macpherson et al., 2006) and Ecuadorian Andes (Chiaradia et al., 2004). It is
354 important to note that our crystallization model differs from the basaltic magma crystallization model
355 of arc magmas in the literature.

356 In our model, the magmas parental to the MMEs and their host granodiorite are the same mafic
357 andesitic magmas in a syn-collisional setting, rather than basaltic magmas in an arc setting of active
358 seafloor subduction advocated in the literature (e.g., Macpherson et al., 2006). That is, the QMS
359 adakitic granodiorites are products of fractional crystallization dominated by the mineral assemblage
360 indicated by the MMEs from mafic andesitic magmas. We can further consider two fractional
361 crystallization models to elucidate the effect of crystallization of the observed mineralogy on trace
362 elements using closed-system Rayleigh fractionation equation: (1) Model A, in reasonable agreement
363 with observed mineral proportions of the MMEs, 50% amphibole, 40% plagioclase, 7.52% biotite, 2.2%
364 apatite, 0.2% zircon and 0.03% sphene; (2) Model B, which incorporates fractionation of garnet, 50%
365 amphibole, 40% plagioclase, 7.6% biotite, 2.4% garnet. The partition coefficients used in the
366 calculations are for intermediate-felsic magmas (Appendix 6). For convenience (see below), the
367 assumed parental magma (Appendix 6) is very similar to the bulk continental crust (BCC) composition
368 (Rudnick and Gao, 2003) (Fig. 15), which is the same as the ~ 60 Ma Linzizong andesite in southern
369 Tibet (Mo et al., 2008; Niu et al., 2013), in terms of major and trace element abundances.

370 Notably, removal of garnet would yield a smooth decrease of LREE-to-HREE pattern (Richards
371 and Kerrich, 2007) with elevated $(Dy/Yb)_N$ and $(La/Yb)_N$ in the evolving melt (Fig. 9c). However, the
372 $(Dy/Yb)_N$ ratio in the QMS adakitic granodiorites remain constant with increasing $(La/Yb)_N$ (Fig. 9c),
373 which indicate that the effect of garnet fractionation in generating the QMS adakitic granodiorites is
374 unimportant. Simple modal calculation of fractional crystallization using Model B indicates that the

participation of garnet is no more than 3% (Fig. 9), but the low garnet proportion in combination with a large amount of amphibole-plagioclase fractionation can hardly generate the adakitic signature shown in the QMS pluton (Figs. 9a-b). Besides, mineralogically, garnet has been observed neither in the QMS MMEs and their host adakitic granodiorite, nor in the coeval igneous rocks in the eastern section of the NQOB. In addition, our preferred source for the QMS MMEs and their host adakitic granodiorite is partial melting of the ocean crust at amphibolite facies conditions (＜40km) (Mo et al., 2008; Niu and O'Hara, 2009; Niu et al., 2013) (see below), rather than the presence of garnet as a residual phase at garnet amphibolite or eclogite conditions.

It is also impossible to generate QMS adakitic granodiorites by fractionation of amphibole-plagioclase alone, because they trend to produce concave-upwards patterns between the MREE and HREE and lead to decreasing $(Dy/Yb)_N$ with increasing $(La/Yb)_N$ (Fig. 9c), owing to the affinity of calcic amphiboles for MREEs over the HREEs (Klein et al., 1997). Additionally, removal of amphibole-plagioclase would result in negative Eu anomalies in the residual melts, which is inconsistent with QMS adakitic granodiorites (Fig. 9d). In the case of our study, we emphasize that the widespread accessory minerals such as zircons and apatites in both QMS host adakitic granodiorite and particularly their cumulate MMEs played a significant role in generating QMS adakitic granodiorites. For example, zircon fractionation would increase $(Dy/Yb)_N$ (Fig. 9c) and the La/Yb and Sr/Y ratios of residue magmas (Figs. 9a-b), because $Kd_{zircon}^{Dy/Yb} = 0.140$, and $Kd_{zircon}^{La/Yb} = 0.005$ (Bea et al., 1994). Apatite fractionation can also increase the Sr/Y ratio (Figs. 9a-b), but decrease $(Dy/Yb)_N$ (Fig. 9c). Importantly, apatite fractionation would increase Eu/Eu* (Fig. 9d), because $Kd_{\text{apatite}}^{\text{Sm}} = 46$, $Kd_{apatite}^{Eu} = 25.5$, $Kd_{apatite}^{Gd} = 43.9$ (Fujimaki et al., 1984). Note that the simple calculation of Model A (Appendix 6; Figs. 9 and 15), which involves a small proportion of zircon, apatite and sphene in

combination with amphibole, biotite and plagioclase to form the fractionation assemblage can explain the characteristics of the QMS adakitic granodiorites. Although uncertainties exist for mineral partition coefficients, our model offers insights into the petrogenesis of the adakitic granodiorite as well as the enclosed MMEs in syn-collisional environments.

6.3 Constraints on the source

As discussed above, the primary magmas parental to the MMEs and their host granodiorite are most consistent with mafic andesitic magmas of ocean crust origin during continental collision. In addition, our new data and the whole-rock Sr-Nd and zircon Hf isotopic data in the literature on the QMS pluton (Tseng et al., 2009; Yu et al., 2015) exhibit quite uniform Sr-Nd-Hf composition (Figs. 10j-l). Though the radiogenic Sr and slightly unradiogenic Nd isotopes indicate the input of crustal materials, the whole-rock ε_{Hf} (t) values (+5.5 to +8.4) of this study and the zircon ε_{Hf} (t) values (+4.2 to +7.7) in the literature (Yu et al., 2015) are indicative of significant mantle input or juvenile mafic continental crust derived from the mantle in no distant past (Zhang et al., 2015). As noted above, many adakitic rocks can be generated from the lower continental crust, but this is not applicable in our study (see above). In our case, the most likely source for the andesitic magmas with inherited mantle isotopic signatures parental to the QMS pluton is partial melting of the remaining part of the North Qilian ocean crust (Chen et al., 2015). On the other hand, contribution from continental crust is also required. This may occur in the melting region or in an evolving magma chamber rather than simple crustal level assimilation, because the Sr-Nd-Hf isotopes for the MMEs and their host granodiorites are closely similar and show a respectively narrow range of variation, and they do not show correlated variations with SiO_2 (Figs. 10j-l). Melting of recycled terrigenous sediments of upper continental crust and

418 remaining part of the North Qilian oceanic crust in the melting region is more likely (Mo et al. 2008;
419 Niu and O'Hara 2009; Chen et al., 2015).

420 In the broad context of the continental collision, the model of partial melting of the remaining part
421 of the ocean crust and the recycled terrigenous sediments has been proposed and tested by Niu and
422 co-workers in southern Tibet, East Kunlun and Qilian Orogenic Belts (e.g., Mo et al., 2008; Niu and
423 O'Hara, 2009; Niu et al., 2013; Huang et al., 2014; Chen et al., 2015; Zhang et al., 2015). In their model,
424 during collision, the underthrusting North Qilian ocean crust would subduct/underthrust slowly, tend to
425 attain thermal equilibrium with the superjacent warm active continental margin, and evolve along a
426 high T/P path in P-T space as a result of retarded subduction and enhanced heating (Appendix Fig. S1).
427 The warm hydrated ocean crust of basaltic composition and sediments of felsic composition with rather
428 similar solidi would melt together under the amphibolite facies conditions (for details see Niu et al.,
429 2013; also see Appendix Fig. S1).

430 Importantly, this model can generate andesitic magmas not only with inherited mantle
431 isotopic signatures but also compositions similar to the bulk continental crust (BCC), except for
432 notable depletion in highly compatible elements like Mg, Cr and Ni (Mo et al., 2008). This model
433 together with experimental results of melting of metabasalt and eclogite (Fig. 13a) implies that the
434 relatively high $Mg^{\#}$ (also high Cr and Ni) contents in QMS adakitic granodiorites may indeed
435 reflect melt interaction with mantle peridotite during ascent. Although magmas produced through
436 the above process lack the adakitic signature, it can be the ideal source that generates QMS
437 adakitic granodiorites through fractional crystallization dominated by mineral assemblages
438 represented by the MMEs. Note that this interpretation is consistent with binary isotope mixing
439 calculations as proposed by Chen et al. (2015) (Figs. 14a-b), and with trace element model

calculations (see above) (Figs. 9 and 15). As illustrated by these mass balance calculations, ~95% ocean crust and ~5% continental materials contribute to the source of the QMS pluton (Fig. 14), and 30%-50% fractional crystallization dominated by mineralogy and modes of the MMEs can lead to the highly evolved granodioritic composition of the QMS pluton with the adakitic signature (Figs. 9 and 15).

7. Conclusions

(1) The zircon U-Pb dating of the QMS pluton yields the same age (~430 Ma) for both the MMEs and their host granodiorite, which is the same as the closure time of the Qilian ocean and continental collision at ~440-420Ma.

(2) The MMEs and their host granodiorite also share the same mineralogy with indistinguishable isotopic compositions, all of which indicate that the MMEs are cumulate formed at earlier stages of the same magmatic system rather than representing mantle melt required by the popular magma mixing model.

(3) The QMS host granodiorite has adakite-like major and trace element features, including high Sr, Sr/Y and La/Yb, but low Y and Yb. By accepting our model for the petrogenesis of the MMEs, it follows that the QMS adakitic granodiorite resulted from fractional crystallization dominated by mineral assemblages represented by the MMEs.

(4) The parental magma for the QMS pluton is best explained as resulting from partial melting of the remaining part of ocean crust together with recycled terrigenous sediments during continental collision. The resulting magma may have also experienced interaction with mantle peridotite during ascent.

Acknowledgments

We thank Li Su for the assistance with whole rock major, trace elements and zircon U-Pb age analysis, Minwu Liu with electron microprobe analysis, and Jinlong Ma, Xirong Liang and Zhongyuan Ren with whole rock Sr-Nd-Hf isotope analysis. Pu Sun, Huixiang Cui and Yuxing Ma are thanked for their help with sample preparation. This work was supported by the National Natural Science Foundation of China (NSFC: 91014003, 41130314), Chinese Academy of Sciences (Innovation Grant Y42217101L) and grants from regional and local authorities (Shandong Province and City of Qingdao), two projects of Chinese Geological Survey Departments and Offices (1212011121092, 1212011220928), and supported by National Oceanography Laboratory in Qingdao.

References

Andersen, T., 2002. Correction of common lead in U-Pb analyses that do not report ^{204}Pb. Chemical Geology 192, 59-79.

Bachmann, O., Dungan, M.A., Bussy, F., 2005. Insights into shallow magmatic processes in large silicic magma bodies: the trace element record in the Fish Canyon magma body, Colorado. Contributions to Mineralogy and Petrology 149, 338-349.

Barbarin, B., 2005. Mafic magmatic enclaves and mafic rocks associated with some granitoids of the central Sierra Nevada batholith, California: nature, origin, and relations with the hosts. Lithos 80, 155-177.

Barbarin, B., Didier, J., 1991. Enclaves of the Mesozoic calc-alkaline granitoids of the Sierra Nevada Batholith, California. Enclaves and granite petrology. Elsevier, Amsterdam 135, 153.

481 Bea, F., Pereira, M., Stroh, A., 1994. Mineral/leucosome trace-element partitioning in a peraluminous
482 migmatite (a laser ablation-ICP-MS study). Chemical Geology 117, 291-312.
483 Black, L.P., Kamo, S.L., Allen, C.M., Aleinikoff, J.N., Davis, D.W., Korsch, R.J., Foudoulis, C., 2003.
484 TEMORA 1: a new zircon standard for Phanerozoic U–Pb geochronology. Chemical Geology 200,
485 155-170.
486 Caricchi, L., Annen, C., Rust, A., Blundy, J., 2012. Insights into the mechanisms and timescales of
487 pluton assembly from deformation patterns of mafic enclaves. Journal of Geophysical Research:
488 Solid Earth (1978–2012) 117.
489 Castillo, P.R., 2006. An overview of adakite petrogenesis. Chinese Science Bulletin 51, 257-268.
490 Castillo, P.R., 2012. Adakite petrogenesis. Lithos 134-135, 304-316.
491 Castillo, P.R., Janney, P.E., Solidum, R.U., 1999. Petrology and geochemistry of Camiguin Island,
492 southern Philippines: insights to the source of adakites and other lavas in a complex arc setting.
493 Contributions to Mineralogy and Petrology 134, 33-51.
494 Castro, A., Moreno‐Ventas, I., De la Rosa, J., 1990. Microgranular enclaves as indicators of
495 hybridization processes in granitoid rocks, Hercynian Belt, Spain. Geological Journal 25, 391-404.
496 Chappell, B., White, A., 1991. Restite enclaves and the restite model, Enclaves and granite petrology.
497 Elsevier Amsterdam, pp. 479-492.
498 Chappell, B., White, A., 1992. I-and S-type granites in the Lachlan Fold Belt. Geological Society of
499 America Special Papers 272, 1-26.
500 Chappell, B., White, A., Wyborn, D., 1987. The importance of residual source material (restite) in
501 granite petrogenesis. Journal of Petrology 28, 1111-1138.
502 Chen, B., He, J., Ma, X., 2009a. Petrogenesis of mafic enclaves from the north Taihang Yanshanian

503 intermediate to felsic plutons: Evidence from petrological, geochemical, and zircon Hf-O isotopic
504 data. Science in China Series D: Earth Sciences 52, 1331-1344.
505 Chen, B., Chen, Z.C., Jahn, B.M., 2009b. Origin of mafic enclaves from the Taihang Mesozoic orogen,
506 north China craton. Lithos 110, 343-358.
507 Chen, B., Jahn, B.M., Suzuki, K., 2013a. Petrological and Nd-Sr-Os isotopic constraints on the origin
508 of high-Mg adakitic rocks from the North China Craton: Tectonic implications. Geology 41,
509 91-94.
510 Chen, B., Chen, C., He, J., Liu, A., 2013b. Origin of Mesozoic high-Mg adakitic rocks from
511 northeastern China: Petrological and Nd-Sr-Os isotopic constraints. Chinese Science Bulletin 58,
512 1941-1953.
513 Chen, S., Niu, Y., Sun, W., Zhang, Y., Li, J., Guo, P., Sun, P., 2015. On the origin of mafic magmatic
514 enclaves (MMEs) in syn-collisional granitoids: evidence from the Baojishan pluton in the North
515 Qilian Orogen, China. Mineralogy and Petrology 109, 577-596.
516 Chen, Y., Song, S., Niu, Y., Wei, C., 2014. Melting of continental crust during subduction initiation: A
517 case study from the Chaidanuo peraluminous granite in the North Qilian suture zone. Geochimica
518 et Cosmochimica Acta 132, 311-336.
519 Chiaradia, M., Fontbote, L., Beate, B., 2004. Cenozoic continental arc magmatism and associated
520 mineralization in Ecuador. Mineralium Deposita 39, 204-222.
521 Chung, S.L., Liu, D., Ji, J., Chu, M. F., Lee, H.Y., Wen, D.J., Lo, C.H., Lee, T.Y., Qian, Q., Zhang, Q.,
522 2003. Adakites from continental collision zones: Melting of thickened lower crust beneath
523 southern Tibet. Geology 31, 1021.
524 Chung, S.L., Chu, M.F., Zhang, Y., Xie, Y., Lo, C.H., Lee, T.Y., Lan, C.Y., Li, X., Zhang, Q., Wang, Y.,

525 2005. Tibetan tectonic evolution inferred from spatial and temporal variations in post-collisional
526 magmatism. Earth-Science Reviews 68, 173-196.
527 Clemens, J., 1989. The importance of residual source material (restite) in granite petrogenesis: a
528 comment. Journal of Petrology 30, 1313-1316.
529 Dahlquist, J., 2002. Mafic microgranular enclaves: early segregation from metaluminous magma
530 (Sierra de Chepes), Pampean Ranges, NW Argentina. Journal of South American Earth Sciences
531 15, 643-655.
532 Defant, M.J., Drummond, M.S., 1990. Derivation of some modern arc magmas by melting of young
533 subducted lithosphere. Nature 347, 662-665.
534 DePaolo, D.J., 1981. A neodymium and strontium isotopic study of the Mesozoic calc-alkaline granitic
535 batholiths of the Sierra Nevada and Peninsular Ranges, California. Journal of Geophysical
536 Research 86, 10470.
537 Didier, J., 1987. Contribution of enclave studies to the understanding of origin and evolution of granitic
538 magmas. Geologische Rundschau 76, 41-50.
539 Dodge, F.C.W., Kistler, R.W., 1990. Some additional observations on inclusions in the granitic rocks of
540 the Sierra Nevada. Journal of Geophysical Research 95, 17841.
541 Donaire, T., Pascual, E., Pin, C., Duthou, J.L., 2005. Microgranular enclaves as evidence of rapid
542 cooling in granitoid rocks: the case of the Los Pedroches granodiorite, Iberian Massif, Spain.
543 Contributions to Mineralogy and Petrology 149, 247-265.
544 Dorais, M.J., Whitney, J.A., Roden, M.F., 1990. Origin of mafic enclaves in the Dinkey Creek pluton,
545 central Sierra Nevada batholith, California. Journal of Petrology 31, 853-881.
546 Ewart, A., Griffin, W., 1994. Application of proton-microprobe data to trace-element partitioning in

volcanic rocks. Chemical Geology 117, 251-284.

Farner, M.J., Lee, C.T.A., Putirka, K.D., 2014. Mafic–felsic magma mixing limited by reactive processes: A case study of biotite-rich rinds on mafic enclaves. Earth and Planetary Science Letters 393, 49-59.

Fujimaki, H., Tatsumoto, M., Aoki, K.I., 1984. Partition coefficients of Hf, Zr, and ree between phenocrysts and groundmasses. Journal of Geophysical Research 89, B662.

Furman, T., Spera, F.J., 1985. Co-mingling of acid and basic magma with implications for the origin of mafic I-type xenoliths: field and petrochemical relations of an unusual dike complex at Eagle Lake, Sequoia National Park, California, USA. Journal of Volcanology and Geothermal Research 24, 151-178.

Gao, S., Rudnick, R.L., Yuan, H.L., Liu, X.M., Liu, Y.S., Xu, W.L., Ling, W.L., Ayers, J., Wang, X.C., Wang, Q.H., 2004. Recycling lower continental crust in the North China Craton. Nature 432, 892–897.

Green, T., Blundy, J., Adam, J., Yaxley, G., 2000. SIMS determination of trace element partition coefficients between garnet, clinopyroxene and hydrous basaltic liquids at 2–7.5 GPa and 1080–1200 C. Lithos 53, 165-187.

He, Y., Li, S., Hoefs, J., Kleinhanns, I.C., 2013. Sr-Nd-Pb isotopic compositions of Early Cretaceous granitoids from the Dabie orogen: Constraints on the recycled lower continental crust. Lithos 156-159, 204-217.

Holden, P., Halliday, A., Stephens, W., 1987. Neodymium and strontium isotope content of microdiorite enclaves points to mantle input to granitoid production. Nature 330, 53-56.

Hoskin, P.W., Schaltegger, U., 2003. The composition of zircon and igneous and metamorphic

569 petrogenesis. Reviews in mineralogy and geochemistry 53, 27-62.
570 Huang, H., Niu, Y., Nowell, G., Zhao, Z., Yu, X., Zhu, D.C., Mo, X., Ding, S., 2014. Geochemical
571 constraints on the petrogenesis of granitoids in the East Kunlun Orogenic belt, northern Tibetan
572 Plateau: Implications for continental crust growth through syn-collisional felsic magmatism.
573 Chemical Geology 370, 1-18.
574 Irving, A.J., Frey, F.A., 1984. Trace element abundances in megacrysts and their host basalts:
575 constraints on partition coefficients and megacryst genesis. Geochimica et Cosmochimica Acta 48,
576 1201-1221.
577 Klein, M., Stosch, H.G., Seck, H., 1997. Partitioning of high field-strength and rare-earth elements
578 between amphibole and quartz-dioritic to tonalitic melts: an experimental study. Chemical
579 Geology 138, 257-271.
580 Le Maitre, R.W., Bateman, P., Dudek, A., Keller, J., Lameyre, J., Le Bas, M., Sabine, P., Schmid, R.,
581 Sorensen, H., Streckeisen, A., 1989. A classification of igneous rocks and glossary of terms:
582 Recommendations of the International Union of Geological Sciences Subcommission on the
583 Systematics of Igneous Rocks. Blackwell Oxford.
584 Leake, B., Arps, C., Birch, W., Gilbert, M., Grice, J., Hawthorne, F., Kato, A., Kisch, H., Krivovichev,
585 V., Linthout, K., 1997. Nomenclature of Amphiboles: Report of the Subcom mittee on Amphiboles
586 of the International Mineralogi cal Association, Commission on New Minerals and Mineral
587 Names. The Canadian Mineralogist 35, 219-246.
588 Lee, C.T., Bachmann, O., 2014. How important is the role of crystal fractionation in making
589 intermediate magmas? Insights from Zr and P systematics. Earth and Planetary Science Letters
590 393, 266-274.

591 Lesher, C.E., 1990. Decoupling of chemical and isotopic exchange during magma mixing. Nature 344,
592 235-237.
593 Li, X.H., Li, W.X., Li, Z.X., Lo, C.H., Wang, J., Ye, M.F., Yang, Y.H., 2009. Amalgamation between
594 the Yangtze and Cathaysia Blocks in South China: Constraints from SHRIMP U–Pb zircon ages,
595 geochemistry and Nd–Hf isotopes of the Shuangxiwu volcanic rocks. Precambrian Research 174,
596 117-128.
597 Liu, L., Qiu, J.S., Li, Z., 2013. Origin of mafic microgranular enclaves (MMEs) and their host quartz
598 monzonites from the Muchen pluton in Zhejiang Province, Southeast China: Implications for
599 magma mixing and crust–mantle interaction. Lithos 160-161, 145-163.
600 Ma, J., Wei, G., Liu, Y., Ren, Z., Xu, Y., Yang, Y., 2013a. Precise measurement of stable (δ $^{88}/^{86}$Sr) and
601 radiogenic ($^{87}Sr/^{86}Sr$) strontium isotope ratios in geological standard reference materials using
602 MC-ICP-MS. Chinese Science Bulletin 58, 3111-3118.
603 Ma, J., Wei, G., Liu, Y., Ren, Z., Xu, Y., Yang, Y., 2013b. Precise measurement of stable neodymium
604 isotopes of geological materials by using MC-ICP-MS. Journal of Analytical Atomic Spectrometry
605 28, 1926.
606 Ma, Q., Zheng, J.P., Xu, Y.G., Griffin, W.L., Zhang, R.S., 2015. Are continental “adakites” derived
607 from thickened or foundered lower crust? Earth and Planetary Science Letters 419, 125-133.
608 Macpherson, C.G., Dreher, S.T., Thirlwall, M.F., 2006. Adakites without slab melting: High pressure
609 differentiation of island arc magma, Mindanao, the Philippines. Earth and Planetary Science
610 Letters 243, 581-593.
611 Mahood, G., Hildreth, W., 1983. Large partition coefficients for trace elements in high-silica rhyolites.
612 Geochimica et Cosmochimica Acta 47, 11-30.

Matsui, Y., Onuma, N., Nagasawa, H., Higuchi, H. and Banno, S., 1977. Crystal structure control in trace element partition between crystal and magma. Tectonics 100, 315-324.

Mo, X., Niu, Y., Dong, G., Zhao, Z., Hou, Z., Zhou, S., Ke, S., 2008. Contribution of syncollisional felsic magmatism to continental crust growth: A case study of the Paleogene Linzizong volcanic Succession in southern Tibet. Chemical Geology 250, 49-67.

Nash, W., Crecraft, H., 1985. Partition coefficients for trace elements in silicic magmas. Geochimica et Cosmochimica Acta 49, 2309-2322.

Niu, Y., Batiza, R., 1997. Trace element evidence from seamounts for recycled oceanic crust in the Eastern Pacific mantle. Earth and Planetary Science Letters 148, 471-483.

Niu, Y., Regelous, M., Wendt, I.J., Batiza, R., O'Hara, M.J., 2002. Geochemistry of near-EPR seamounts: importance of source vs. process and the origin of enriched mantle component. Earth and Planetary Science Letters 199, 327-345.

Niu, Y., O'Hara, M.J., 2003. Origin of ocean island basalts: A new perspective from petrology, geochemistry, and mineral physics considerations. Journal of Geophysical Research: Solid Earth (1978–2012) 108.

Niu, Y., 2005. Generation and evolution of basaltic magmas: some basic concepts and a new view on the origin of Mesozoic–Cenozoic basaltic volcanism in eastern China. Geological Journal of China Universities 11, 9-46.

Niu, Y., O'Hara, M.J., 2009. MORB mantle hosts the missing Eu (Sr, Nb, Ta and Ti) in the continental crust: New perspectives on crustal growth, crust–mantle differentiation and chemical structure of oceanic upper mantle. Lithos 112, 1-17.

Niu, Y., Zhao, Z., Zhu, D.C., Mo, X., 2013. Continental collision zones are primary sites for net

635 continental crust growth — A testable hypothesis. Earth-Science Reviews 127, 96-110.
636 Pabst, A., 1928. Observations on inclusions in the granitic rocks of the Sierra Nevada. University of
637 California Publications in Geological Sciences 17, 325-386.
638 Pearce, J.A., Norry, M.J., 1979. Petrogenetic implications of Ti, Zr, Y, and Nb variations in volcanic
639 rocks. Contributions to mineralogy and petrology 69, 33-47.
640 Pietranik, A., Koepke, J., Puziewicz, J., 2006. Crystallization and resorption in plutonic plagioclase:
641 Implications on the evolution of granodiorite magma (Gęsiniec granodiorite, Strzelin Crystalline
642 Massif, SW Poland). Lithos 86, 260-280.
643 Prowatke, S., Klemme, S., 2006. Trace element partitioning between apatite and silicate melts.
644 Geochimica et Cosmochimica Acta 70, 4513-4527.
645 Qian, Q., Hermann, J., 2013. Partial melting of lower crust at 10–15 kbar: constraints on adakite and
646 TTG formation. Contributions to Mineralogy and Petrology 165, 1195-1224.
647 Rapp, R.P., Watson, E.B., 1995. Dehydration melting of metabasalt at 8–32 kbar: implications for
648 continental growth and crust-mantle recycling. Journal of Petrology 36, 891-931.
649 Richards, J.P., Kerrich, R., 2007. Special paper: adakite-like rocks: their diverse origins and
650 questionable role in metallogenesis. Economic Geology 102, 537-576.
651 RodrIguez, C., Selles, D., Dungan, M., Langmuir, C., Leeman, W., 2007. Adakitic dacites formed by
652 intracrustal crystal fractionation of water-rich parent magmas at Nevado de Longavi Volcano
653 (36.2° S; Andean Southern Volcanic Zone, Central Chile). Journal of Petrology 48, 2033-2061.
654 Ronov, A., Yaroshevsky, A., 1976. A new model for the chemical structure of the Earth's crust.
655 Geochemistry International 13, 89-121.
656 Rudnick, R., Gao, S., 2003. Composition of the continental crust. Treatise on geochemistry 3, 1-64.

657 Schnetzler, C., Philpotts, J.A., 1970. Partition coefficients of rare-earth elements between igneous
658 matrix material and rock-forming mineral phenocrysts—II. Geochimica et Cosmochimica Acta 34,
659 331-340.
660 Sen, C., Dunn, T., 1994. Dehydration melting of a basaltic composition amphibolite at 1.5 and 2.0 GPa:
661 implications for the origin of adakites. Contributions to Mineralogy and Petrology 117, 394-409.
662 Song, S., Su, L., Niu, Y., Zhang, L., Zhang, G., 2007. Petrological and geochemical constraints on the
663 origin of garnet peridotite in the North Qaidam ultrahigh-pressure metamorphic belt, northwestern
664 China. Lithos 96, 243-265.
665 Song, S., Niu, Y., Wei, C., Ji, J., Su, L., 2010a. Metamorphism, anatexis, zircon ages and tectonic
666 evolution of the Gongshan block in the northern Indochina continent—An eastern extension of the
667 Lhasa Block. Lithos 120, 327-346.
668 Song, S., Su, L., Li, X.H., Zhang, G., Niu, Y., Zhang, L., 2010b. Tracing the 850-Ma continental flood
669 basalts from a piece of subducted continental crust in the North Qaidam UHPM belt, NW China.
670 Precambrian Research 183, 805-816.
671 Song, S., Niu, Y., Su, L., Xia, X., 2013. Tectonics of the North Qilian orogen, NW China. Gondwana
672 Research 23, 1378-1401.
673 Song, S., Niu, Y., Su, L., Wei, C., Zhang, L., 2014a. Adakitic (tonalitic-trondhjemitic) magmas
674 resulting from eclogite decompression and dehydration melting during exhumation in response to
675 continental collision. Geochimica et Cosmochimica Acta 130, 42-62.
676 Song, S., Niu, Y., Su, L., Zhang, C., Zhang, L., 2014b. Continental orogenesis from ocean subduction,
677 continent collision/subduction, to orogen collapse, and orogen recycling: The example of the
678 North Qaidam UHPM belt, NW China. Earth-Science Reviews 129, 59-84.

679 Streck, M.J., Leeman, W.P., Chesley, J., 2007. High-magnesian andesite from Mount Shasta: A product
680 of magma mixing and contamination, not a primitive mantle melt. Geology 35, 351.
681 Sun, S.S., McDonough, W., 1989. Chemical and isotopic systematics of oceanic basalts: implications
682 for mantle composition and processes. Geological Society, London, Special Publications 42,
683 313-345.
684 Thomas, J., Bodnar, R., Shimizu, N., Sinha, A., 2002. Determination of zircon/melt trace element
685 partition coefficients from SIMS analysis of melt inclusions in zircon. Geochimica et
686 Cosmochimica Acta 66, 2887-2901.
687 Tseng, C.Y., Yang, H.J., Yang, H.Y., Liu, D., Wu, C., Cheng, C.K., Chen, C.H., Ker, C.M., 2009.
688 Continuity of the North Qilian and North Qinling orogenic belts, Central Orogenic System of
689 China: Evidence from newly discovered Paleozoic adakitic rocks. Gondwana Research 16,
690 285-293.
691 Vernon, R., 1984. Microgranitoid enclaves in granites—globules of hybrid magma quenched in a
692 plutonic environment. Nature 309, 438-439.
693 Vernon, R.H., 1983. Restite, xenoliths and microgranitoid enclaves in granites. Journal and Proceedings
694 of the Royal Society of New South Wales 116, 77–103.
695 Wang, J., Wu, C., Cai, Z., Guo, Y., Wu, J., Liu, X., 2006a. Early Paleozoic high-Mg adakite froin
696 Yindongliang in the eastern section of the North Qilian: Implications for geodynamics and Cu-Au
697 mineralization.. Acta Petrol Sinica 22, 2655–2664. (in Chinese with English abstract)
698 Wang, Q., McDermott, F., Xu, J.F., Bellon, H., Zhu, Y.T., 2005. Cenozoic K-rich adakitic volcanic
699 rocks in the Hohxil area, northern Tibet: Lower-crustal melting in an intracontinental setting.
700 Geology 33, 465.

Wang, Q., Wyman, D.A., Xu, J.F., Zhao, Z.H., Jian, P., Xiong, X.L., Bao, Z.W., Li, C.F., Bai, Z.H., 2006b. Petrogenesis of Cretaceous adakitic and shoshonitic igneous rocks in the Luzong area, Anhui Province (eastern China): Implications for geodynamics and Cu–Au mineralization. Lithos 89, 424-446.

Wang, Q., Wyman, D.A., Xu, J., Jian, P., Zhao, Z., Li, C., Xu, W., Ma, J., He, B., 2007. Early Cretaceous adakitic granites in the Northern Dabie Complex, central China: Implications for partial melting and delamination of thickened lower crust. Geochimica et Cosmochimica Acta 71, 2609-2636.

Wang, Q., Wyman, D.A., Xu, J., Dong, Y., Vasconcelos, P.M., Pearson, N., Wan, Y., Dong, H., Li, C., Yu, Y., Zhu, T., Feng, X., Zhang, Q., Zi, F., Chu, Z., 2008. Eocene melting of subducting continental crust and early uplifting of central Tibet: Evidence from central-western Qiangtang high-K calc-alkaline andesites, dacites and rhyolites. Earth and Planetary Science Letters 272, 158-171.

Wang, Q., Li, X.H., Jia, X.H., Wyman, D., Tang, G.J., Li, Z.X., Ma, L., Yang, Y.H., Jiang, Z.Q., Gou, G.N., 2013. Late Early Cretaceous adakitic granitoids and associated magnesian and potassium‐rich mafic enclaves and dikes in the Tunchang–Fengmu area, Hainan Province (South China): Partial melting of lower crust and mantle, and magma hybridization. Chemical Geology 328, 222-243.

Wiedenbeck, M., Alle, P., Corfu, F., Griffin, W., Meier, M., Oberli, F., Quadt, A.v., Roddick, J., Spiegel, W., 1995. Three natural zircon standards for U-Th-Pb, Lu-Hf, trace element and REE analyses. Geostandards newsletter 19, 1-23.

Xiong, X.L., Adam, J., Green, T.H., 2005. Rutile stability and rutile/melt HFSE partitioning during

partial melting of hydrous basalt: Implications for TTG genesis. Chemical Geology 218, 339-359.

Xu, J.F., Shinjo, R., Defant, M.J., Wang, Q., Rapp, R.P., 2002. Origin of Mesozoic adakitic intrusive rocks in the Ningzhen area of east China: Partial melting of delaminated lower continental crust? Geology 30, 1111.

Xu, W., Gao, S., Wang, Q., Wang, D., Liu, Y., 2006. Mesozoic crustal thickening of the eastern North China craton: Evidence from eclogite xenoliths and petrologic implications. Geology 34, 721-724.

Yu, S., Zhang, J., Qin, H., Sun, D., Zhao, X., Cong, F., Li, Y., 2015. Petrogenesis of the early Paleozoic low-Mg and high-Mg adakitic rocks in the North Qilian orogenic belt, NW China: Implications for transition from crustal thickening to extension thinning. Journal of Asian Earth Sciences 107, 122-139.

Zhang, C., Ma, C., Holtz, F., 2010. Origin of high-Mg adakitic magmatic enclaves from the Meichuan pluton, southern Dabie orogen (central China): Implications for delamination of the lower continental crust and melt-mantle interaction. Lithos 119, 467-484.

Zhang, J., Meng, F., Wan, Y., 2007. A cold Early Palaeozoic subduction zone in the North Qilian Mountains, NW China: petrological and U-Pb geochronological constraints. Journal of Metamorphic Geology 25, 285-304.

Zhang, Y., Niu, Y., Hu, Y., Liu, J., Ye, L., Kong, J., Duan, M., 2015. The syncollisional granitoid magmatism and continental crust growth in the West Kunlun Orogen, China - Evidence from geochronology and geochemistry of the Arkarz pluton. Lithos. doi: 10.1016/j.lithos.2015.05.007 (in press).

Figure captions：

Fig.1: (a) Simplified geological map of the North Qilian Orogen showing distributions of the main tectonic units (modified after Song et al., 2013; Chen et al., 2015). (b) Simplified map of the Qumushan (QMS) and Baojishan (BJS) area in the eastern section of the North Qilian Orogen. U-Pb ages are shown for granodiorite and MMEs in the BJS and QMS plutons from Chen et al. (2015), Yu et al. (2015) and this study as indicated.

Fig. 2: Photographs of the adakitic granodiorite and the MMEs in the field and in thin-sections. (a), (b) and (c) showing the sharp contact of MMEs of varying size with their host granodiorite with MMEs being finer-grained than the host; (d) showing the mineral assemblage of the adakitic host granodiorite (QMS12-02host) and (e), (f) showing the mineral assemblage of MMEs (QMS12-02MME, QMS12-06MME). Amp = amphibole; Bt = biotite; Pl= plagioclase; Qz = quartz; Ap = apatite; Zrn= zircon. Plates c-f are taken under cross-polarized light.

Fig. 3: Photomicrographs showing a plagioclase crystal with a high-Ca core rimmed by a euhedral overgrowth of low-Ca plagioclase in both (a) adakitic rocks (e.g., QMS12-04host) and (b) MMEs (e.g., QMS12-04MME). Numerals are the An contents. See Appendix 2 for compositional data.

Fig. 4: Chemical compositions of amphiboles from the host granodiorite and MMEs in the amphibole classification diagram (Leake et al., 1997). Data from the host granodiorites and the MMEs of BJS pluton (Chen et al., 2015) are also shown for comparison.

Fig. 5: Concordia diagrams of LA-ICP-MS U-Pb zircon age data and representative CL images of zircon grains showing spots for the host adakitic granodiorites (a, c) and the MMEs (b, d) in the QMS pluton.

765 **Fig. 6:** Classification diagrams of the host granodiorites and the MMEs in the QMS pluton. (a) Total
766 alkalis *vs*. SiO_2 (Le Maitre et al., 1989), (b) K_2O *vs*. SiO_2, and (c) A/NK *vs.* A/CNK. The blue circles
767 and squares are data from BJS granodiorites and their MMEs (Chen et al., 2015), and the open circles
768 are literature data on the QMS granodiorites (Wang et al., 2006a; Tseng et al., 2009; Yu et al., 2015).
769 **Fig. 7:** (a) Chondrite normalized REE patterns for the QMS host adakitic granodiorites and the MMEs;
770 (b) host rock-normalized REE patterns of MMEs. Chondrite REE values and bulk continental crust
771 (BCC) are from Sun and McDonough (1989) and Rudnick and Gao (2003), respectively. Shaded fields
772 of BJS granodiorite and the MMEs are from Chen et al. (2015).
773 **Fig. 8:** Average ocean crust-normalized (OC; Niu and O'Hara, 2003) trace element patterns for the
774 QMS host adakitic granodiorites and the MMEs.
775 **Fig. 9:** Plots of (a) Sr/Y vs. Y, where fields of adakite, and normal arc andesite-dacite-rhyolite are from
776 Defant and Drummond (1990); (b) La/Yb vs. Yb, discrimination lines are from Richards and Kerrich
777 (2007); (c) $(Dy/Yb)_N$ vs $(La/Yb)_N$, and (d) Eu/Eu* vs. Sr. Results in a-d using Rayleigh fractional
778 crystallization models indicate the effects of garnet, amphibole, plagioclase, zircon and apatite
779 fractionation on Sr/Y and Y (a), on La/Yb and Yb (b), on $(Dy/Yb)_N$ and $(La/Yb)_N$ (c), and on Eu/Eu*
780 and Sr (d). The partition coefficients used and modeling details are given in Appendix 6. Two
781 crystallization models were designed to elucidate the effect of crystallization on bulk-rock (assumed to
782 approximate melt) trace element systematics: (1) Model A, in reasonable agreement with observed
783 mineral proportions of the MMEs, 50% amphibole, 40% plagioclase, 7.52% biotite, 2.2% apatite, 0.2%
784 zircon and 0.03% sphene; (2) Model B, 50% amphibole, 40% plagioclase, 7.6% biotite, 2.4% garnet.
785 Data sources for the QMS and BJS plutons are the same as in Fig. 6. Amp = amphibole; Bt = biotite;
786 Pl= plagioclase; Ap = apatite; Zrn=zircon; Grt = garnet; Spn=sphene.

Fig. 10: SiO_2 variation diagrams of (a) MgO, (b) $Fe_2O_3^T$, (c) TiO_2, (d) CaO, (e) MnO, (f) P_2O_5, (g) Eu, (h) Hf, (i) La/Sm, (j) $^{87}Sr/^{86}Sr_{(t)}$, (k) $\varepsilon_{Nd}(t)$ and (l) $\varepsilon_{Hf}(t)$. Fractional crystallization trends in g–i: the inverse linear trend of SiO_2 versus Eu and Hf indicate the effects of plagioclase and zircon fractional crystallization, respectively. Because Sm is incorporated more easily than Hf in amphibole (Fujimaki et al., 1984; Klein et al., 1997), amphibole crystallization will cause Hf/Sm increase in residual magmas (i). Crustal contamination and (or) basalt-rhyolite mixing trend in j-l are after Wang et al. (2008). Data sources of the QMS and BJS pluton are the same as in Fig. 6. The average zircon $\varepsilon_{Hf}(t)$ isotopic data (6.2±2, 2σ) calculated from Yu et al. (2015) is also presented in l.

Fig. 11: (a) SiO_2 versus P_2O_5; (b) SiO_2 versus Zr. Data for Island arc basalt (n=284 for P and 277 for Zr), boninite (n=37 for P and 34 for Zr) and rhyolite (n=66 for P and 45 for Zr) are from the Georoc database (http://georoc.mpch-mainz.gwdg.de/georoc/). Dashed and solid lines in a-b are hypothetical mixing lines and linear trend defined the QMS granodiorite and their MMEs, respectively. Data sources of the QMS and BJS plutons are the same as in Fig. 6.

Fig. 12: Cartoon illustrating a possible scenario for MME formation. Earlier crystallized cumulate with the mineral assemblage of amphibole, biotite, plagioclase and accessory minerals such as zircon and apatite (a), which was later disturbed by subsequent magma replenishment in the magma chamber, constituting MMEs in the dominant host granodiorite.

Fig. 13: Plots of (a) SiO_2 versus $Mg^{\#}$; (b) Na_2O versus K_2O. Data sources: classical adakite, resulting from partial melting of subducted ocean crust in modern arcs, are from the GeoRoc database (http://georoc.mpch-mainz.gwdg.de/georoc/); Tibet Plateau (Chung et al., 2003; Wang et al., 2005), Dabie Orogen (He et al., 2013; Wang et al., 2007), Yangtze Craton (Xu et al., 2002; Wang et al., 2006b); North China Craton (Chen et al., 2013a; Ma et al., 2015) , experimental data (Sen and Dunn,

1994; Rapp and Watson, 1995. Data sources of the QMS and BJS plutons are the same as in Fig. 6.

Fig. 14: (a) Nd–Sr and (b) Nd-Hf isotope diagrams for the QMS adakitic rocks and their MMEs. The MORB data are from Niu and Batiza (1997) and Niu et al. (2002), other data sources are the same as Fig. 13. Binary isotope mixing calculations between North Qilian Ocean MORB (average composition: Sr=159.6 ppm, Nd=10.5 ppm, Hf=2.41, $^{87}Sr/^{76}Sr_{(t)}$=0.7054, ε_{Nd} (t)=5.44, ε_{Hf} (t)=9.93) and Mohe Basement (average composition: Sr=586 ppm, Nd=32.97 ppm, Hf=3.44, $^{87}Sr/^{76}Sr_{(t)}$=0.7234, ε_{Nd} (t)=-19.80, ε_{Hf} (t)=-43.65) are after Chen et al. (2015) and referrences therein. $K=[(Sr/Nd)_{MORB}]/[(Sr/Nd)_{Mohe\ basement}]$, where K_{max}, K_{min}, and $K_{average}$ are the maximum, minimum and average values respectively.

Fig. 15: Shows 30%, 40%, 50% and 60% fractional crystallization of mineral assemblages of Model A and Model B from the assumed magma along with the BCC and QMS adakitic granodiorites and their MMEs on primitive mantle normalized multi-element diagram. The light red and green shaded regions are the field of QMS adakitic granodiorite and MMEs, respectively.

Appendix Fig. S1: Simplified phase diagram showing hydrous solidi of basalts and granitic rocks modified from Niu et al. (2013) (after Niu, 2005). The red line with arrow illustrates the concept of the underthrusting North Qilian oceanic crust evolve along a high T/P path as a result of retarded subducting and enhanced heating upon continental collision at a prior active continental margin setting.

Appendix tables captions:

Appendix 1: U-Th-Pb analyses by LA-ICP-MS for zircons from host granodiorites (QMS12-04host and QMS12-10host) and the mafic magmatic enclaves (QMS12-04MME and QMS12-10MME).

Appendix 2: Microprobe analysis of representative plagioclase in the host granodiorites and the mafic magmatic enclaves.

Appendix 3: Microprobe analysis of representative amphibole in the host granodiorites and the mafic magmatic enclaves.

Appendix 4: Whole-rock major and trace elements analysis of the host adakitic granodiorites and the mafic magmatic enclaves in the NQOB.

Appendix 5: Whole rock Sr-Nd-Hf isotopic analyses for the host adakitic granodiorites and the mafic magmatic enclaves in the NQOB.

Appendix 6: Relevant partition coefficients, assumed melt and model compositions.

Syn-collisional adakitic granodiorites formed by fractional crystallization: insights from their enclosed mafic magmatic enclaves (MMEs) in the Qumushan pluton, North Qilian Orogen at the northern margin of the Tibetan Plateau

Shuo Chen [a,b*], Yaoling Niu [a, c*], Jiyong Li [a,b], Wenli Sun [a], Yu Zhang [d], Yan Hu[a,b], Fengli Shao [a,b]

[a] Institute of Oceanology, Chinese Academy of Sciences, Qingdao 266071, China.

[b] University of Chinese Academy of Sciences, Beijing 100049, China

[c] Department of Earth Sciences, Durham University, Durham DH1 3LE, UK

[d] School of Earth Sciences, Lanzhou University, Lanzhou 730000, China

***Corresponding authors:**

Mr. Shuo Chen (chenshuo528@foxmail.com)

Professor Yaoling Niu (yaoling.niu@foxmail.com)

Abstract

The Qumushan (QMS) syn-collisional granodiorite, which is located in the eastern section of the North Qilian Orogen at the northern margin of the Greater Tibetan Plateau, has typical adakitic characteristics and also contains abundant mafic magmatic enclaves (MMEs). This recognition offers an unprecedented insight into the petrogenesis of both the adakitic host granodiorite and the enclosed MMEs. The MMEs and their host granodiorites share many characteristics in common, including identical crystallization age (~430 Ma), same mineralogy, similar mineral chemistry and whole-rock isotopic compositions, indicating their genetic link. The MMEs are most consistent with being of cumulate origin formed at earlier stages of the same magmatic system that produced the QMS adakitic granodiorite. Subsequent replenishment of adakitic magmas could have disturbed the cumulate piles as "MMEs" dispersed in the adakitic granodiorite host during emplacement. The geochemical data and petrogenetic modeling of trace elements suggest that the QMS adakitic host granodiorite is most consistent with fractional crystallization dominated by the mineral assemblage of the MMEs. The parental magma for the QMS granodiorite is best explained as resulting from partial melting of the ocean crust together with recycled terrigenous sediments during continental collision, which may have also experienced interaction with mantle peridotite during ascent.

Keywords: Adakitic rocks; Mafic magmatic enclaves; Cumulate; Syn-collisional granodiorite; North Qilian Orogen

1. **Introduction**

"Adakite" was introduced by Defant and Drummond (1990) after the name of Adak Island in the Aleutian arc. It refers to a group of intermediate-felsic igneous rocks observed in modern oceanic and continental arcs genetically associated with seafloor subduction. They are characterized by high Sr, light rare earth elements (REEs), Sr/Y (>40) and La/Yb (>20), low Y and heavy REEs, and lack of obvious Eu anomalies. It was initially considered that adakites were derived by partial melting of young (≤ 25Myrs) and warm subducting/subducted ocean crust in subduction zones (Defant and Drummond, 1990). The origin of adakite has since been one of the most popular subjects of research in igneous petrology due to its use for tectonic finger-printing (see Castillo, 2006, 2012), yet recent studies have shown that adakite or rocks with adakitic compositions can be produced in various ways and in different settings (Castillo et al., 1999; Xu et al., 2002; Chung et al., 2003, 2005; Wang et al., 2005, 2007; Macpherson et al., 2006; RodrIguez et al., 2007; Streck et al., 2007; He et al., 2013; Chen et al., 2013a; Song et al., 2014a). Because adakite is defined on the basis of certain trace element characteristics as detailed above, geochemistry in combination with experimental geochemistry has been widely used to discuss the petrogenesis of adakites and adakitic rocks (e.g., Defant and Drummond, 1990; Sen and Dunn, 1994; Castillo et al., 1999; Xu et al., 2002; Wang et al., 2005; Xiong et al., 2005; Castillo, 2006, 2012). However, a petrological approach is essential for petrological problems and is expected to offer insights into the petrogenesis of adakites and adakitic rocks. Indeed, mafic magmatic enclaves (MMEs) hosted in adakitic rocks have been recently recognized, and the processes of the MME formation may offer a fresh perspective on the petrogenesis of the adakitic host (e.g., RodrIguez et al., 2007; Chen et al., 2013b).

In this paper, we report our petrological, mineralogical and geochemical analyses and

63 trace-element modeling on an MME-bearing adakitic pluton well exposed in the eastern section of the
64 North Qilian orogenic belt (NQOB) (Fig. 1a). This pluton was previously studied using the "standard"
65 geochemical method with the MMEs being overlooked (e.g., Wang et al., 2006a; Tseng et al., 2009; Yu
66 et al., 2015). Here we present a simple but effective model of fractional crystallization to successfully
67 address both the origin of MMEs and their host adakitic granodiorite.

68 **2. Geological setting**

69 The NW-SE-trending NQOB is located between the Alashan Block to the northeast and the Qilian
70 Block to the southwest, and is offset to the northwest by the Altyn-Tagh Fault (Fig.1a). It is made up of
71 Early Paleozoic subduction-zone complexes including ophiolitic melanges, blueschists and eclogites,
72 Silurian flysch formations, Devonian molasse, and Carboniferous to Triassic sedimentary cover
73 sequences (Fig. 1a) (Song et al., 2007, 2013; Zhang et al., 2007). It is composed of three subunits, i.e.,
74 (1) the southern ophiolite belt, (2) the middle arc magmatic belt and (3) the northern back-arc basin
75 ophiolite-volcanic belt (Fig. 1a) (Song et al., 2007, 2013; Zhang et al., 2007; Chen et al., 2014). It is
76 generally accepted that the NQOB is an Early Paleozoic suture zone, which records a long tectonic
77 history from seafloor spreading/subduction to the ultimate continental collision and mountain-building
78 (see Song et al., 2013). The Qumushan (QMS) pluton we studied is about 60km^2 in outcrop located in
79 the eastern section of the NQOB. It lies approximately 10 km southeast of the Baojishan (BJS) pluton
80 (Fig.1b). The QMS pluton intruded the Ordovician sedimentary and metamorphic rocks of Yingou
81 group (Fig.1b). MMEs are widespread in the host granodiorite (Fig. 2a).

3. Analytical methods

3.1. Zircon U–Pb ages

Zircons were separated by using combined methods of heavy liquid and magnetic techniques before hand-picking under a binocular microscope. The selected zircons were set in an epoxy mount that was polished to expose zircon interiors. Cathodoluminescence (CL) images were taken at China University of Geosciences in Wuhan (CUGW) to examine the internal structure of individual zircon grains. The zircon U-Pb dating was done using LA-ICP-MS at China University of Geosciences in Beijing (CUGB). The instrument consists of an Agilent 7500a quadrupole inductively coupled plasma mass spectrometry (ICP-MS) coupled with a UP-193 Solid-State laser (193 nm, New Wave Research Inc.). Laser spot size was set to be ~30μm. Zircon 91500 (Wiedenbeck et al., 1995) and a secondary standard zircon TEMORA (417 Ma) (Black et al., 2003) was used as an external standard. The analytical procedure is given in Song et al. (2010a). Isotopic ratios and element concentrations of zircons were calculated using GLITTER (ver. 4.4, Macquarie University). Common Pb correction was applied using the method of Andersen (2002). Results are given in ~~Appendix A~~Appendix 1.

3.2. Mineral compositions

Mineral chemistry was determined using a JXA-8100 microprobe at Chang'an University, China. The operating conditions were a 15 kV accelerating potential with a probe current of 10 nA and the electron beam diameter of 1μm. Results are given in ~~Appendix B~~Appendix 2 and ~~Appendix C~~Appendix 3.

3.3. Major and trace elements

The bulk-rock major and trace elements were analyzed using Leeman Prodigy inductively coupled plasma-optical emission spectroscopy (ICP-OES) and Agilent-7500a inductively coupled plasma mass spectrometry (ICP-MS) at CUGB, respectively. The analytical uncertainties are generally less than 1% for most major elements with the exception of TiO_2 (~1.5%) and P_2O_5 (~2.0%). The loss on ignition was measured by placing 1 g of sample powder in the furnace at 1000°C for several hours before cooling in a desiccator and reweighting. The analytical details are given in Song et al. (2010b). The data are presented in ~~Table 1~~Appendix 4.

3.4. Whole-rock Sr-Nd-Hf isotopes

Whole-rock Sr-Nd-Hf isotopic analyses were done in Guangzhou Institute of Geochemistry, Chinese Academy of Sciences (GIG-CAS). The rock powders were digested and dissolved in HF-HNO_3 acid mixtures and dried on a hot-plate. Sr-Nd-Hf fractions were separated using small Sr Spec resin columns to obtain Sr and Nd-Hf bearing fractions. Sr isotopic compositions were determined using a Neptune Plus multi-collector ICP-MS (MC-ICP-MS) following Ma et al. (2013a). Nd fractions were then separated by passing through cation columns followed by HDEHP columns. Separation of Hf from the matrix and rare earth elements was carried out using a combined method of Eichrom RE and HDEHP columns. Nd and Hf isotopic compositions were determined using a Micromass Isoprobe MC-ICP-MS following Li et al. (2009) and Ma et al. (2013b). Repeated analysis of NBS-987 run during the same period of sample analysis gave $^{87}Sr/^{86}Sr$=0.710283±27 (2σ, n=13). Repeated analysis of BHVO-2 and JB-3 during the same period of sample analysis yielded $^{143}Nd/^{144}Nd$ 0.512977±14 (2σ, n=8) and 0.513053±18 (2σ, n=13), respectively. During the course of this study, the

mean $^{176}Hf/^{177}Hf$ ratios for BHVO-2 and JB-3 are respectively 0.283099±15 (2σ, n = 13) and 0.283216 ± 15 (2σ, n=6). All measured $^{87}Sr/^{86}Sr$, $^{143}Nd/^{144}Nd$ and $^{176}Hf/^{177}Hf$ ratios were normalized to $^{86}Sr/^{88}Sr$ = 0.1194, $^{146}Nd/^{144}Nd$ =0.7219 and $^{179}Hf/^{177}Hf$ = 0.7325, respectively. The USGS rock standards JB-3 and BHVO-2 run with our samples give values consistent with the reported reference values (GeoREM, http://georem.mpch-mainz.gwdg.de/). Results are given in ~~Table 2~~Appendix 5.

4. Petrography and mineral chemistry

4.1. Granodiorite

The QMS pluton is of granodioritic composition with a mineral assemblage of plagioclase (45 vol. %–50 vol. %), quartz (35 vol. %-42 vol. %), amphibole (3 vol. %-10 vol. %), biotite (2 vol. %-10 vol. %), minor K-feldspar, and accessory minerals such as apatite, sphene, zircon and Fe-Ti oxides (Fig. 2d). Plagioclase crystals are euhedral to subhedral, and are of oligoclase composition with An_{12-24} (Fig. 3a). Zoned-plagioclase crystals display normal zoning with more anorthitic cores rimmed by less calcic compositions (Fig. 3a). Amphibole is always present as euhedral to subhedral crystals despite the variably small abundances (Fig. 2d). Amphibole grains are usually homogeneous and rarely display disequilibrium textures. Amphiboles from the host granodiorite can be classified as edenite (~~Appendix C~~Appendix 3, Fig. 4) following Leake et al. (1997). They have medium SiO_2, and low TiO_2 (0.37-1.24 wt. %), Na_2O (0.87-1.48 wt. %) and K_2O (0.29-1.69 wt. %).

4.2. Mafic magmatic enclave

MMEs are abundant in the QMS pluton (Fig. 2a), showing varying shape and size from centimeters to tens of centimeters in diameter (Fig. 2a). They differ from the host by having finer

grain-size (Figs. 2a-c), but have the same mineralogy albeit with greater mafic modes (e.g., 35-50 vol.% amphibole, 5-15 vol.% biotite, 40-50 vol.% plagioclase, minor quartz, K-feldspar, along with accessory minerals such as apatite, sphene, zircon and Fe-Ti oxides), thus giving a dioritic bulk composition. Plagioclase mostly occurs as subhedral grains with compositions similar to those in the host granodiorite. Zoned-plagioclase in the MMEs shows a compositional continuum with cores slightly more anorthitic than the rims (Fig. 3b). Amphibole in the MMEs is compositionally identical to that in the host granodiorite (Fig. 4). Biotite is yellow brown with subhedral to euhedral forms. The MMEs show no chilled margins nor textures of crystal resorption or reactive overgrowth. These rocks mainly exhibit porphyritic-like textures.

5. Results

5.1. Zircon U–Pb ages

Four samples (2 host-MME pairs) were chosen for dating. In CL images (Figs. 5a, c), zircons from the host granodiorites (QMS12-04host and QMS12-10host) are transparent, colorless, and mostly euhedral columnar crystals of varying size (~150-300μm long with length/width ratio of 1:1-3:1) with well-developed oscillatory zoning. The zircons have varying U (~ 28-386 ppm) and Th (~ 69-423 ppm) with Th/U ratio of 0.3-1.4. All these characteristics are consistent with the zircons being of magmatic origin (Hoskin and Schaltegger, 2003). After excluding discordant ages, zircons from the two host granodiorite samples yielded weighted mean $^{206}Pb/^{238}U$ ages of 429.7 ±2.5 Ma (1σ, MSWD=0.15, n=23) and 431.5 ±2.6 Ma (1σ, MSWD=0.19, n=20), respectively (Figs. 5a, c), representing the crystallization age (~430 Ma) of the host granodiorite. These age data are in agreement with those in the literature (Tseng et al., 2009; Yu et al., 2015).

Zircons from the MMEs (QMS12-04MME and QMS12-10MME) show similar optical properties to those in the host with oscillatory zoning (Figs. 5b, d) and varying size (~150-200μm in length length/width ratio of ~ 1:1-2:1). They have varying Th (27-548 ppm), U (50-541 ppm), and Th/U (0.1-2.4). They are also of magmatic origin. Zircons in the 2 MMEs yielded the same weighted mean ages as zircons in the host within error, i.e. 429.6 ±2.8 Ma (1σ, MSWD=0.48, n=18) and 431.2 ±2.8 Ma (1σ, MSWD=0.2, n=19), respectively (Figs. 5b, d).

5.2. Major and trace elements

Eleven representative QMS granodiorite samples and their hosted MMEs (including 5 host-MME pairs) were analyzed for whole-rock major and trace element compositions (~~Table 1~~Appendix 4). The granodiorite samples have high SiO_2 (64.37-65.49 wt.%), Al_2O_3 (16.09-17.61 wt.%), Na_2O (4.86-5.12 wt.%) and Na_2O/K_2O (2.11-3.82) with medium total alkalis (Na_2O+K_2O = 6.46-7.25 wt.%), and plot in the granodiorite field (Fig. 6a). They have low $Fe_2O_3^T$ (2.86-3.43 wt.%), MgO (2.14-2.60 wt.%) and CaO (3.60-4.10 wt.%). They are calc-alkaline (Fig. 6b) and metaluminous to weakly peraluminous (A/CNK= 0.93 to 1.03) (Fig. 6c), which is typical for I-type granitoids (Chappell and White, 1992). In contrast, the MMEs plot in the fields of diorite, monzodiorite and monzonite (Fig. 6a). They are compositionally high-K calc-alkaline to calc-alkaline (Fig. 6b), and metaluminous with A/CNK ranging from 0.74 to 0.84 (Fig. 6c). They have lower SiO_2 (52.06-58.59 wt.%), higher $Fe_2O_3^T$ (6.12-8.50 wt.%), MgO (5.09-7.22 wt.%), CaO (4.99-6.57 wt.%), P_2O_5 (0.49-1.01 wt.%), and slightly higher $Mg^{\#}$ (0.63-0.68; $Mg^{\#}=Mg/[Mg+Fe^{2+}]$) than the host granodiorites.

In the chondrite-normalized REE diagram, the QMS granodiorite samples are characterized by a relatively flat heavy REE (HREE) pattern ($[Dy/Yb]_N$ = 1.32-1.54), slightly negative to positive Eu

anomalies (Eu/Eu*=0.88-1.13), and lower total REE contents (ΣREE=76-134 ppm) than the hosted MMEs. The REE patterns of the QMS granodiorites are similar to the field defined by the BJS granodiorites (cf. Chen et al., 2015) (Fig. 7), but display greater light REE (LREE) enrichment ($[La/Sm]_N$ = 4.77-5.36). The MMEs show similar REE patterns, but have significantly higher HREEs (Fig. 7a, b), which is consistent with greater modes of REE-enriched minerals (e.g., amphibole, apatite and zircon). They have negative Eu anomalies (Eu/Eu*=0.6-0.8).

In the multi-element spider diagram (Fig. 8), the host granodiorite and MMEs both show enrichment of large ion lithophile elements (LILE, e.g., P, K, Pb) and depletion in high field strength elements (HFSE, e.g., Nb, Ta and Ti). Sr appears to have a positive anomaly in the host (Sr/Sr*=1.66-2.96), but varying anomalies for the MMEs (Sr/Sr*=0.5-1.19). In particular, compared to the BJS granodiorites (Chen et al., 2015), the QMS granodiorite samples have adakitic signatures with high Sr/Y and La/Yb ratios, and lower Y and Yb abundances, thus plotting in the adakite fields in the discrimination diagrams (Figs. 9a-b), while most MMEs plot in the normal arc rock field.

5.3. Sr-Nd-Hf isotopic geochemistry

Whole-rock Sr-Nd-Hf isotopic compositions for the MMEs and their host granodiorite are given in ~~Table 2~~Appendix 5. The initial $^{87}Sr/^{86}Sr_{(t)}$, $\varepsilon_{Nd}(t)$ and $\varepsilon_{Hf}(t)$ values are calculated at 430 Ma using the zircon age data (see Fig. 5 above). On the plots of $^{87}Sr/^{86}Sr_{(t)}$, $\varepsilon_{Nd}(t)$ and $\varepsilon_{Hf}(t)$ against SiO_2 (Figs. 10j-l), both host granodiorite and MME samples are indistinguishable and overlapping within a narrow range (also see ~~Table 2~~Appendix 5).

On SiO_2-variation diagrams (Fig. 10), the MMEs and their host granodiorite define linear trends for most elements (e.g., TiO_2, $Fe_2O_3^T$, MnO, MgO, CaO, P_2O_5, Eu and Hf abundances) and trace

element ratio (e.g., Hf/Sm) (Figs. 10a-i), but show no correlations of initial Sr, Nd, and Hf isotopic compositions with SiO_2 (Figs. 10j-l).

6. Discussion

6.1. Petrogenesis of the mafic magmatic enclaves

Several models have been proposed for the origin of MMEs in the literature, including foreign xenoliths (usually country rocks; e.g., Vernon, 1983; Xu et al., 2006), refractory and residual phase assemblages derived from granitoid sources (e.g., the restite model; Chappell et al., 1987; Chappell and White, 1991), chilled material or cumulate of early-formed co-genetic crystals (e.g., Dodge and Kistler, 1990; Dahlquist, 2002; Donaire et al., 2005; RodrIguez et al., 2007; Niu et al., 2013; Huang et al., 2014; Chen et al., 2015), and basaltic melt material incompletely digested and homogenized during a magma mixing process (e.g., Vernon, 1983; Didier, 1987; Castro et al., 1990; Dorais et al., 1990; Barbarin and Didier, 1991; Chappell and White, 1991; Barbarin, 2005; Chen et al., 2009a, 2013b; Wang et al., 2013). We critically evaluate these interpretations below.

6.1.1. Textural and chemical relationships of the MMEs and their hosts

The textural and chemical relationships of the QMS MMEs and their host granodiorite concur with the findings for the BJS pluton (Chen et al., 2015), and are summarized as follows: (1) the MMEs in the QMS granodiorites are ellipsoidal, or elongate, show no chilled margins，no textures of crystal resorption nor reactive overgrowth, but exhibit typical magmatic texture (Figs. 2a-f); (2) they have a mineral assemblage identical to, and more mafic phases than, their host granodiorite (Figs. 2c-f); (3) they have mineral compositions (e.g., amphibole and plagioclase) identical to those of their host (Fig.

225 3-4); (4) they have the same age (~430 Ma) as their host (Fig. 5); (5) their different major and trace
226 element abundances from their hosts are controlled largely by mineral modal proportions, i.e., MMEs
227 have greater modes of REE-enriched minerals (amphibole, apatite and zircon) and thus have higher
228 MgO, Fe_2O_3, CaO and trace elements easily incorporated into these phases (e.g., TiO_2, P_2O_5, Hf and
229 HREEs) (Figs. 10a-i); and (6) more importantly, they have overlapping and indistinguishable Sr-Nd-Hf
230 isotopes with their host granodiorite (Figs. 10j-l).

231 Any successful models for the origin of MMEs must be consistent with these observations.
232 Models for MMEs as foreign xenoliths from country rocks (e.g., Xu et al., 2006) can be readily rejected,
233 as there is no evidence of reaction textures for the MMEs. Likewise, the identical age (~430 Ma) of the
234 MMEs and their host as well as the magmatic textures, constitute a strong argument against the restite
235 origin (e.g., Chappell et al., 1987). In addition, the MMEs do not contain peraluminous minerals and
236 their metaluminous composition (Fig. 6c) also excludes their derivation by melting of peraluminous
237 restites (Barbarin, 2005). Therefore, the most straightforward interpretation is that the MMEs and their
238 hosts formed as different products of a common magmatic system.

239 *6.1.2. Assessing the origin of magma mixing*

240 Similar observations mentioned above between the MMEs and their host granitoids have been
241 identified first by Pabst (1928) and by many others since then. The MMEs were thus described as
242 "autoliths", referring to "cogenetic" or part of the same system. Despite the "autoliths" nature of the
243 MMEs with the host, this interpretation has been questioned: (1) Why are isotopic values of some
244 MMEs intermediate between those of crustal and mantle materials (e.g., DePaolo, 1981; Barbarin,
245 2005)? (2) Why are the MMEs fine-grained (e.g., Barbarin and Didier, 1991)? Because of these

246 questions, a model of magma mixing between mantle-derived mafic magma and crust-derived felsic
247 magma was proposed to address the above issues: (1) the intermediate isotopic values of the MMEs
248 were commonly interpreted as the result of magma mixing between a mantle-derived mafic magma and
249 a crust-derived felsic magma, because a mafic magma derived from upper mantle provides not only
250 material but also the heat necessary for melting and subsequently mixing with the crustal rocks (e.g.,
251 Barbarin, 2005); (2) the fine-grained MMEs were interpreted as due to quenching against host felsic
252 magmas (e.g., Vernon, 1984; Furman and Spera, 1985; Barbarin, 2005), owing to their higher liquidus
253 and solidus temperatures compared to felsic magmas. As a result, the magma mixing model has been
254 the most popular interpretation for the petrogenesis of the MMEs (see critical review by Niu et al.,
255 2013).

256 Actually, there are many compelling lines of evidence for magma mixing in many granitoids,
257 especially (1) where a clear isotopic contrast exists between the MMEs and the hosts (e.g., Holden et
258 al., 1987; Chen et al., 2009b; Liu et al., 2013); and (or) (2) where disequilibrium features occur in the
259 MMEs, e.g., complex zoning of clinopyroxene crystals that have distinctly low-MgO cores surrounded
260 by high-MgO rims (e.g., Chen et al., 2013a; Wang et al., 2013), or resorption textures or reversed
261 zoning of plagioclase (Pietranik et al., 2006; Chen et al., 2009a, 2009b). In the case of our study,
262 however, none of the above has been observed. Instead, many lines of evidence argue against the
263 magma mixing origin.

264 First, the MMEs and their host granodiorites in the QMS pluton have overlapping and
265 indistinguishable Sr-Nd-Hf isotopes (vs. isotopic contrast in magma mixing model). In spite of this,
266 some authors would still argue that the isotopic and mineral compositional similarity between the
267 enclaves and the host could result from chemical and isotopic equilibration during magma mixing, (e.g.,

Dorais et al., 1990; Barbarin, 2005; Chen et al., 2009b; Zhang et al., 2010) using some experimental interpretations that isotopic equilibration is generally more easily achieved than chemical equilibration (Lesher, 1990). However, we emphasize that it is physically unlikely that isotopes become homogenized whereas major and trace elements are not (Niu et al., 2013), because isotopes are "carried" by the relevant chemical elements and isotopic diffusion cannot take place without the diffusion of the "carrying" elements (Chen et al., 2015). In fact, there are two forceful arguments against thermal and chemical equilibration: (1) the MMEs exhibit no textures of crystal resorption or reactive overgrowth (Figs. 2b-c), and (2) plagioclase in the MMEs and their host granodiorite shows no compositional or textural disequilibrium (Fig. 3). In addition, although the fine-grained texture of the MMEs could be interpreted as resulting from quenching in the magma mixing model, quenching of the mafic magma would lead to a significantly high viscosity contrast between the solidified enclaves and the felsic host magma, thereby inhibiting deformation, mechanical mixing (Caricchi et al., 2012; Farner et al., 2014) and isotope homogenization between the MMEs and the host.

Second, strongly correlated variations between major and trace elements (Figs. 10a-i) are consistent with modal mineralogy control, as the result of magma evolution (i.e., the MMEs are cumulate and the host represents residual melt) rather than mixing of two magmas with entirely different origins because magma mixing is a complex, multi-stage process in which linear trends can be disturbed (e.g., Clemens, 1989; Donaire et al., 2005; Chen et al., 2015). Moreover, the distinctive high abundances of some elements in the MMEs, such as Zr and P (Fig. 11), cannot be explained by magma mixing because these elements are controlled by the presence of accessory phases, such as zircon and apatite. As shown in Fig. 11, mantle derived basaltic magmas would have much lower Zr and P_2O_5 than in the QMS MMEs. For example, quantitative calculations by Lee and Bachmann (2014) suggested that

10-20% melting of an upper mantle with 5 ppm Zr and 0.019 wt.% P_2O_5 (equivalent to that estimated for depleted mid-ocean ridge basalt mantle), would yield primary liquids with 25-50 ppm Zr and 0.1-0.2 wt.% P_2O_5. These concentrations are much lower than in the QMS MMEs. Additionally, boninites are thought to result from partial melting of highly depleted harzburgitic mantle peridotites induced by subduction-zone slab dehydration (Niu, 2005), but they also have lower Zr and P_2O_5 contents (Fig. 11). More importantly, magma mixing between a basalt with any silicic end-member (e.g., rhyolite) would generate a mixing array (Figs. 11a-b, the dash lines) totally different from the linear trend (Figs. 11a-b, the solid lines) defined by the QMS granodiorite and their MMEs. In contrast, all of these observations are consistent with the interpretation that the MMEs represent earlier cumulate with greater amounts of zircon and apatite than their hosts (e.g., Donaire et al., 2005).

6.1.3. Formation of the mafic magmatic enclaves

The foregoing observations, illustrations and discussion leave us with the best interpretation that the MMEs represent the earlier crystallized cumulate that were later disturbed by subsequent melt replenishment and induced magma convection in the magma chamber. As illustrated in Fig. 12, when a primitive magma body is emplaced into a cold environment (e.g., developing a magma chamber) with the wall-rock having temperatures below the liquidus of the magma, magma quench and rapid crystallization are inevitable because of the thermal contrast. For an andesitic primitive magma parental to the syn-collisional granitoids (Niu et al., 2013), the first major liquidus phases would be amphibole, biotite, plagioclase and accessory minerals such as zircon and apatite, and rapid quench will facilitate abundant nucleation without between-nuclei space for rapid growth, thus resulting in the formation of fine-grained cumulate (Chen et al., 2015). This is a fundamentally important petrologic concept with

311 which any interpretation must comply. This early formed fine-grained mafic cumulate piles (largely
312 plastic before complete solidification) can be readily disturbed by subsequent magma replenishment
313 and induced convection, resulting in the dispersion of the MMEs in the host granodiorite.

314 *6.2 Petrogenesis of QMS adakitic granodiorite*

315 *6.2.1 Implication from the MMEs*

316 Recently, mixing of basaltic and felsic magmas was proposed for the genesis of some high-Mg
317 and low SiO_2 adakitic rocks from Mount Shasta and the North China Craton using the presence of
318 ubiquitous MMEs as evidence (Chen et al., 2013b) and also based on the disequilibrium petrographic
319 characteristics in high-Mg andesites (Streck et al., 2007; Chen et al., 2013a). This interpretation could
320 be reasonable, but it is not the case here because there is no petrographic and compositional evidence
321 for magma mixing as elaborated above. That is, the MMEs in the QMS adakitic granodiorite are not
322 evidence for magma mixing, but rather they are of cumulate origin without direct asthenospheric
323 mantle participation (e.g., Dahlquist, 2002). More importantly, the MMEs comprise dominantly
324 amphibole and plagioclase, which are common cumulate minerals of andesitic melts. If the parental
325 melts were basaltic, the typical cumulate from such evolved basaltic melt would be gabbro dominated
326 by clinopyroxene and plagioclase (Chen et al., 2015). It can be inferred from this important petrological
327 concept that the parental magmas of the MMEs and their host granodiorite was mafic andesitic (Niu et
328 al., 2013; Chen et al., 2015).

329 *6.2.2 Assessing the model of melting of mafic lower continental crust*

330 To date, some intra-continental high-MgO or -$Mg^{\#}$ (also high Cr and Ni contents) adakitic rocks

have been considered to originate from melting of delaminated lower crust (e.g., Xu et al., 2002; Gao et al., 2004; Wang et al., 2006b). By accepting and applying this model, it has been previously interpreted that the QMS adakitic rocks were derived from delaminated lower crust, and they subsequently interacted with mantle peridotite during ascent (Tseng et al., 2009; Yu et al., 2015). Although this model seems plausible and applicable to the QMS adakitic rocks, it has more difficulties than certainties. First, the QMS adakitic granodiorites have lower $(Dy/Yb)_N$, $(La/Yb)_N$, and distinctive low K_2O/Na_2O ratios (Fig. 13b), which are significantly different from the composition of adakitic rocks inferred to be derived from partial melting of the thickened or delaminated lower continental crust. Second, the Nd and Hf isotopic data of the QMS adakitic granodiorite indicate a significant mantle input, which is also inconsistent with those of lower continental crust origin (Fig. 14a). Finally, the existence of the Paleo-Qilian ocean is manifested by the ophiolites and eclogites in the North Qilian orogenic belt; the ocean basin started its subduction at ~520 Ma, and was eventually closed at the end of the Ordovician (~445 Ma) followed by continental collision (see Song et al., 2013). Accordingly, the coeval (~430 Ma) MMEs and their adakitic host granodiorite of the QMS pluton are best interpreted as a magmatic response to the collision between the Qilian-Qaidam block and Alashan block, thereby being contrary to the environment of crustal extension required by a delaminated lower crustal origin. In fact, continuous lithosphere extension and delamination in the NQOB occurred at <400 Ma, which resulted in strong magmatic activity and formed a number of diorite-granodiorite-granite plutons with ages of ~400–360 Ma (Song et al., 2013, 2014b).

6.2.3 A fractional crystallization model for the petrogenesis of the QMS adakitic granodiorites

An origin of adakitic rocks by fractional crystallization has been proposed in the literature.

However, it should be noted that all these crystallization models require basaltic parental magmas derived from the metasomatized mantle wedge in arc settings, such as in the complex Philippine arc (Castillo et al., 1999; Macpherson et al., 2006) and Ecuadorian Andes (Chiaradia et al., 2004). It is important to note that our crystallization model differs from the basaltic magma crystallization model of arc magmas in the literature.

In our model, the magmas parental to the MMEs and their host granodiorite are the same mafic andesitic magmas in a syn-collisional setting, rather than basaltic magmas in an arc setting of active seafloor subduction advocated in the literature (e.g., Macpherson et al., 2006). That is, the QMS adakitic granodiorites are products of fractional crystallization dominated by the mineral assemblage indicated by the MMEs from mafic andesitic magmas. We can further consider two fractional crystallization models to elucidate the effect of crystallization of the observed mineralogy on trace elements using closed-system Rayleigh fractionation equation: (1) Model A, in reasonable agreement with observed mineral proportions of the MMEs, 50% amphibole, 40% plagioclase, 7.52% biotite, 2.2% apatite, 0.2% zircon and 0.03% sphene; (2) Model B, which incorporates fractionation of garnet, 50% amphibole, 40% plagioclase, 7.6% biotite, 2.4% garnet. The partition coefficients used in the calculations are for intermediate-felsic magmas (~~Table 3~~Appendix 6). For convenience (see below), the assumed parental magma (~~Table 3~~Appendix 6) is very similar to the bulk continental crust (BCC) composition (Rudnick and Gao, 2003) (Fig. 15), which is the same as the ~ 60 Ma Linzizong andesite in southern Tibet (Mo et al., 2008; Niu et al., 2013), in terms of major and trace element abundances.

Notably, removal of garnet would yield a smooth decrease of LREE-to-HREE pattern (Richards and Kerrich, 2007) with elevated $(Dy/Yb)_N$ and $(La/Yb)_N$ in the evolving melt (Fig. 9c). However, the $(Dy/Yb)_N$ ratio in the QMS adakitic granodiorites remain constant with increasing $(La/Yb)_N$ (Fig. 9c),

374 which indicate that the effect of garnet fractionation in generating the QMS adakitic granodiorites is
375 unimportant. Simple modal calculation of fractional crystallization using Model B indicates that the
376 participation of garnet is no more than 3% (Fig. 9), but the low garnet proportion in combination with a
377 large amount of amphibole-plagioclase fractionation can hardly generate the adakitic signature shown
378 in the QMS pluton (Figs. 9a-b). Besides, mineralogically, garnet has been observed neither in the QMS
379 MMEs and their host adakitic granodiorite, nor in the coeval igneous rocks in the eastern section of the
380 NQOB. In addition, our preferred source for the QMS MMEs and their host adakitic granodiorite is
381 partial melting of the ocean crust at amphibolite facies conditions (＜40km) (Mo et al., 2008; Niu and
382 O'Hara, 2009; Niu et al., 2013) (see below), rather than the presence of garnet as a residual phase at
383 garnet amphibolite or eclogite conditions.

384 It is also impossible to generate QMS adakitic granodiorites by fractionation of
385 amphibole-plagioclase alone, because they trend to produce concave-upwards patterns between the
386 MREE and HREE and lead to decreasing $(Dy/Yb)_N$ with increasing $(La/Yb)_N$ (Fig. 9c), owing to the
387 affinity of calcic amphiboles for MREEs over the HREEs (Klein et al., 1997). Additionally, removal of
388 amphibole-plagioclase would result in negative Eu anomalies in the residual melts, which is
389 inconsistent with QMS adakitic granodiorites (Fig. 9d). In the case of our study, we emphasize that the
390 widespread accessory minerals such as zircons and apatites in both QMS host adakitic granodiorite and
391 particularly their cumulate MMEs played a significant role in generating QMS adakitic granodiorites.
392 For example, zircon fractionation would increase $(Dy/Yb)_N$ (Fig. 9c) and the La/Yb and Sr/Y ratios of
393 residue magmas (Figs. 9a-b), because $Kd_{zircon}^{Dy/Yb} = 0.140$, and $Kd_{zircon}^{La/Yb} = 0.005$ (Bea et al., 1994).
394 Apatite fractionation can also increase the Sr/Y ratio (Figs. 9a-b), but decrease $(Dy/Yb)_N$ (Fig. 9c).
395 Importantly, apatite fractionation would increase Eu/Eu* (Fig. 9d), because $Kd_{apatite}^{Sm} = 46$,

396 $Kd^{Eu}_{apatite} = 25.5$, $Kd^{Gd}_{apatite} = 43.9$ (Fujimaki et al., 1984). Note that the simple calculation of Model A
397 (~~Table 3~~Appendix 6; Figs. 9 and 15), which involves a small proportion of zircon, apatite and sphene in
398 combination with amphibole, biotite and plagioclase to form the fractionation assemblage can explain
399 the characteristics of the QMS adakitic granodiorites. Although uncertainties exist for mineral partition
400 coefficients, our model offers insights into the petrogenesis of the adakitic granodiorite as well as the
401 enclosed MMEs in syn-collisional environments.

402 *6.3 Constraints on the source*

403 As discussed above, the primary magmas parental to the MMEs and their host granodiorite are
404 most consistent with mafic andesitic magmas of ocean crust origin during continental collision. In
405 addition, our new data and the whole-rock Sr-Nd and zircon Hf isotopic data in the literature on the
406 QMS pluton (Tseng et al., 2009; Yu et al., 2015) exhibit quite uniform Sr-Nd-Hf composition (Figs.
407 10j-l). Though the radiogenic Sr and slightly unradiogenic Nd isotopes indicate the input of crustal
408 materials, the whole-rock ε_{Hf} (t) values (+5.5 to +8.4) of this study and the zircon ε_{Hf} (t) values (+4.2 to
409 +7.7) in the literature (Yu et al., 2015) are indicative of significant mantle input or juvenile mafic
410 continental crust derived from the mantle in no distant past (Zhang et al., 2015). As noted above, many
411 adakitic rocks can be generated from the lower continental crust, but this is not applicable in our study
412 (see above). In our case, the most likely source for the andesitic magmas with inherited mantle isotopic
413 signatures parental to the QMS pluton is partial melting of the remaining part of the North Qilian ocean
414 crust (Chen et al., 2015). On the other hand, contribution from continental crust is also required. This
415 may occur in the melting region or in an evolving magma chamber rather than simple crustal level
416 assimilation, because the Sr-Nd-Hf isotopes for the MMEs and their host granodiorites are closely

similar and show a respectively narrow range of variation, and they do not show correlated variations with SiO_2 (Figs. 10j-l). Melting of recycled terrigenous sediments of upper continental crust and remaining part of the North Qilian oceanic crust in the melting region is more likely (Mo et al. 2008; Niu and O'Hara 2009; Chen et al., 2015).

In the broad context of the continental collision, the model of partial melting of the remaining part of the ocean crust and the recycled terrigenous sediments has been proposed and tested by Niu and co-workers in southern Tibet, East Kunlun and Qilian Orogenic Belts (e.g., Mo et al., 2008; Niu and O'Hara, 2009; Niu et al., 2013; Huang et al., 2014; Chen et al., 2015; Zhang et al., 2015). In their model, during collision, the underthrusting North Qilian ocean crust would subduct/underthrust slowly, tend to attain thermal equilibrium with the superjacent warm active continental margin, and evolve along a high T/P path in P-T space as a result of retarded subduction and enhanced heating (Appendix Fig. S1). The warm hydrated ocean crust of basaltic composition and sediments of felsic composition with rather similar solidi would melt together under the amphibolite facies conditions (for details see Niu et al., 2013; also see Appendix Fig. S1).

Importantly, this model can generate andesitic magmas not only with inherited mantle isotopic signatures but also compositions similar to the bulk continental crust (BCC), except for notable depletion in highly compatible elements like Mg, Cr and Ni (Mo et al., 2008). This model together with experimental results of melting of metabasalt and eclogite (Fig. 13a) implies that the relatively high $Mg^{\#}$ (also high Cr and Ni) contents in QMS adakitic granodiorites may indeed reflect melt interaction with mantle peridotite during ascent. Although magmas produced through the above process lack the adakitic signature, it can be the ideal source that generates QMS adakitic granodiorites through fractional crystallization dominated by mineral assemblages

represented by the MMEs. Note that this interpretation is consistent with binary isotope mixing calculations as proposed by Chen et al. (2015) (Figs. 14a-b), and with trace element model calculations (see above) (Figs. 9 and 15). As illustrated by these mass balance calculations, ~95% ocean crust and ~5% continental materials contribute to the source of the QMS pluton (Fig. 14), and 30%-50% fractional crystallization dominated by mineralogy and modes of the MMEs can lead to the highly evolved granodioritic composition of the QMS pluton with the adakitic signature (Figs. 9 and 15).

7. Conclusions

(1) The zircon U-Pb dating of the QMS pluton yields the same age (~430 Ma) for both the MMEs and their host granodiorite, which is the same as the closure time of the Qilian ocean and continental collision at ~440-420Ma.

(2) The MMEs and their host granodiorite also share the same mineralogy with indistinguishable isotopic compositions, all of which indicate that the MMEs are cumulate formed at earlier stages of the same magmatic system rather than representing mantle melt required by the popular magma mixing model.

(3) The QMS host granodiorite has adakite-like major and trace element features, including high Sr, Sr/Y and La/Yb, but low Y and Yb. By accepting our model for the petrogenesis of the MMEs, it follows that the QMS adakitic granodiorite resulted from fractional crystallization dominated by mineral assemblages represented by the MMEs.

(4) The parental magma for the QMS pluton is best explained as resulting from partial melting of the remaining part of ocean crust together with recycled terrigenous sediments during continental collision.

460 The resulting magma may have also experienced interaction with mantle peridotite during ascent.

461 **Acknowledgments**

462 We thank Li Su for the assistance with whole rock major, trace elements and zircon U-Pb age
463 analysis, Minwu Liu with electron microprobe analysis, and Jinlong Ma, Xirong Liang and Zhongyuan
464 Ren with whole rock Sr-Nd-Hf isotope analysis. Pu Sun, Huixiang Cui and Yuxing Ma are thanked for
465 their help with sample preparation. This work was supported by the National Natural Science
466 Foundation of China (NSFC: 91014003, 41130314), Chinese Academy of Sciences (Innovation Grant
467 Y42217101L) and grants from regional and local authorities (Shandong Province and City of Qingdao),
468 two projects of Chinese Geological Survey Departments and Offices (1212011121092,
469 1212011220928), and supported by National Oceanography Laboratory in Qingdao.

470

471 **References**

472 Andersen, T., 2002. Correction of common lead in U-Pb analyses that do not report ^{204}Pb. Chemical
473 Geology 192, 59-79.
474 Bachmann, O., Dungan, M.A., Bussy, F., 2005. Insights into shallow magmatic processes in large
475 silicic magma bodies: the trace element record in the Fish Canyon magma body, Colorado.
476 Contributions to Mineralogy and Petrology 149, 338-349.
477 Barbarin, B., 2005. Mafic magmatic enclaves and mafic rocks associated with some granitoids of the
478 central Sierra Nevada batholith, California: nature, origin, and relations with the hosts. Lithos 80,
479 155-177.

480 Barbarin, B., Didier, J., 1991. Enclaves of the Mesozoic calc-alkaline granitoids of the Sierra Nevada
481 Batholith, California. Enclaves and granite petrology. Elsevier, Amsterdam 135, 153.
482 Bea, F., Pereira, M., Stroh, A., 1994. Mineral/leucosome trace-element partitioning in a peraluminous
483 migmatite (a laser ablation-ICP-MS study). Chemical Geology 117, 291-312.
484 Black, L.P., Kamo, S.L., Allen, C.M., Aleinikoff, J.N., Davis, D.W., Korsch, R.J., Foudoulis, C., 2003.
485 TEMORA 1: a new zircon standard for Phanerozoic U–Pb geochronology. Chemical Geology 200,
486 155-170.
487 Caricchi, L., Annen, C., Rust, A., Blundy, J., 2012. Insights into the mechanisms and timescales of
488 pluton assembly from deformation patterns of mafic enclaves. Journal of Geophysical Research:
489 Solid Earth (1978–2012) 117.
490 Castillo, P.R., 2006. An overview of adakite petrogenesis. Chinese Science Bulletin 51, 257-268.
491 Castillo, P.R., 2012. Adakite petrogenesis. Lithos 134-135, 304-316.
492 Castillo, P.R., Janney, P.E., Solidum, R.U., 1999. Petrology and geochemistry of Camiguin Island,
493 southern Philippines: insights to the source of adakites and other lavas in a complex arc setting.
494 Contributions to Mineralogy and Petrology 134, 33-51.
495 Castro, A., Moreno‐Ventas, I., De la Rosa, J., 1990. Microgranular enclaves as indicators of
496 hybridization processes in granitoid rocks, Hercynian Belt, Spain. Geological Journal 25, 391-404.
497 Chappell, B., White, A., 1991. Restite enclaves and the restite model, Enclaves and granite petrology.
498 Elsevier Amsterdam, pp. 479-492.
499 Chappell, B., White, A., 1992. I-and S-type granites in the Lachlan Fold Belt. Geological Society of
500 America Special Papers 272, 1-26.
501 Chappell, B., White, A., Wyborn, D., 1987. The importance of residual source material (restite) in

granite petrogenesis. Journal of Petrology 28, 1111-1138.

Chen, B., He, J., Ma, X., 2009a. Petrogenesis of mafic enclaves from the north Taihang Yanshanian intermediate to felsic plutons: Evidence from petrological, geochemical, and zircon Hf-O isotopic data. Science in China Series D: Earth Sciences 52, 1331-1344.

Chen, B., Chen, Z.C., Jahn, B.M., 2009b. Origin of mafic enclaves from the Taihang Mesozoic orogen, north China craton. Lithos 110, 343-358.

Chen, B., Jahn, B.M., Suzuki, K., 2013a. Petrological and Nd-Sr-Os isotopic constraints on the origin of high-Mg adakitic rocks from the North China Craton: Tectonic implications. Geology 41, 91-94.

Chen, B., Chen, C., He, J., Liu, A., 2013b. Origin of Mesozoic high-Mg adakitic rocks from northeastern China: Petrological and Nd-Sr-Os isotopic constraints. Chinese Science Bulletin 58, 1941-1953.

Chen, S., Niu, Y., Sun, W., Zhang, Y., Li, J., Guo, P., Sun, P., 2015. On the origin of mafic magmatic enclaves (MMEs) in syn-collisional granitoids: evidence from the Baojishan pluton in the North Qilian Orogen, China. Mineralogy and Petrology 109, 577-596.

Chen, Y., Song, S., Niu, Y., Wei, C., 2014. Melting of continental crust during subduction initiation: A case study from the Chaidanuo peraluminous granite in the North Qilian suture zone. Geochimica et Cosmochimica Acta 132, 311-336.

Chiaradia, M., Fontbote, L., Beate, B., 2004. Cenozoic continental arc magmatism and associated mineralization in Ecuador. Mineralium Deposita 39, 204-222.

Chung, S.L., Liu, D., Ji, J., Chu, M. F., Lee, H.Y., Wen, D.J., Lo, C.H., Lee, T.Y., Qian, Q., Zhang, Q., 2003. Adakites from continental collision zones: Melting of thickened lower crust beneath

524 southern Tibet. Geology 31, 1021.
525 Chung, S.L., Chu, M.F., Zhang, Y., Xie, Y., Lo, C.H., Lee, T.Y., Lan, C.Y., Li, X., Zhang, Q., Wang, Y.,
526 2005. Tibetan tectonic evolution inferred from spatial and temporal variations in post-collisional
527 magmatism. Earth-Science Reviews 68, 173-196.
528 Clemens, J., 1989. The importance of residual source material (restite) in granite petrogenesis: a
529 comment. Journal of Petrology 30, 1313-1316.
530 Dahlquist, J., 2002. Mafic microgranular enclaves: early segregation from metaluminous magma
531 (Sierra de Chepes), Pampean Ranges, NW Argentina. Journal of South American Earth Sciences
532 15, 643-655.
533 Defant, M.J., Drummond, M.S., 1990. Derivation of some modern arc magmas by melting of young
534 subducted lithosphere. Nature 347, 662-665.
535 DePaolo, D.J., 1981. A neodymium and strontium isotopic study of the Mesozoic calc-alkaline granitic
536 batholiths of the Sierra Nevada and Peninsular Ranges, California. Journal of Geophysical
537 Research 86, 10470.
538 Didier, J., 1987. Contribution of enclave studies to the understanding of origin and evolution of granitic
539 magmas. Geologische Rundschau 76, 41-50.
540 Dodge, F.C.W., Kistler, R.W., 1990. Some additional observations on inclusions in the granitic rocks of
541 the Sierra Nevada. Journal of Geophysical Research 95, 17841.
542 Donaire, T., Pascual, E., Pin, C., Duthou, J.L., 2005. Microgranular enclaves as evidence of rapid
543 cooling in granitoid rocks: the case of the Los Pedroches granodiorite, Iberian Massif, Spain.
544 Contributions to Mineralogy and Petrology 149, 247-265.
545 Dorais, M.J., Whitney, J.A., Roden, M.F., 1990. Origin of mafic enclaves in the Dinkey Creek pluton,

546 central Sierra Nevada batholith, California. Journal of Petrology 31, 853-881.
547 Ewart, A., Griffin, W., 1994. Application of proton-microprobe data to trace-element partitioning in
548 volcanic rocks. Chemical Geology 117, 251-284.
549 Farner, M.J., Lee, C.T.A., Putirka, K.D., 2014. Mafic–felsic magma mixing limited by reactive
550 processes: A case study of biotite-rich rinds on mafic enclaves. Earth and Planetary Science
551 Letters 393, 49-59.
552 Fujimaki, H., Tatsumoto, M., Aoki, K.I., 1984. Partition coefficients of Hf, Zr, and ree between
553 phenocrysts and groundmasses. Journal of Geophysical Research 89, B662.
554 Furman, T., Spera, F.J., 1985. Co-mingling of acid and basic magma with implications for the origin of
555 mafic I-type xenoliths: field and petrochemical relations of an unusual dike complex at Eagle Lake,
556 Sequoia National Park, California, USA. Journal of Volcanology and Geothermal Research 24,
557 151-178.
558 Gao, S., Rudnick, R.L., Yuan, H.L., Liu, X.M., Liu, Y.S., Xu, W.L., Ling, W.L., Ayers, J., Wang, X.C.,
559 Wang, Q.H., 2004. Recycling lower continental crust in the North China Craton. Nature 432,
560 892–897.
561 Green, T., Blundy, J., Adam, J., Yaxley, G., 2000. SIMS determination of trace element partition
562 coefficients between garnet, clinopyroxene and hydrous basaltic liquids at 2–7.5 GPa and
563 1080–1200 C. Lithos 53, 165-187.
564 He, Y., Li, S., Hoefs, J., Kleinhanns, I.C., 2013. Sr-Nd-Pb isotopic compositions of Early Cretaceous
565 granitoids from the Dabie orogen: Constraints on the recycled lower continental crust. Lithos
566 156-159, 204-217.
567 Holden, P., Halliday, A., Stephens, W., 1987. Neodymium and strontium isotope content of microdiorite

568 enclaves points to mantle input to granitoid production. Nature 330, 53-56.
569 Hoskin, P.W., Schaltegger, U., 2003. The composition of zircon and igneous and metamorphic
570 petrogenesis. Reviews in mineralogy and geochemistry 53, 27-62.
571 Huang, H., Niu, Y., Nowell, G., Zhao, Z., Yu, X., Zhu, D.C., Mo, X., Ding, S., 2014. Geochemical
572 constraints on the petrogenesis of granitoids in the East Kunlun Orogenic belt, northern Tibetan
573 Plateau: Implications for continental crust growth through syn-collisional felsic magmatism.
574 Chemical Geology 370, 1-18.
575 Irving, A.J., Frey, F.A., 1984. Trace element abundances in megacrysts and their host basalts:
576 constraints on partition coefficients and megacryst genesis. Geochimica et Cosmochimica Acta 48,
577 1201-1221.
578 Klein, M., Stosch, H.G., Seck, H., 1997. Partitioning of high field-strength and rare-earth elements
579 between amphibole and quartz-dioritic to tonalitic melts: an experimental study. Chemical
580 Geology 138, 257-271.
581 Le Maitre, R.W., Bateman, P., Dudek, A., Keller, J., Lameyre, J., Le Bas, M., Sabine, P., Schmid, R.,
582 Sorensen, H., Streckeisen, A., 1989. A classification of igneous rocks and glossary of terms:
583 Recommendations of the International Union of Geological Sciences Subcommission on the
584 Systematics of Igneous Rocks. Blackwell Oxford.
585 Leake, B., Arps, C., Birch, W., Gilbert, M., Grice, J., Hawthorne, F., Kato, A., Kisch, H., Krivovichev,
586 V., Linthout, K., 1997. Nomenclature of Amphiboles: Report of the Subcom mittee on Amphiboles
587 of the International Mineralogi cal Association, Commission on New Minerals and Mineral
588 Names. The Canadian Mineralogist 35, 219-246.
589 Lee, C.T., Bachmann, O., 2014. How important is the role of crystal fractionation in making

intermediate magmas? Insights from Zr and P systematics. Earth and Planetary Science Letters 393, 266-274.

Lesher, C.E., 1990. Decoupling of chemical and isotopic exchange during magma mixing. Nature 344, 235-237.

Li, X.H., Li, W.X., Li, Z.X., Lo, C.H., Wang, J., Ye, M.F., Yang, Y.H., 2009. Amalgamation between the Yangtze and Cathaysia Blocks in South China: Constraints from SHRIMP U–Pb zircon ages, geochemistry and Nd–Hf isotopes of the Shuangxiwu volcanic rocks. Precambrian Research 174, 117-128.

Liu, L., Qiu, J.S., Li, Z., 2013. Origin of mafic microgranular enclaves (MMEs) and their host quartz monzonites from the Muchen pluton in Zhejiang Province, Southeast China: Implications for magma mixing and crust–mantle interaction. Lithos 160-161, 145-163.

Ma, J., Wei, G., Liu, Y., Ren, Z., Xu, Y., Yang, Y., 2013a. Precise measurement of stable (δ $^{88}/^{86}$Sr) and radiogenic ($^{87}Sr/^{86}Sr$) strontium isotope ratios in geological standard reference materials using MC-ICP-MS. Chinese Science Bulletin 58, 3111-3118.

Ma, J., Wei, G., Liu, Y., Ren, Z., Xu, Y., Yang, Y., 2013b. Precise measurement of stable neodymium isotopes of geological materials by using MC-ICP-MS. Journal of Analytical Atomic Spectrometry 28, 1926.

Ma, Q., Zheng, J.P., Xu, Y.G., Griffin, W.L., Zhang, R.S., 2015. Are continental “adakites” derived from thickened or foundered lower crust? Earth and Planetary Science Letters 419, 125-133.

Macpherson, C.G., Dreher, S.T., Thirlwall, M.F., 2006. Adakites without slab melting: High pressure differentiation of island arc magma, Mindanao, the Philippines. Earth and Planetary Science Letters 243, 581-593.

612 Mahood, G., Hildreth, W., 1983. Large partition coefficients for trace elements in high-silica rhyolites.
613 Geochimica et Cosmochimica Acta 47, 11-30.
614 Matsui, Y., Onuma, N., Nagasawa, H., Higuchi, H. and Banno, S., 1977. Crystal structure control in
615 trace element partition between crystal and magma. Tectonics 100, 315-324.
616 Mo, X., Niu, Y., Dong, G., Zhao, Z., Hou, Z., Zhou, S., Ke, S., 2008. Contribution of syncollisional
617 felsic magmatism to continental crust growth: A case study of the Paleogene Linzizong volcanic
618 Succession in southern Tibet. Chemical Geology 250, 49-67.
619 Nash, W., Crecraft, H., 1985. Partition coefficients for trace elements in silicic magmas. Geochimica et
620 Cosmochimica Acta 49, 2309-2322.
621 Niu, Y., Batiza, R., 1997. Trace element evidence from seamounts for recycled oceanic crust in the
622 Eastern Pacific mantle. Earth and Planetary Science Letters 148, 471-483.
623 Niu, Y., Regelous, M., Wendt, I.J., Batiza, R., O'Hara, M.J., 2002. Geochemistry of near-EPR
624 seamounts: importance of source vs. process and the origin of enriched mantle component. Earth
625 and Planetary Science Letters 199, 327-345.
626 Niu, Y., O'Hara, M.J., 2003. Origin of ocean island basalts: A new perspective from petrology,
627 geochemistry, and mineral physics considerations. Journal of Geophysical Research: Solid Earth
628 (1978–2012) 108.
629 Niu, Y., 2005. Generation and evolution of basaltic magmas: some basic concepts and a new view on
630 the origin of Mesozoic–Cenozoic basaltic volcanism in eastern China. Geological Journal of
631 China Universities 11, 9-46.
632 Niu, Y., O'Hara, M.J., 2009. MORB mantle hosts the missing Eu (Sr, Nb, Ta and Ti) in the continental
633 crust: New perspectives on crustal growth, crust–mantle differentiation and chemical structure of

oceanic upper mantle. Lithos 112, 1-17.

Niu, Y., Zhao, Z., Zhu, D.C., Mo, X., 2013. Continental collision zones are primary sites for net continental crust growth — A testable hypothesis. Earth-Science Reviews 127, 96-110.

Pabst, A., 1928. Observations on inclusions in the granitic rocks of the Sierra Nevada. University of California Publications in Geological Sciences 17, 325-386.

Pearce, J.A., Norry, M.J., 1979. Petrogenetic implications of Ti, Zr, Y, and Nb variations in volcanic rocks. Contributions to mineralogy and petrology 69, 33-47.

Pietranik, A., Koepke, J., Puziewicz, J., 2006. Crystallization and resorption in plutonic plagioclase: Implications on the evolution of granodiorite magma (Gęsiniec granodiorite, Strzelin Crystalline Massif, SW Poland). Lithos 86, 260-280.

Prowatke, S., Klemme, S., 2006. Trace element partitioning between apatite and silicate melts. Geochimica et Cosmochimica Acta 70, 4513-4527.

Qian, Q., Hermann, J., 2013. Partial melting of lower crust at 10–15 kbar: constraints on adakite and TTG formation. Contributions to Mineralogy and Petrology 165, 1195-1224.

Rapp, R.P., Watson, E.B., 1995. Dehydration melting of metabasalt at 8–32 kbar: implications for continental growth and crust-mantle recycling. Journal of Petrology 36, 891-931.

Richards, J.P., Kerrich, R., 2007. Special paper: adakite-like rocks: their diverse origins and questionable role in metallogenesis. Economic Geology 102, 537-576.

RodrIguez, C., Selles, D., Dungan, M., Langmuir, C., Leeman, W., 2007. Adakitic dacites formed by intracrustal crystal fractionation of water-rich parent magmas at Nevado de Longavi Volcano (36.2° S; Andean Southern Volcanic Zone, Central Chile). Journal of Petrology 48, 2033-2061.

Ronov, A., Yaroshevsky, A., 1976. A new model for the chemical structure of the Earth's crust.

Geochemistry International 13, 89-121.

Rudnick, R., Gao, S., 2003. Composition of the continental crust. Treatise on geochemistry 3, 1-64.

Schnetzler, C., Philpotts, J.A., 1970. Partition coefficients of rare-earth elements between igneous matrix material and rock-forming mineral phenocrysts—II. Geochimica et Cosmochimica Acta 34, 331-340.

Sen, C., Dunn, T., 1994. Dehydration melting of a basaltic composition amphibolite at 1.5 and 2.0 GPa: implications for the origin of adakites. Contributions to Mineralogy and Petrology 117, 394-409.

Song, S., Su, L., Niu, Y., Zhang, L., Zhang, G., 2007. Petrological and geochemical constraints on the origin of garnet peridotite in the North Qaidam ultrahigh-pressure metamorphic belt, northwestern China. Lithos 96, 243-265.

Song, S., Niu, Y., Wei, C., Ji, J., Su, L., 2010a. Metamorphism, anatexis, zircon ages and tectonic evolution of the Gongshan block in the northern Indochina continent—An eastern extension of the Lhasa Block. Lithos 120, 327-346.

Song, S., Su, L., Li, X.H., Zhang, G., Niu, Y., Zhang, L., 2010b. Tracing the 850-Ma continental flood basalts from a piece of subducted continental crust in the North Qaidam UHPM belt, NW China. Precambrian Research 183, 805-816.

Song, S., Niu, Y., Su, L., Xia, X., 2013. Tectonics of the North Qilian orogen, NW China. Gondwana Research 23, 1378-1401.

Song, S., Niu, Y., Su, L., Wei, C., Zhang, L., 2014a. Adakitic (tonalitic-trondhjemitic) magmas resulting from eclogite decompression and dehydration melting during exhumation in response to continental collision. Geochimica et Cosmochimica Acta 130, 42-62.

Song, S., Niu, Y., Su, L., Zhang, C., Zhang, L., 2014b. Continental orogenesis from ocean subduction,

678 continent collision/subduction, to orogen collapse, and orogen recycling: The example of the
679 North Qaidam UHPM belt, NW China. Earth-Science Reviews 129, 59-84.
680 Streck, M.J., Leeman, W.P., Chesley, J., 2007. High-magnesian andesite from Mount Shasta: A product
681 of magma mixing and contamination, not a primitive mantle melt. Geology 35, 351.
682 Sun, S.S., McDonough, W., 1989. Chemical and isotopic systematics of oceanic basalts: implications
683 for mantle composition and processes. Geological Society, London, Special Publications 42,
684 313-345.
685 Thomas, J., Bodnar, R., Shimizu, N., Sinha, A., 2002. Determination of zircon/melt trace element
686 partition coefficients from SIMS analysis of melt inclusions in zircon. Geochimica et
687 Cosmochimica Acta 66, 2887-2901.
688 Tseng, C.Y., Yang, H.J., Yang, H.Y., Liu, D., Wu, C., Cheng, C.K., Chen, C.H., Ker, C.M., 2009.
689 Continuity of the North Qilian and North Qinling orogenic belts, Central Orogenic System of
690 China: Evidence from newly discovered Paleozoic adakitic rocks. Gondwana Research 16,
691 285-293.
692 Vernon, R., 1984. Microgranitoid enclaves in granites—globules of hybrid magma quenched in a
693 plutonic environment. Nature 309, 438-439.
694 Vernon, R.H., 1983. Restite, xenoliths and microgranitoid enclaves in granites. Journal and Proceedings
695 of the Royal Society of New South Wales 116, 77–103.
696 Wang, J., Wu, C., Cai, Z., Guo, Y., Wu, J., Liu, X., 2006a. Early Paleozoic high-Mg adakite froin
697 Yindongliang in the eastern section of the North Qilian: Implications for geodynamics and Cu-Au
698 mineralization.. Acta Petrol Sinica 22, 2655–2664. (in Chinese with English abstract)
699 Wang, Q., McDermott, F., Xu, J.F., Bellon, H., Zhu, Y.T., 2005. Cenozoic K-rich adakitic volcanic

rocks in the Hohxil area, northern Tibet: Lower-crustal melting in an intracontinental setting. Geology 33, 465.

Wang, Q., Wyman, D.A., Xu, J.F., Zhao, Z.H., Jian, P., Xiong, X.L., Bao, Z.W., Li, C.F., Bai, Z.H., 2006b. Petrogenesis of Cretaceous adakitic and shoshonitic igneous rocks in the Luzong area, Anhui Province (eastern China): Implications for geodynamics and Cu–Au mineralization. Lithos 89, 424-446.

Wang, Q., Wyman, D.A., Xu, J., Jian, P., Zhao, Z., Li, C., Xu, W., Ma, J., He, B., 2007. Early Cretaceous adakitic granites in the Northern Dabie Complex, central China: Implications for partial melting and delamination of thickened lower crust. Geochimica et Cosmochimica Acta 71, 2609-2636.

Wang, Q., Wyman, D.A., Xu, J., Dong, Y., Vasconcelos, P.M., Pearson, N., Wan, Y., Dong, H., Li, C., Yu, Y., Zhu, T., Feng, X., Zhang, Q., Zi, F., Chu, Z., 2008. Eocene melting of subducting continental crust and early uplifting of central Tibet: Evidence from central-western Qiangtang high-K calc-alkaline andesites, dacites and rhyolites. Earth and Planetary Science Letters 272, 158-171.

Wang, Q., Li, X.H., Jia, X.H., Wyman, D., Tang, G.J., Li, Z.X., Ma, L., Yang, Y.H., Jiang, Z.Q., Gou, G.N., 2013. Late Early Cretaceous adakitic granitoids and associated magnesian and potassium‐rich mafic enclaves and dikes in the Tunchang–Fengmu area, Hainan Province (South China): Partial melting of lower crust and mantle, and magma hybridization. Chemical Geology 328, 222-243.

Wiedenbeck, M., Alle, P., Corfu, F., Griffin, W., Meier, M., Oberli, F., Quadt, A.v., Roddick, J., Spiegel, W., 1995. Three natural zircon standards for U-Th-Pb, Lu-Hf, trace element and REE analyses.

722 Geostandards newsletter 19, 1-23.
723 Xiong, X.L., Adam, J., Green, T.H., 2005. Rutile stability and rutile/melt HFSE partitioning during
724 partial melting of hydrous basalt: Implications for TTG genesis. Chemical Geology 218, 339-359.
725 Xu, J.F., Shinjo, R., Defant, M.J., Wang, Q., Rapp, R.P., 2002. Origin of Mesozoic adakitic intrusive
726 rocks in the Ningzhen area of east China: Partial melting of delaminated lower continental crust?
727 Geology 30, 1111.
728 Xu, W., Gao, S., Wang, Q., Wang, D., Liu, Y., 2006. Mesozoic crustal thickening of the eastern North
729 China craton: Evidence from eclogite xenoliths and petrologic implications. Geology 34, 721-724.
730 Yu, S., Zhang, J., Qin, H., Sun, D., Zhao, X., Cong, F., Li, Y., 2015. Petrogenesis of the early Paleozoic
731 low-Mg and high-Mg adakitic rocks in the North Qilian orogenic belt, NW China: Implications for
732 transition from crustal thickening to extension thinning. Journal of Asian Earth Sciences 107,
733 122-139.
734 Zhang, C., Ma, C., Holtz, F., 2010. Origin of high-Mg adakitic magmatic enclaves from the Meichuan
735 pluton, southern Dabie orogen (central China): Implications for delamination of the lower
736 continental crust and melt-mantle interaction. Lithos 119, 467-484.
737 Zhang, J., Meng, F., Wan, Y., 2007. A cold Early Palaeozoic subduction zone in the North Qilian
738 Mountains, NW China: petrological and U-Pb geochronological constraints. Journal of
739 Metamorphic Geology 25, 285-304.
740 Zhang, Y., Niu, Y., Hu, Y., Liu, J., Ye, L., Kong, J., Duan, M., 2015. The syncollisional granitoid
741 magmatism and continental crust growth in the West Kunlun Orogen, China - Evidence from
742 geochronology and geochemistry of the Arkarz pluton. Lithos. doi: 10.1016/j.lithos.2015.05.007
743 (in press).

744

745 **Figure captions：**

746 **Fig.1:** (a) Simplified geological map of the North Qilian Orogen showing distributions of the main
747 tectonic units (modified after Song et al., 2013; Chen et al., 2015). (b) Simplified map of the Qumushan
748 (QMS) and Baojishan (BJS) area in the eastern section of the North Qilian Orogen. U-Pb ages are
749 shown for granodiorite and MMEs in the BJS and QMS plutons from Chen et al. (2015), Yu et al.
750 (2015) and this study as indicated.

751 **Fig. 2:** Photographs of the adakitic granodiorite and the MMEs in the field and in thin-sections. (a), (b)
752 and (c) showing the sharp contact of MMEs of varying size with their host granodiorite with MMEs
753 being finer-grained than the host; (d) showing the mineral assemblage of the adakitic host granodiorite
754 (QMS12-02host) and (e), (f) showing the mineral assemblage of MMEs (QMS12-02MME,
755 QMS12-06MME). Amp = amphibole; Bt = biotite; Pl= plagioclase; Qz = quartz; Ap = apatite; Zrn=
756 zircon. Plates c-f are taken under cross-polarized light.

757 **Fig. 3:** Photomicrographs showing a plagioclase crystal with a high-Ca core rimmed by a euhedral
758 overgrowth of low-Ca plagioclase in both (a) adakitic rocks (e.g., QMS12-04host) and (b) MMEs (e.g.,
759 QMS12-04MME). Numerals are the An contents. See ~~Appendix B~~Appendix 2 for compositional data.

760 **Fig. 4:** Chemical compositions of amphiboles from the host granodiorite and MMEs in the amphibole
761 classification diagram (Leake et al., 1997). Data from the host granodiorites and the MMEs of BJS
762 pluton (Chen et al., 2015) are also shown for comparison.

763 **Fig. 5:** Concordia diagrams of LA-ICP-MS U-Pb zircon age data and representative CL images of
764 zircon grains showing spots for the host adakitic granodiorites (a, c) and the MMEs (b, d) in the QMS

765 pluton.

766 **Fig. 6:** Classification diagrams of the host granodiorites and the MMEs in the QMS pluton. (a) Total
767 alkalis *vs*. SiO_2 (Le Maitre et al., 1989), (b) K_2O *vs*. SiO_2, and (c) A/NK *vs*. A/CNK. The blue circles
768 and squares are data from BJS granodiorites and their MMEs (Chen et al., 2015), and the open circles
769 are literature data on the QMS granodiorites (Wang et al., 2006a; Tseng et al., 2009; Yu et al., 2015).

770 **Fig. 7:** (a) Chondrite normalized REE patterns for the QMS host adakitic granodiorites and the MMEs;
771 (b) host rock-normalized REE patterns of MMEs. Chondrite REE values and bulk continental crust
772 (BCC) are from Sun and McDonough (1989) and Rudnick and Gao (2003), respectively. Shaded fields
773 of BJS granodiorite and the MMEs are from Chen et al. (2015).

774 **Fig. 8:** Average ocean crust-normalized (OC; Niu and O'Hara, 2003) trace element patterns for the
775 QMS host adakitic granodiorites and the MMEs.

776 **Fig. 9:** Plots of (a) Sr/Y vs. Y, where fields of adakite, and normal arc andesite-dacite-rhyolite are from
777 Defant and Drummond (1990); (b) La/Yb vs. Yb, discrimination lines are from Richards and Kerrich
778 (2007); (c) $(Dy/Yb)_N$ vs $(La/Yb)_N$, and (d) Eu/Eu* vs. Sr. Results in a-d using Rayleigh fractional
779 crystallization models indicate the effects of garnet, amphibole, plagioclase, zircon and apatite
780 fractionation on Sr/Y and Y (a), on La/Yb and Yb (b), on $(Dy/Yb)_N$ and $(La/Yb)_N$ (c), and on Eu/Eu*
781 and Sr (d). The partition coefficients used and modeling details are given in ~~Table 3~~Appendix 6. Two
782 crystallization models were designed to elucidate the effect of crystallization on bulk-rock (assumed to
783 approximate melt) trace element systematics: (1) Model A, in reasonable agreement with observed
784 mineral proportions of the MMEs, 50% amphibole, 40% plagioclase, 7.52% biotite, 2.2% apatite, 0.2%
785 zircon and 0.03% sphene; (2) Model B, 50% amphibole, 40% plagioclase, 7.6% biotite, 2.4% garnet.
786 Data sources for the QMS and BJS plutons are the same as in Fig. 6. Amp = amphibole; Bt = biotite;

Pl= plagioclase; Ap = apatite; Zrn=zircon; Grt = garnet; Spn=sphene.

Fig. 10: SiO_2 variation diagrams of (a) MgO, (b) $Fe_2O_3^T$, (c) TiO_2, (d) CaO, (e) MnO, (f) P_2O_5, (g) Eu, (h) Hf, (i) La/Sm, (j) $^{87}Sr/^{86}Sr_{(t)}$, (k) $\varepsilon_{Nd}(t)$ and (l) $\varepsilon_{Hf}(t)$. Fractional crystallization trends in g–i: the inverse linear trend of SiO_2 versus Eu and Hf indicate the effects of plagioclase and zircon fractional crystallization, respectively. Because Sm is incorporated more easily than Hf in amphibole (Fujimaki et al., 1984; Klein et al., 1997), amphibole crystallization will cause Hf/Sm increase in residual magmas (i). Crustal contamination and (or) basalt-rhyolite mixing trend in j-l are after Wang et al. (2008). Data sources of the QMS and BJS pluton are the same as in Fig. 6. The average zircon $\varepsilon_{Hf}(t)$ isotopic data (6.2±2, 2σ) calculated from Yu et al. (2015) is also presented in l.

Fig. 11: (a) SiO_2 versus P_2O_5; (b) SiO_2 versus Zr. Data for Island arc basalt (n=284 for P and 277 for Zr), boninite (n=37 for P and 34 for Zr) and rhyolite (n=66 for P and 45 for Zr) are from the Georoc database (http://georoc.mpch-mainz.gwdg.de/georoc/). Dashed and solid lines in a-b are hypothetical mixing lines and linear trend defined the QMS granodiorite and their MMEs, respectively. Data sources of the QMS and BJS plutons are the same as in Fig. 6.

Fig. 12: Cartoon illustrating a possible scenario for MME formation. Earlier crystallized cumulate with the mineral assemblage of amphibole, biotite, plagioclase and accessory minerals such as zircon and apatite (a), which was later disturbed by subsequent magma replenishment in the magma chamber, constituting MMEs in the dominant host granodiorite.

Fig. 13: Plots of (a) SiO_2 versus $Mg^{\#}$; (b) Na_2O versus K_2O. Data sources: classical adakite, resulting from partial melting of subducted ocean crust in modern arcs, are from the GeoRoc database (http://georoc.mpch-mainz.gwdg.de/georoc/); Tibet Plateau (Chung et al., 2003; Wang et al., 2005), Dabie Orogen (He et al., 2013; Wang et al., 2007), Yangtze Craton (Xu et al., 2002; Wang et al.,

2006b); North China Craton (Chen et al., 2013a; Ma et al., 2015) , experimental data (Sen and Dunn, 1994; Rapp and Watson, 1995. Data sources of the QMS and BJS plutons are the same as in Fig. 6.

Fig. 14: (a) Nd–Sr and (b) Nd-Hf isotope diagrams for the QMS adakitic rocks and their MMEs. The MORB data are from Niu and Batiza (1997) and Niu et al. (2002), other data sources are the same as Fig. 13. Binary isotope mixing calculations between North Qilian Ocean MORB (average composition: Sr=159.6 ppm, Nd=10.5 ppm, Hf=2.41, $^{87}Sr/^{76}Sr_{(t)}$=0.7054, ε_{Nd} (t)=5.44, ε_{Hf} (t)=9.93) and Mohe Basement (average composition: Sr=586 ppm, Nd=32.97 ppm, Hf=3.44, $^{87}Sr/^{76}Sr_{(t)}$=0.7234, ε_{Nd} (t)=-19.80, ε_{Hf} (t)=-43.65) are after Chen et al. (2015) and referrences therein. $K=[(Sr/Nd)_{MORB}]/[(Sr/Nd)_{Mohe\ basement}]$, where K_{max}, K_{min}, and $K_{average}$ are the maximum, minimum and average values respectively.

Fig. 15: Shows 30%, 40%, 50% and 60% fractional crystallization of mineral assemblages of Model A and Model B from the assumed magma along with the BCC and QMS adakitic granodiorites and their MMEs on primitive mantle normalized multi-element diagram. The light red and green shaded regions are the field of QMS adakitic granodiorite and MMEs, respectively.

Appendix Fig. S1: Simplified phase diagram showing hydrous solidi of basalts and granitic rocks modified from Niu et al. (2013) (after Niu, 2005). The red line with arrow illustrates the concept of the underthrusting North Qilian oceanic crust evolve along a high T/P path as a result of retarded subducting and enhanced heating upon continental collision at a prior active continental margin setting.

Table captions:

~~Table 1: Whole-rock major and trace elements analysis of the host adakitic granodiorites and the mafic~~

~~magmatic enclaves in the NQOB.~~

~~Table 2: Whole-rock Sr-Nd-Hf isotopic analyses for the host adakitic granodiorites and the mafic magmatic enclaves in the NQOB.~~

~~Table 3: Relevant partition coefficients, assumed melt and model compositions.~~

~~Appendix A~~Appendix 1: U-Th-Pb analyses by LA-ICP-MS for zircons from host granodiorites (QMS12-04host and QMS12-10host) and the mafic magmatic enclaves (QMS12-04MME and QMS12-10MME).

~~Appendix B~~Appendix 2: Microprobe analysis of representative plagioclase in the host granodiorites and the mafic magmatic enclaves.

~~Appendix C~~Appendix 3: Microprobe analysis of representative amphibole in the host granodiorites and the mafic magmatic enclaves.

Appendix 4: Whole-rock major and trace elements analysis of the host adakitic granodiorites and the mafic magmatic enclaves in the NQOB.

Appendix 5: Whole rock Sr-Nd-Hf isotopic analyses for the host adakitic granodiorites and the mafic magmatic enclaves in the NQOB.

Appendix 6: Relevant partition coefficients, assumed melt and model compositions.

Figure 1

Click here to download high resolution image

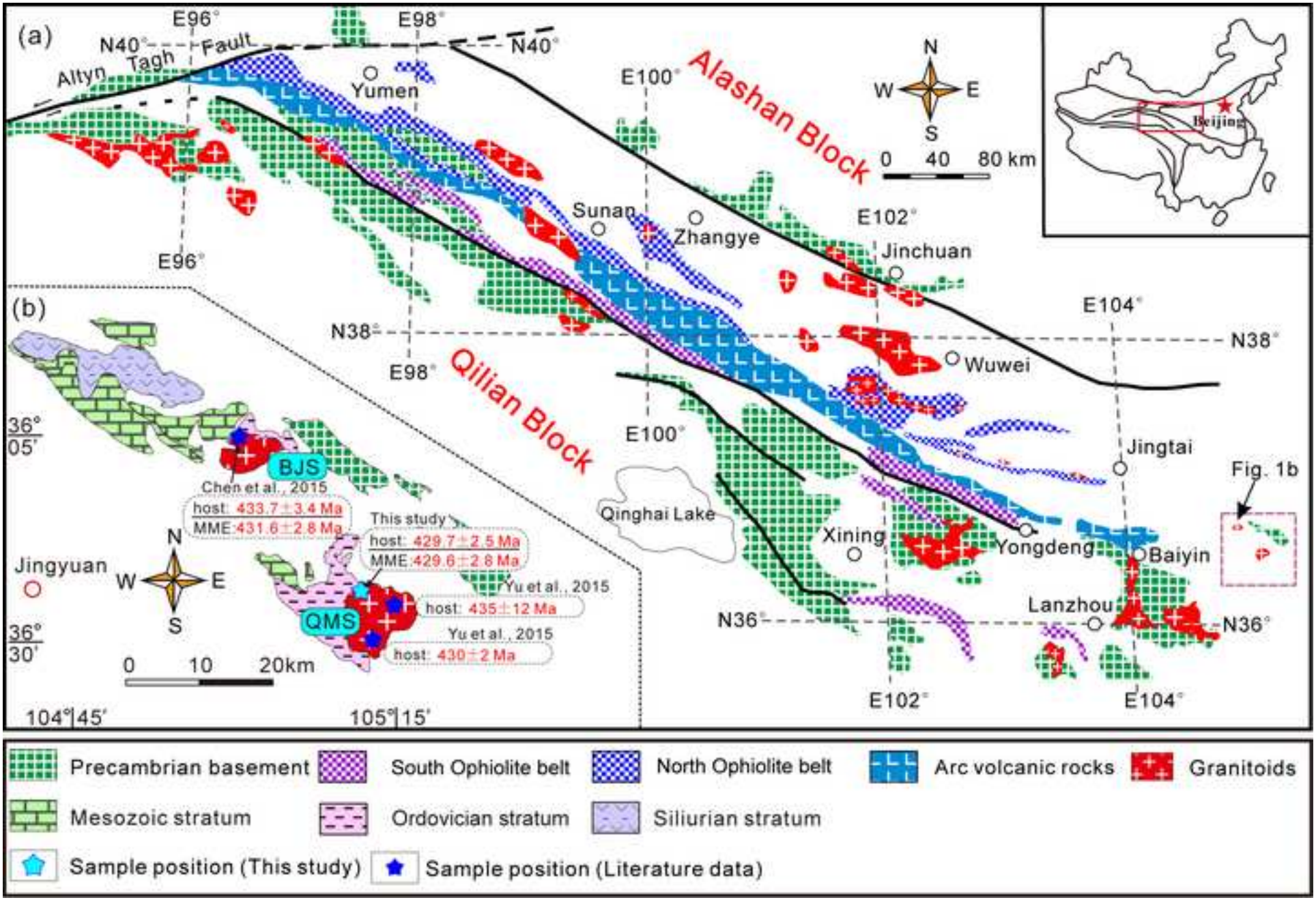

Figure 2

Click here to download high resolution image

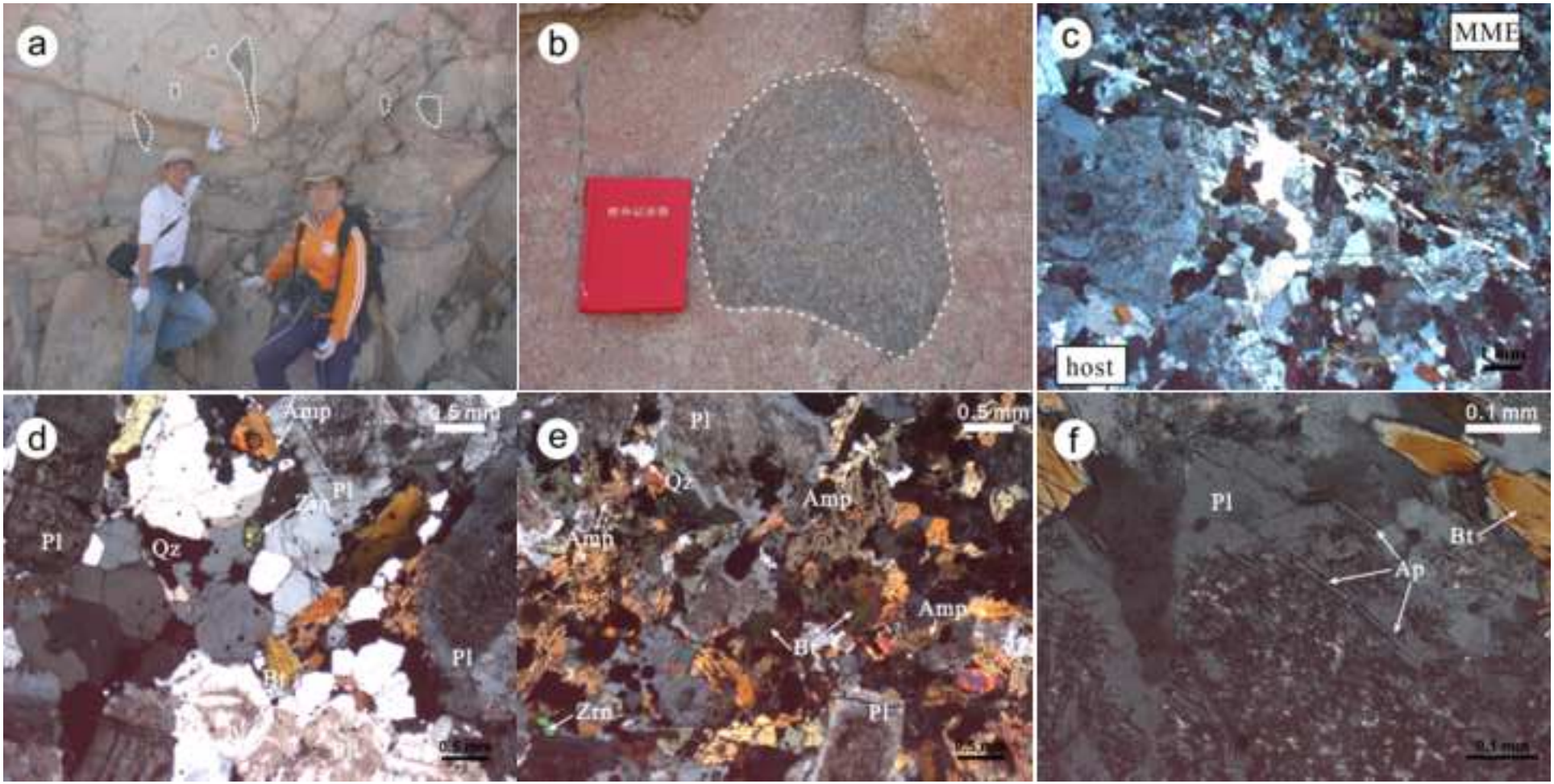

Figure 3

Click here to download high resolution image

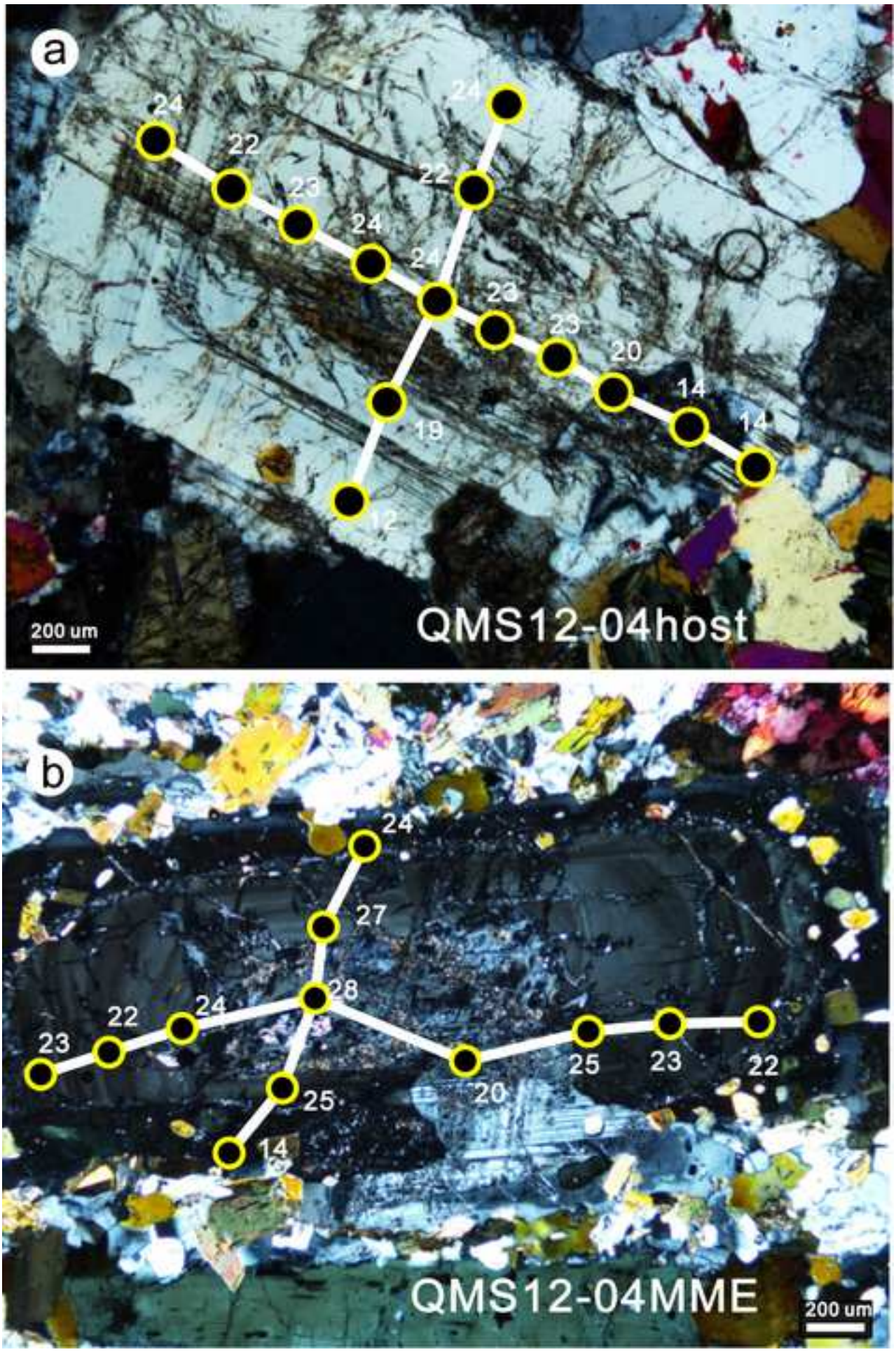

Figure 4

Click here to download high resolution image

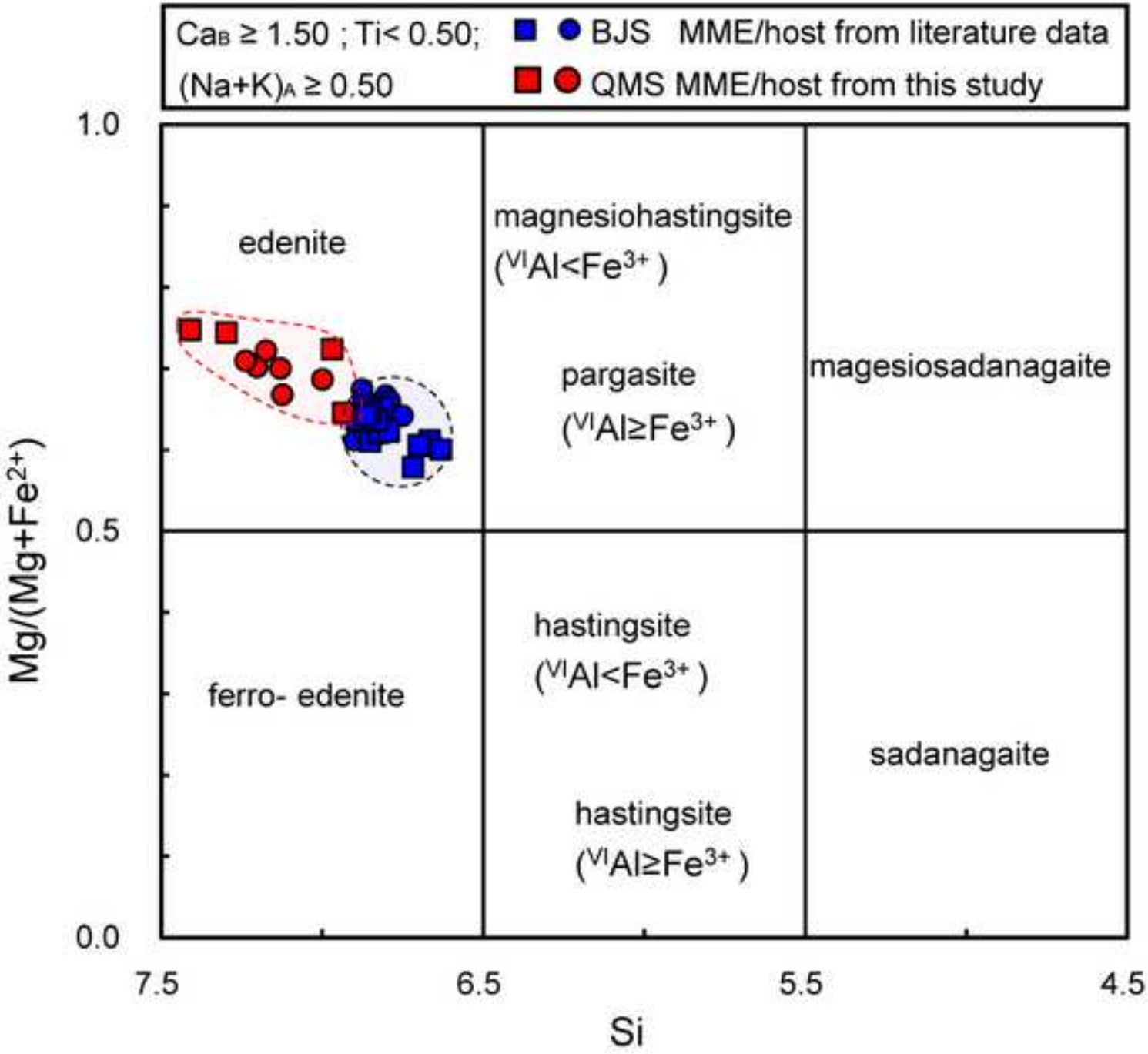

Figure 5

Click here to download high resolution image

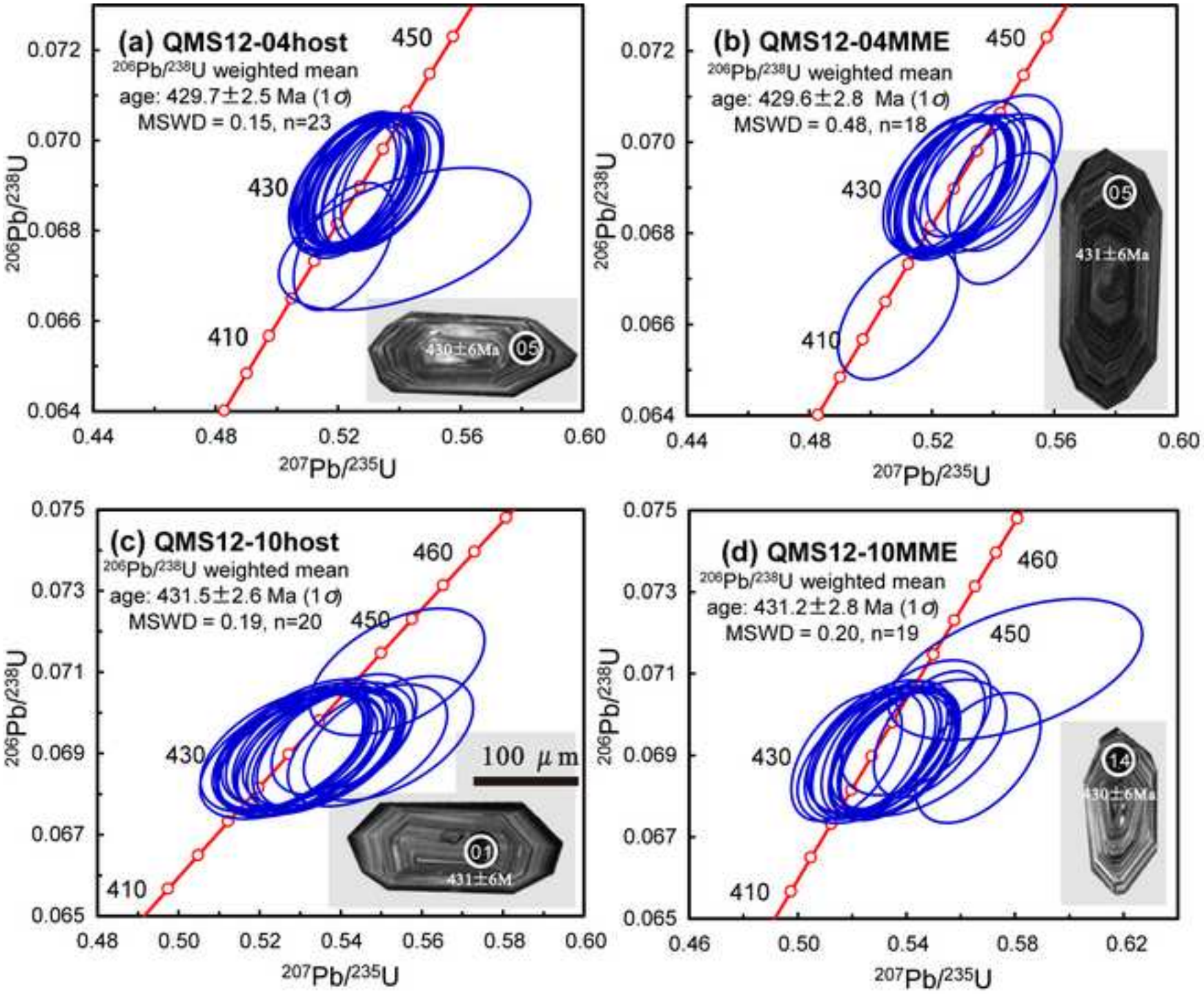

Figure 6

Click here to download high resolution image

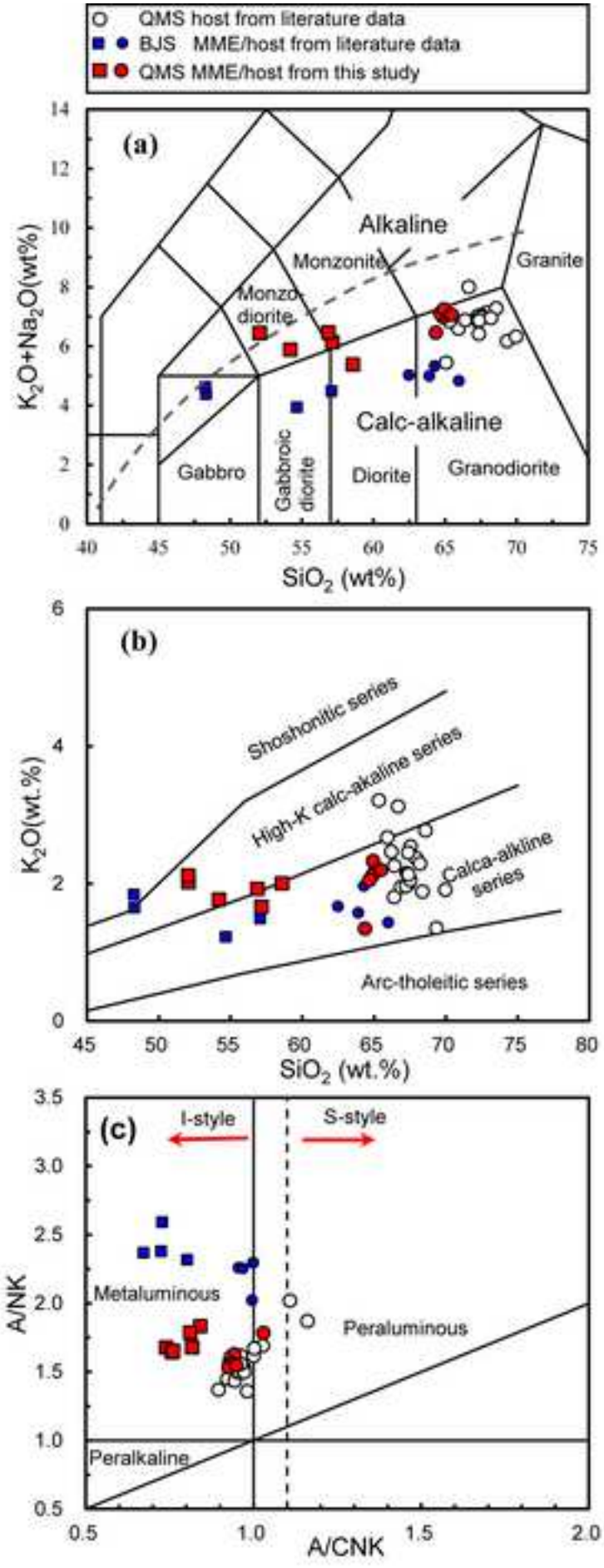

Figure 7

Click here to download high resolution image

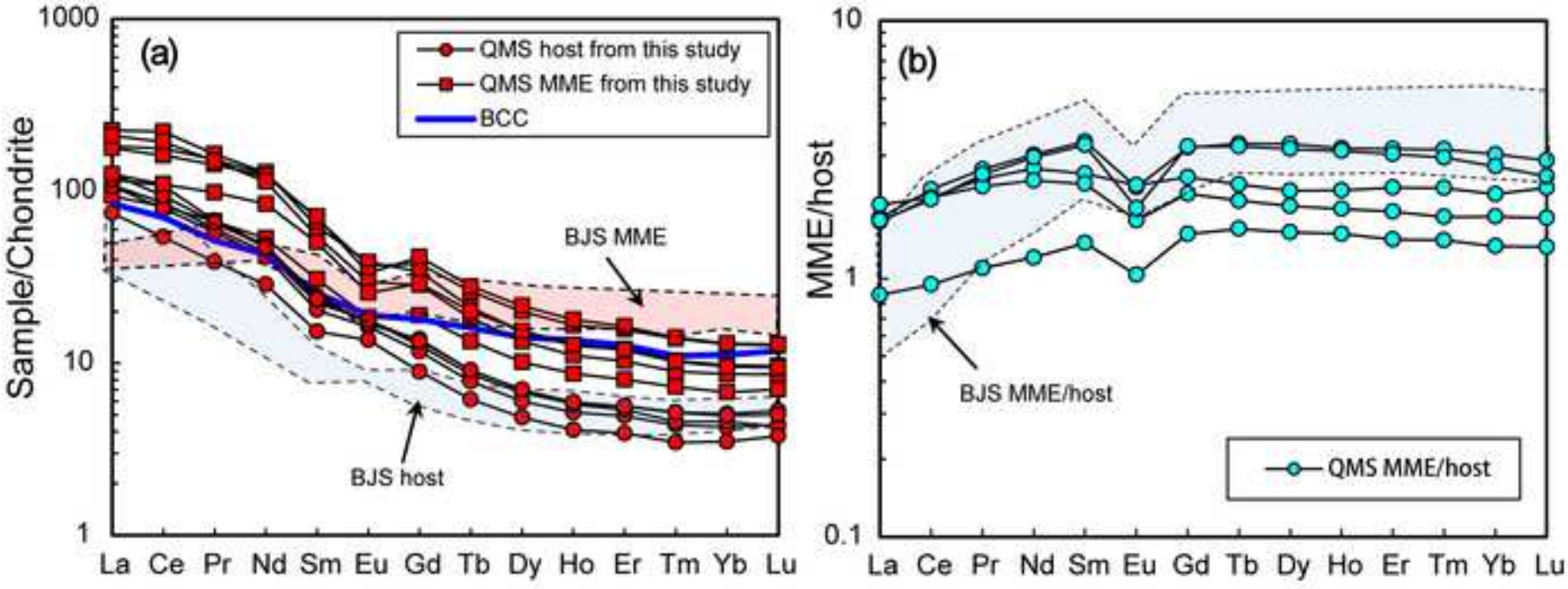

Figure 8

Click here to download high resolution image

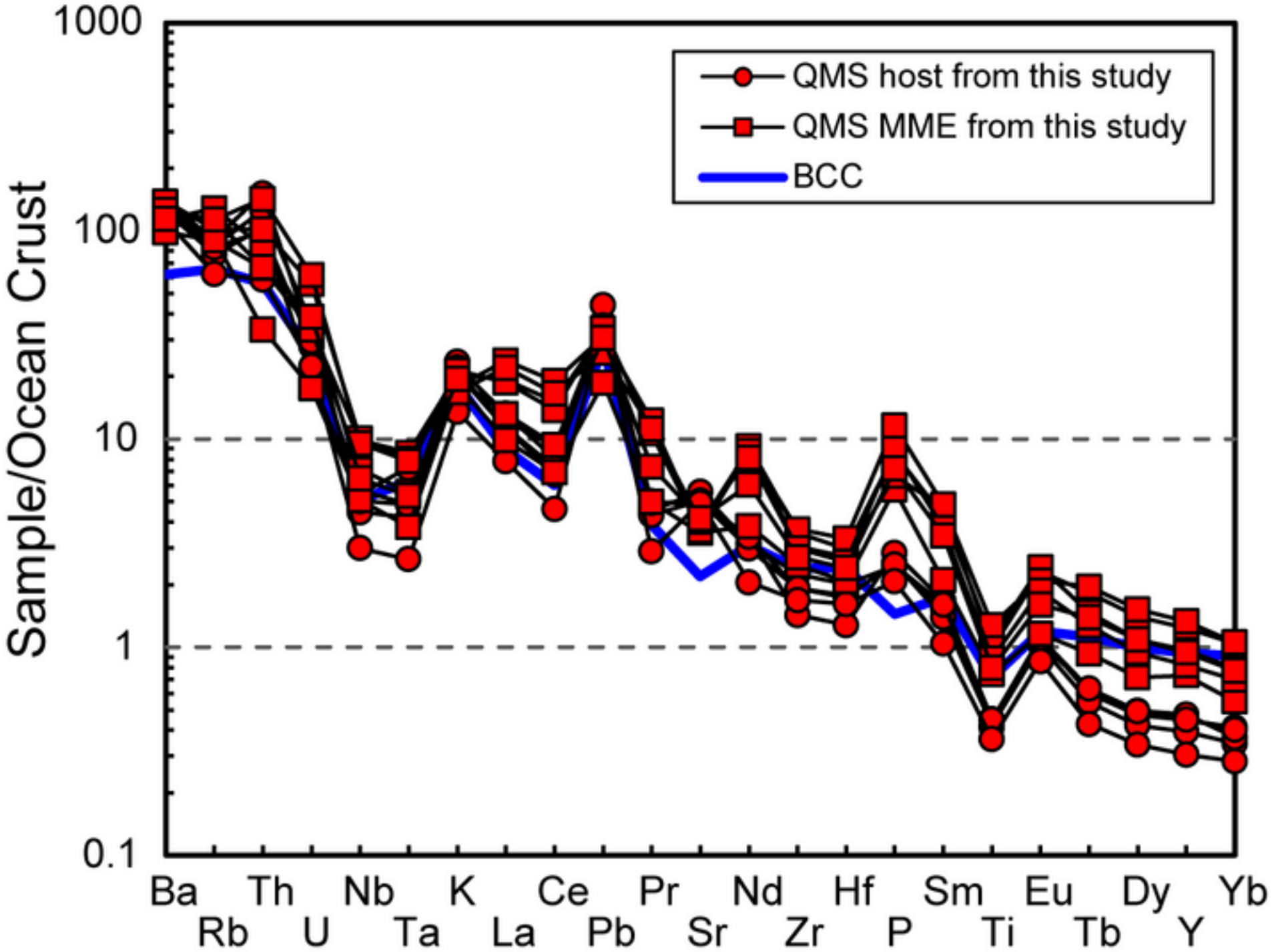

Figure 9

Click here to download high resolution image

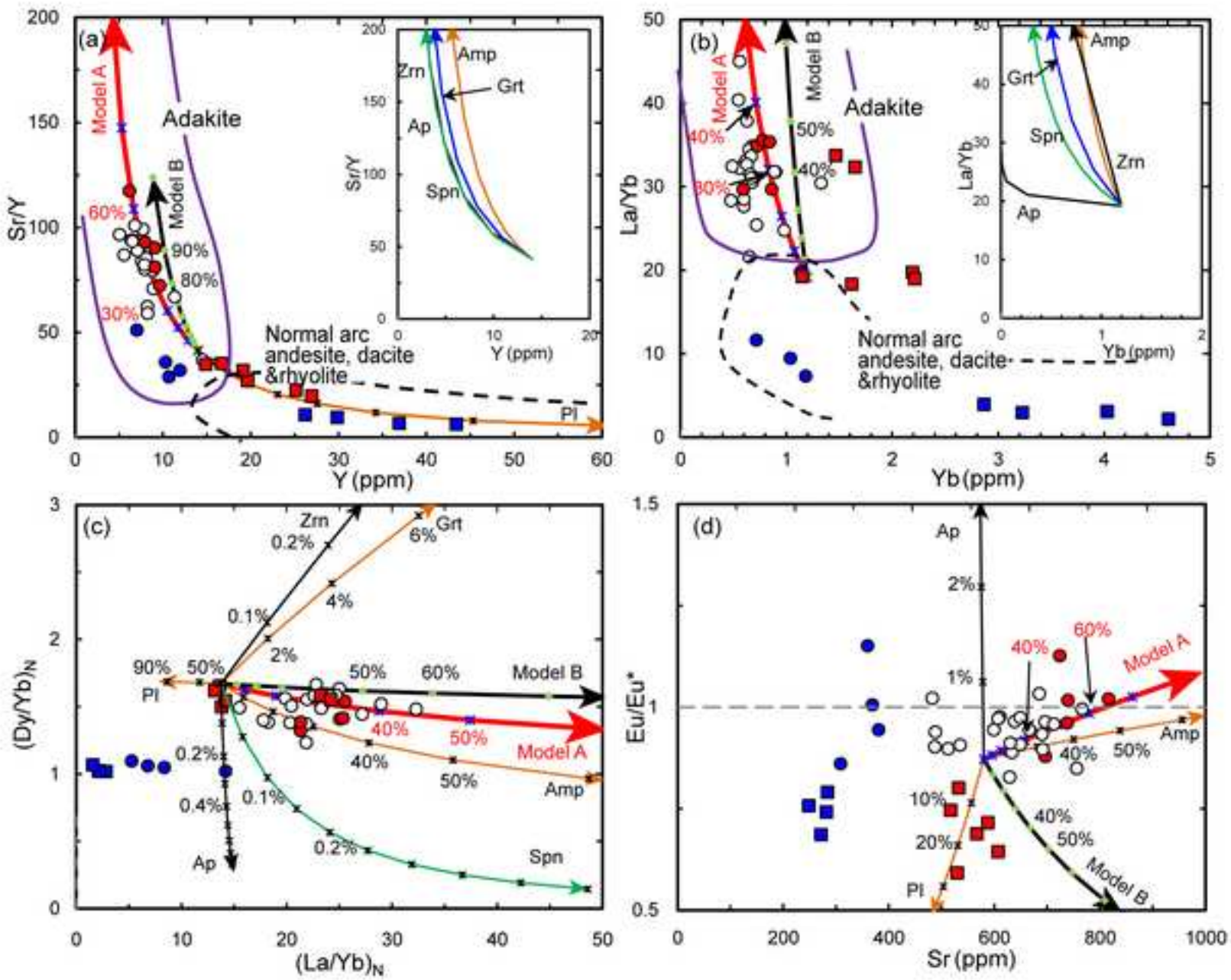

Figure

Click here to download high resolution image

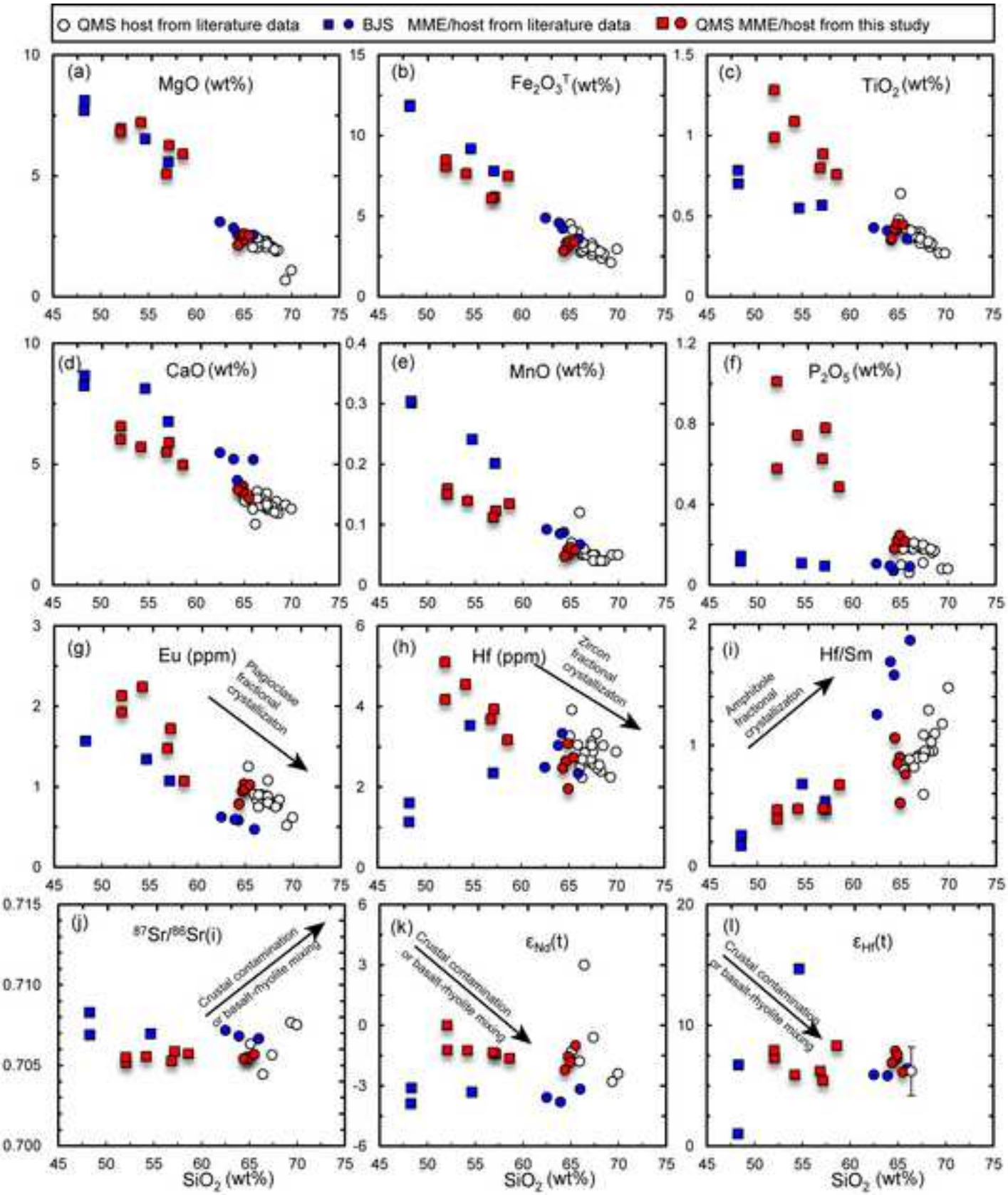

Figure

Click here to download high resolution image

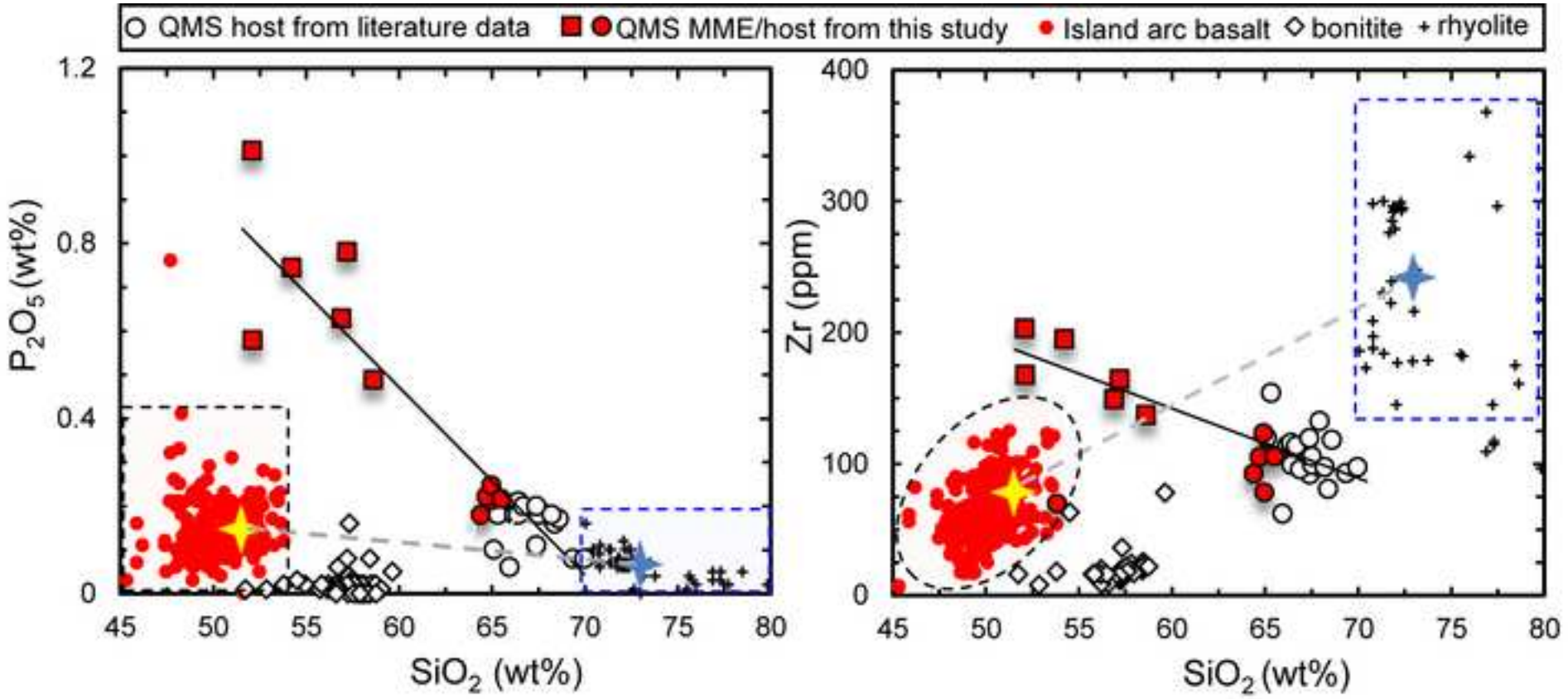

Figure 12

Click here to download high resolution image

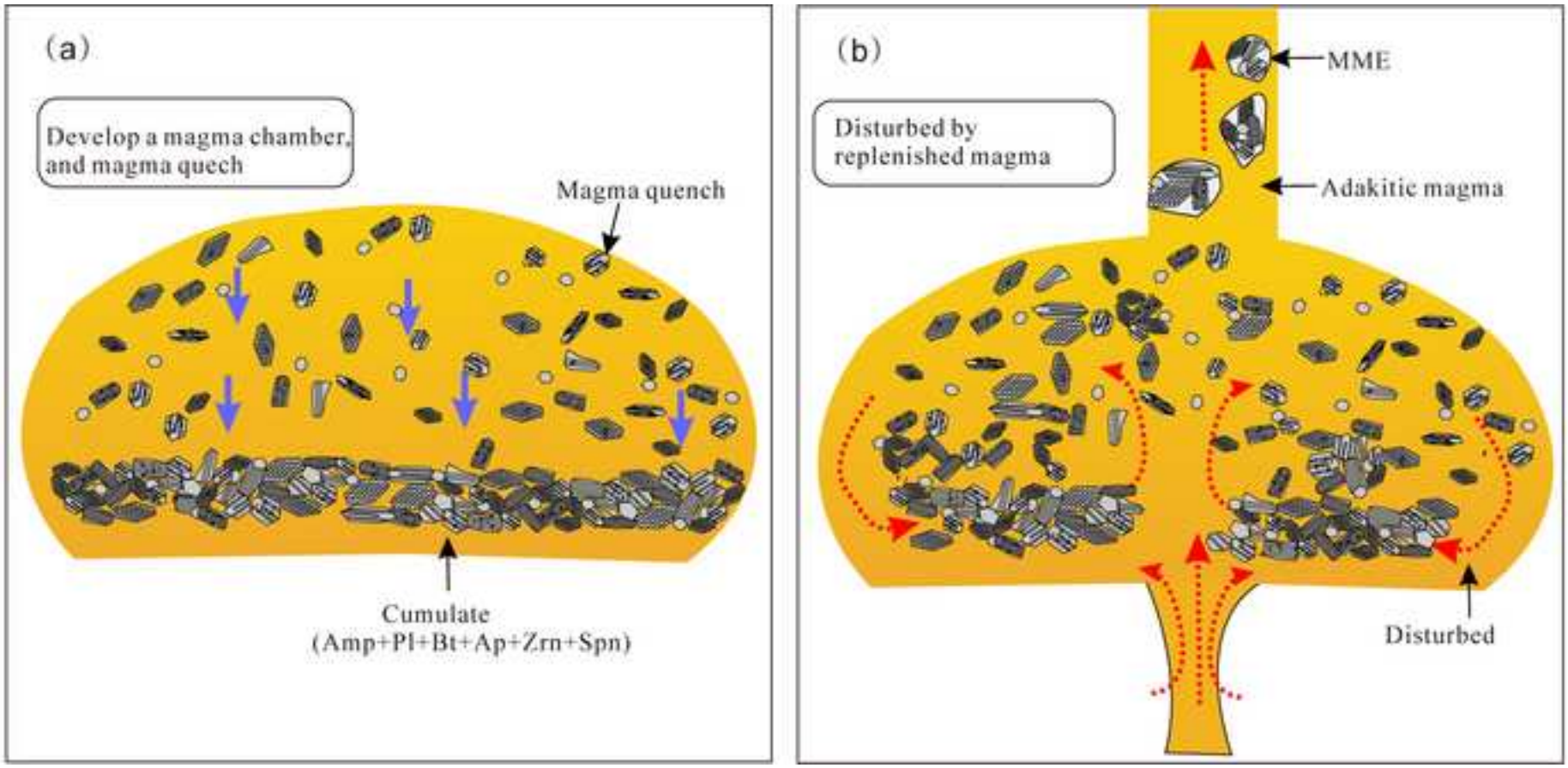

Figure

Click here to download high resolution image

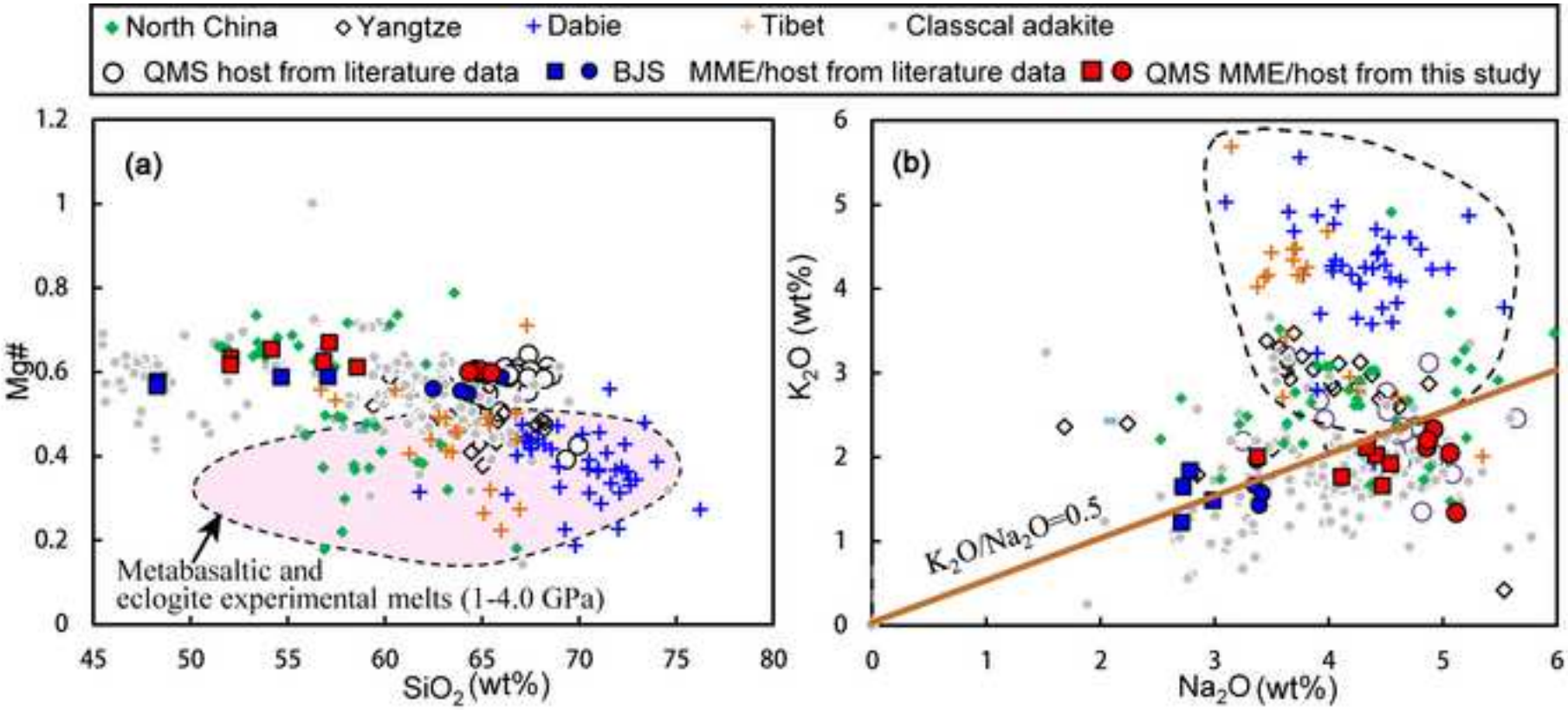

Figure 14

Click here to download high resolution image

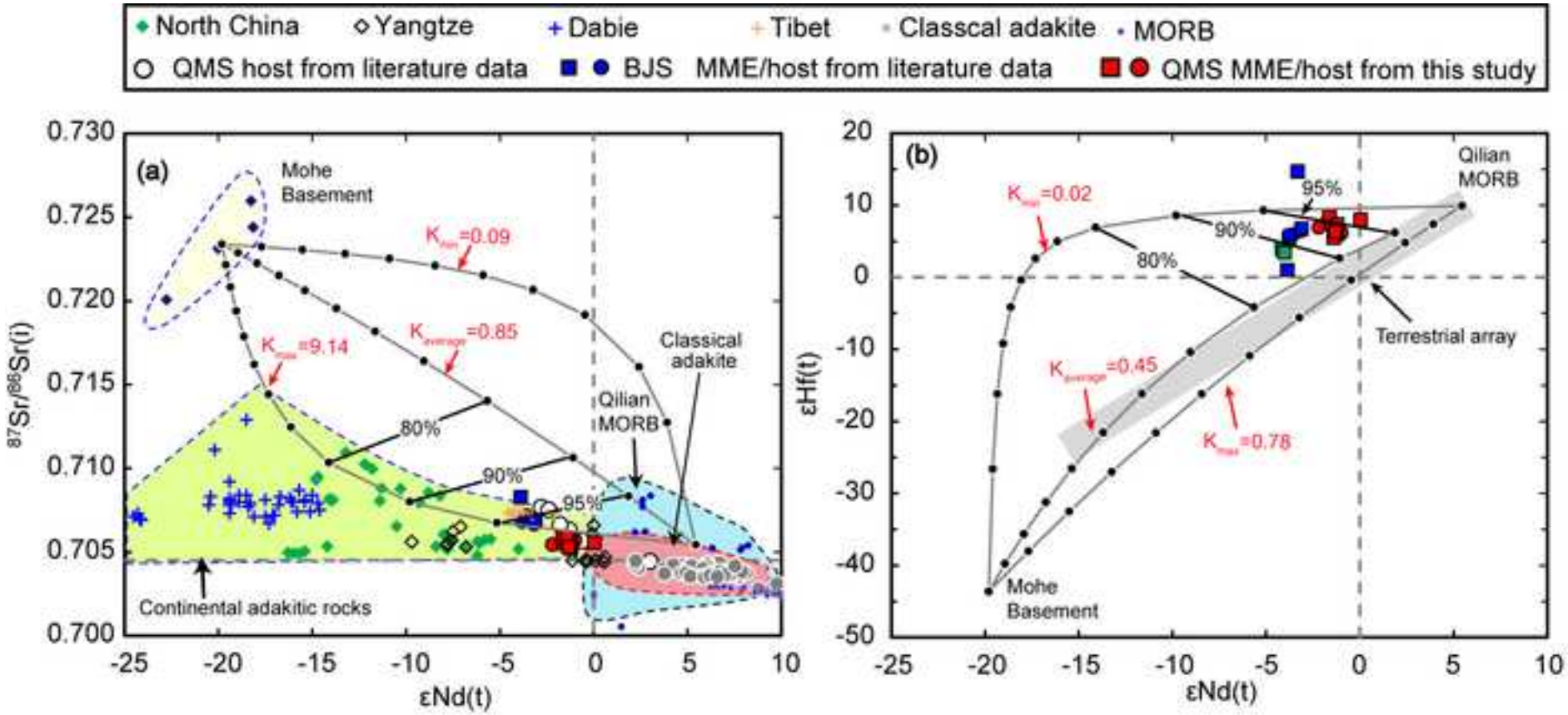

Figure 15

Click here to download high resolution image

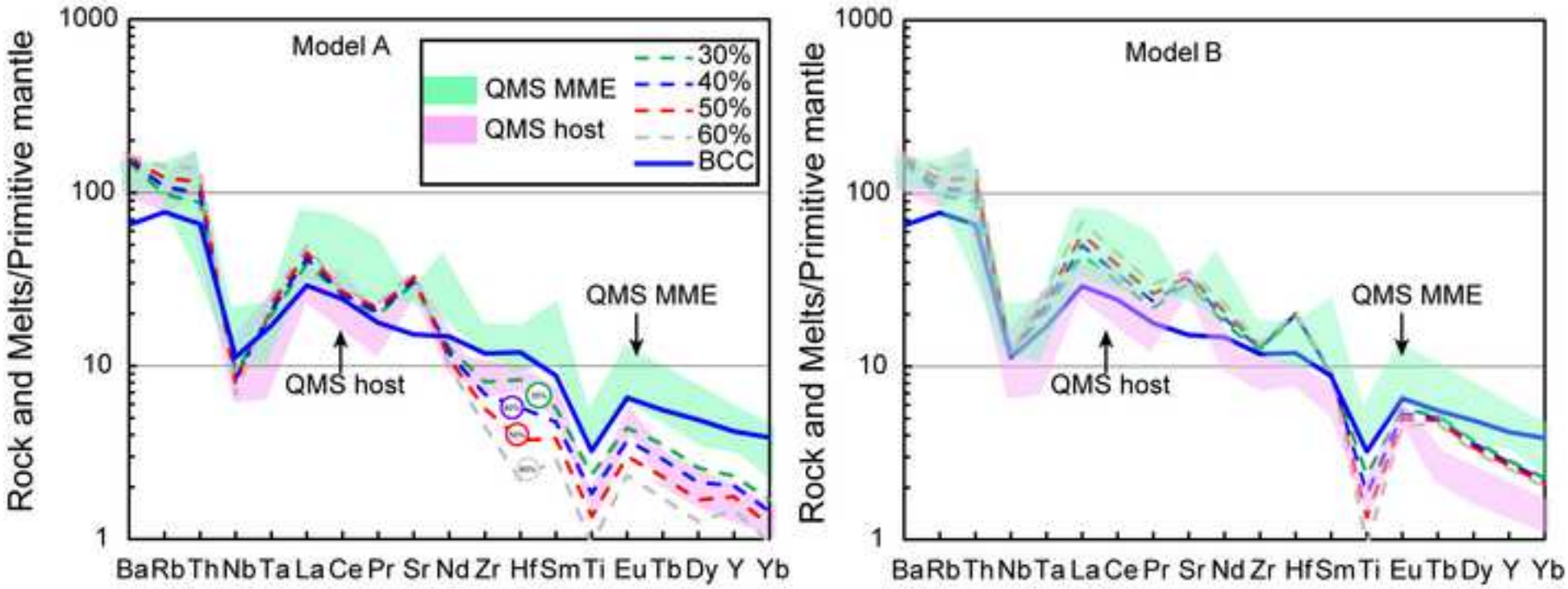

Appendix Fig.S1

Click here to download high resolution image

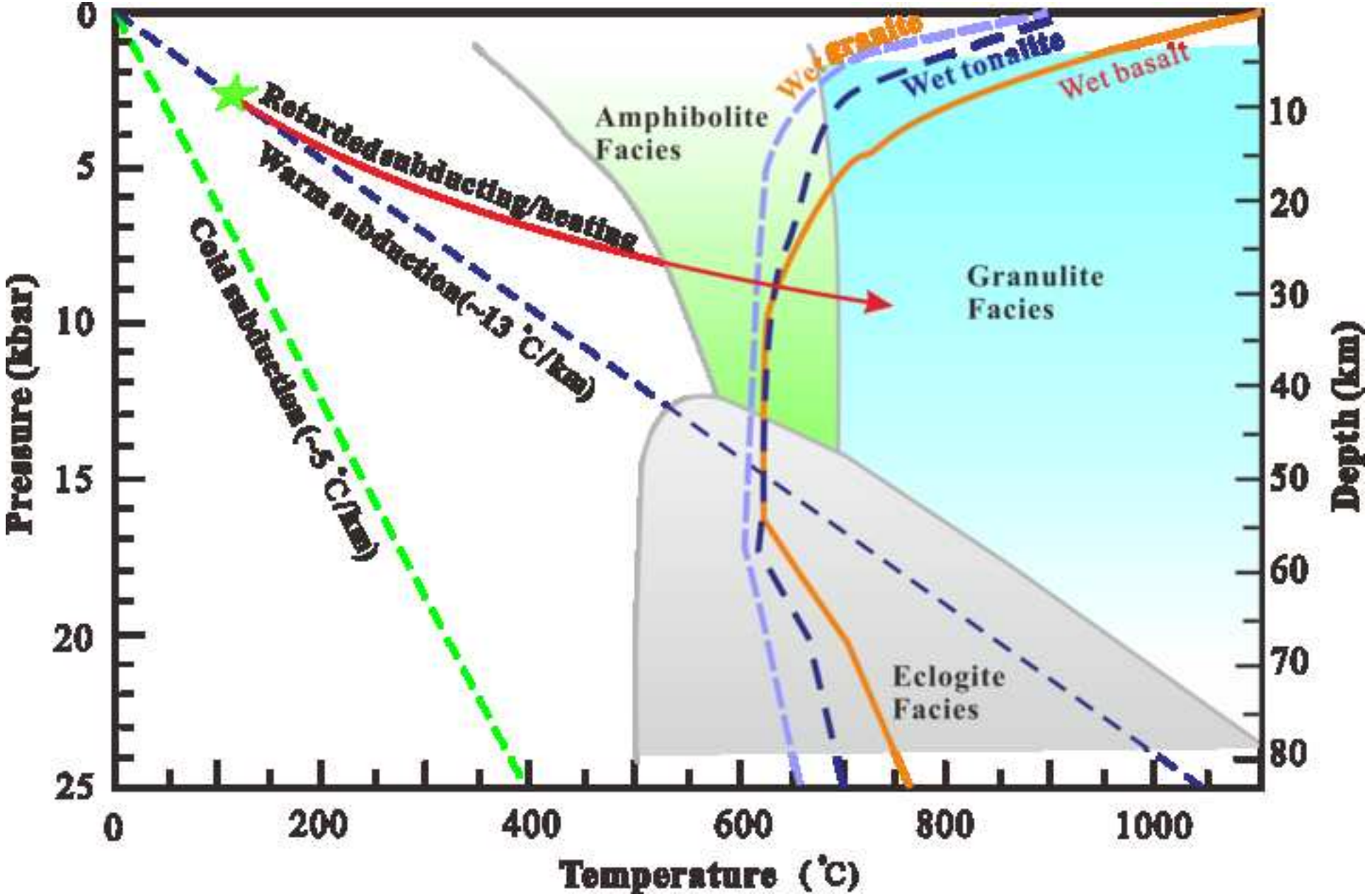

Appendix tables

Click here to download Supplementary Interactive Plot Data (CSV): Appendix tables.xlsx